2015

The Stratal Architecture of the False River Point Bar (Lower Mississippi River, LA)

Alexandra Lechnowskyj
Louisiana State University and Agricultural and Mechanical College

THE STRATAL ARCHITECTURE OF THE FALSE RIVER POINT BAR (LOWER MISSISSIPPI RIVER, LA)

A Thesis

Submitted to the Graduate Faculty of the
Louisiana State University and
Agricultural and Mechanical College
in partial fulfillment of the
requirements for the degree of
Master of Science

in

The Department of Geology and Geophysics

by
Alexandra N. Lechnowskyj
B.S., San Diego State University, 2013
December 2015

ACKNOWLEDGEMENTS

I would like to thank Louisiana State University and ExxonMobil for making this project possible through their collaboration and research funding. I would also like to thank Doctor Peter Clift for his joint efforts in research and for guiding me throughout my pursuit of my graduate degree.

A very special thanks goes out to the three property owners of False River, LA, who allowed me to collect field data on their properties. Without their participation and interest in furthering the research efforts of LSU this project would not have been possible. Respectively, I want to first thank the Jumonville family: J.E. Jumonville, his wife, and their son Dutcher. Their reception and encouragement over both field seasons were a very large asset. I would also like to thank Claude Jumonville for his patience in allowing us to access his land, and Walter Bueche, Jr., who took a strong interest in the project and was always willing to give any needed assistance while navigating his property. Additionally, I want to thank Betty Woody for granting access to myself and my crew, and Glen Ray Cline, for his immense patience in dealing with the many field issues that can arise in muddy and wet weather. Without the cumulative understanding and support of the people of False River, this project would not have been possible.

Lastly, I would like to thank the crew of Professional Technical Support Services, Inc., for not only putting effort into the project, but for taking the time to make sure the job was done correctly and efficiently. Individually, I want to thank the owner of the company, Scott Bergeron, for his vast amount of assistance regarding log interpretation and technical understanding, and for answering the dozens of emails I sent to him on a weekly basis.

TABLE OF CONTENTS

ABSTRACT

The False River point bar system is located roughly thirty miles north of Baton Rouge, LA. It is an oxbow lake cut off from the Mississippi River, and represents a large-scale modern analogue to the ancient systems of northeastern Alberta, Canada, specifically those of the Athabasca Oils Sands. While previous work has been done regarding the general architecture of a point bar, there is still complexity associated with larger scale systems, as studies have been mostly based on small and medium-scale examples.

Examination of the point bar was done through a combination of coring and geophysical logging, followed by software analysis of the logs in order to identify facies packages and trends within three different areas of the bar (early upstream apex, late stage near apex, and downstream late simple bar stage to late compound bar stage). Three facies packages were interpreted: Top bar, interbedded heterolithic strata, and high-net facies (sand-rich).

Although early to late stage simple bar growth demonstrated predictable facies stacking trends, facies related late stage compound bar growth and active abandonment from the main river channel were unpredictable based on small-scale simple models. Permeability differences within sand-rich packages also decreased in the downstream end of the bar, demonstrating a difference in sand quality within seemingly identical facies packages which has previously been overlooked.

1. INTRODUCTION

A meandering river is a river with a notably sinuous pattern, and whose position within an alluvial plain (also referred to as a zone of river migration) moves throughout time (Reading, 1986) (Fig.1.1). These rivers represent an end member for fluvial systems and contrast with the braided type, which anastomose across a wide plain. A number of factors may control whether a river is braided or meandering and a single river may switch from one mode to another as a result of changing climate, sea level, or tectonic state. Movement of a meandering channel across the alluvial plain is often recorded in depositional features known as point bar deposits. These are constantly being built and eroded as the meanders migrate, but may be preserved if the meander experiences a cut-off event in which the stream is effectively short circuited, which allows the meander loop to be preserved as an oxbow lake, with much of the stratigraphy in the subsurface maintained (Fisk, 1947; Reading, 1986; Saucier, 1969, 1994).

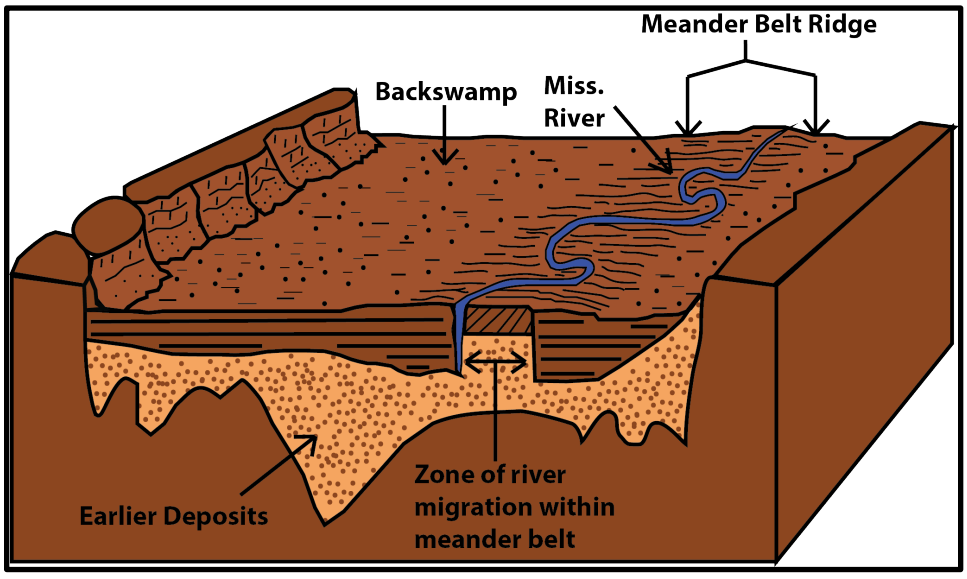

Figure 1.1. The alluvial valley of the Mississippi River, highlighting the main features of the meander system. The zone of river migration sits within the boundaries of the meander belt ridge. Outside of the ridge is the backswamp (floodplain) area. The alluvial plain is estimated to be 150 km wide, with large vertical exaggeration. Modified from Saucier (1994) and Reading (1986).

Point bar complexes provide crucial data regarding the history and path of ancient river systems and these may be preserved in the geological record if there is sufficient accommodation space, especially in the form of tectonically driven basin subsidence if the point bar is to preserved for millions of years or longer. Present-day rivers such as the Mississippi can be studied in order to provide analogues for ancient systems so that their internal architecture can be examined and explained in terms of the fluvial processes that built them. This is especially crucial when considering large scale bars like that seen in False River, Louisiana (Fig. 1.2), in which the sheer size of the structure introduces complexities not usually seen or studied in smaller systems (Hubbard et al., 2011). To date, most detailed studies have concentrated on smaller and medium sized systems (Gibling, 2006).

The False River point bar holds out a special opportunity to understand how these bodies are constructed. Fisk and Saucier (1947; 1994) recognized some of the basic features of this and other point bars in their early papers, which studied the course of the Mississippi River through southern Louisiana, and provided the stratigraphic basis upon which this study was built. While previous work has been done regarding the general architecture of a point bar, there is still complexity associated with larger scale systems that has yet to be understood, especially in association with the suspected large hydrocarbon reserves that may be stored within them (Sheperd, 2009). Point bars are not homogenous blocks of sand, but show internal heterogeneity linked to the changing currents and sediment supply that built the bar. Understanding where these heterogeneities are and why they form represents an important question both theoretically and economically.

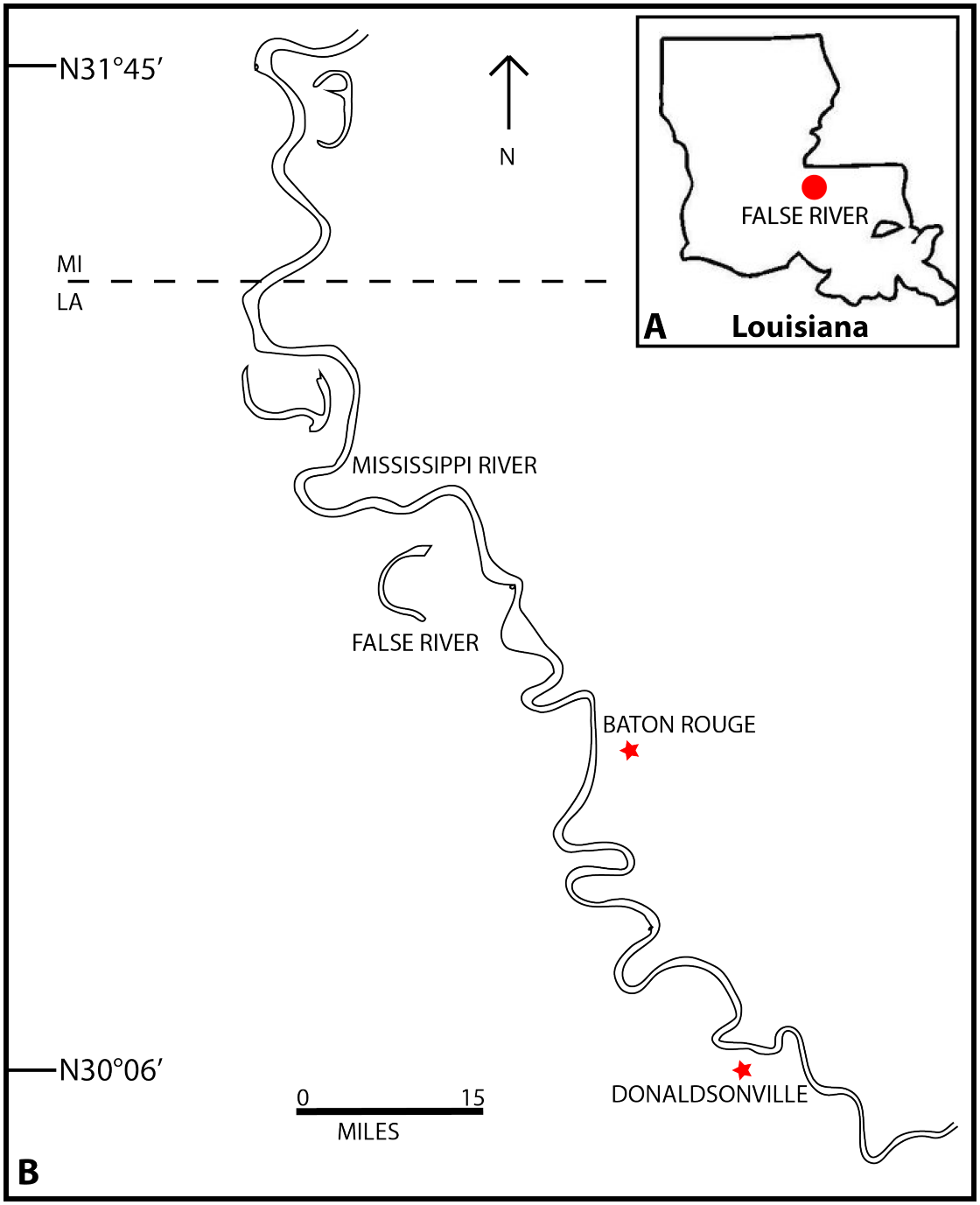

Figure 1.2. Location of the False River study area. A depicts the entire state of Louisiana, with the red circle representing False River. False River is shown in B as an oxbow lake. Red stars indicate major cities.

Point bars from studies such as Fisk and Saucier recognized a general ‘1 D’ model of formation, in which sediment is eroded from the cutbank (outer curve of the channel) due to bank caving. This material is then deposited on the opposite leeward side, forming a point bar

deposit as the river meander migrates (Fig. 1.3). Eventually, the meander is cut off from the main river channel because of either chute cutoff or neck cutoff, with the difference being the abruptness of the transition between the bedload and suspended sediment (Reading, 1986; Fisk, 1947). These early models, which assumed a uniform river sediment load, established the basic fining-up and outwards sequence of a simple point bar system, but lacked the fine scale heterogeneity seen in later models, and which form the focus of this paper (Fustic et al., 2012; Labrecque et al., 2011; Willis and Tang, 2010). In later models of larger scale systems, the assumption of a uniform river load is replaced by seasonal or longer-term discharge variability (Fustic et al., 2012). This could include spring melting, monsoonal summer rains, or longer-term changes linked to climatic phenomena such as El Nino. Flooding events are considered crucial in forming discontinuities in the point bar since they can impact stratigraphy, especially in relation to the formation of chutes and mud rip-ups (Fisk, 1947; Fustic, 2007; Fustic et al., 2012; Reading, 1987).

Fustic et al. (2012) studied the difference between the upper and lower units of a point bar, in which the lower portion is characterized by trough cross-bedded sandy strata, and the upper by Incline Heterolithic Strata (IHS). IHS is characterized by interbedded sands, silts and clays, and is recognized as the laterally accreting units of the point bar, in which the original accretionary angle of construction is recorded (Thomas et al., 1987). This accretionary growth is recognized on the surface of the bar as scroll bar topography, with frequent interruptions by reorientation surfaces. Reorientation surfaces, while still relatively misunderstood, were theorized by Musial et al. (2011) as erosional surfaces representing boundaries between different phases of construction within the point bar. This paper builds on ongoing research regarding these surfaces. Reorientation surfaces are important because fluid flow across the boundaries is

poorly understood, as is the continuity of the strata that define them and the exact mechanisms of formation (Fustic et al., 2007; Fustic et al., 2011; Musial et al., 2012).

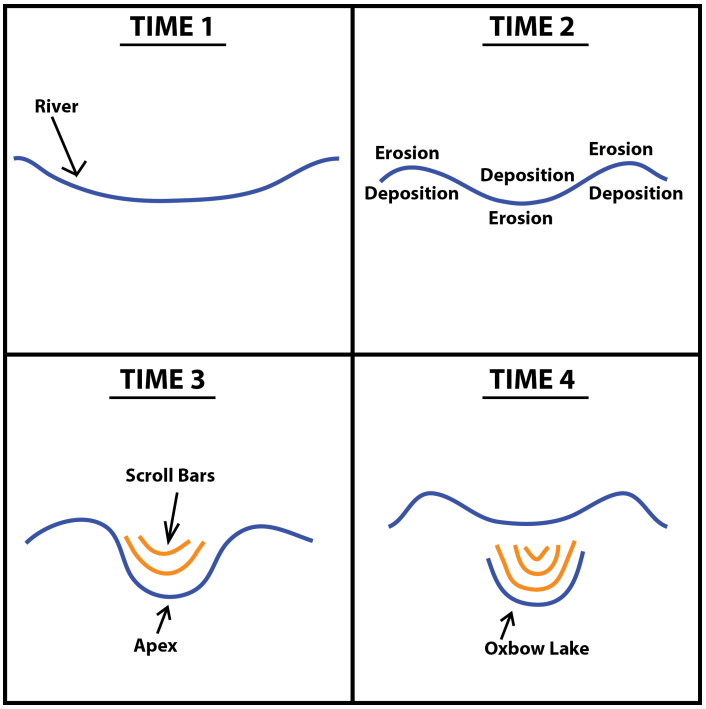

Figure 1.3. Generalized model of point bar development. Time 1 shows the path of a river, with deposition and erosion beginning to occur, causing curvature. Point bars begin developing in Time 2, with deposition on the concave side of the bend and erosion on the convex side. In Time 3, scroll bars remain as surface expression of the point bars growth, with the apex being the center point of the curve of the point bar at the riverbed. As deposition and erosion continue, neck cut-off begins to occur, resulting in an oxbow lake cut off from the main flow of the river, as seen in Time 4.

Also of question is the accretionary angle of the reorientation surfaces, as well as the strata bounded within them. It is unknown how the angle of accretion changes after larger flooding events, and how continuous strata are within these phases of construction. Floods are targets because they represent times of rapid changes in the fluvial system. Fustic et al. (2011) noted that dip becomes more variable in upper IHS settings, especially in those dominated by lateral migration, as opposed to down-valley translation, caused by the sinuosity of the meander.

When observing a well preserved, large point bar from above, features can sometimes be observed on the surface which give clues as to the mechanisms of formation, such as scroll bars

(Fig. 1.3). Scroll bars are elongated ridges of sediment that roughly parallel the point bar growth, and are attributed to large flooding events that deposit sands, silts and clays as levees along the bank of the river (Fisk, 1947). Most importantly, because they form alluvial ridges above the elevation of the floodplain, they can be seen in aerial photographs and may be used as historical clues regarding point bar formation and subsurface stratigraphic architecture (Fisk, 1947, Hubbard et al., 2011). Since scroll bar orientation is directly linked to the type of migration responsible for forming the bar, scrolls can be used to visually define the bar in terms of lateral or translational migration (Fustic, 2007; Hubbard et al., 2011; Smith et al., 2011). While IHS is seen in bars formed by either method, the main difference lies in the orientation of the channel apex to that of the scroll bars seen at the surface. In translation, erosion and accretion occur in a down-valley direction, creating scroll bars sub parallel to the channel downstream of the apex (Fig. 1.3). In contrast, scroll bars will form parallel to the apex of the abandoned channel if the bar was formed from lateral migration (Fustic, 2007). False River may further complicate these models due to the presence of multiple apexes and asymmetrical scroll bar topography.

It is necessary to expand on the current knowledge regarding point bar topography in order to develop new models to enhance the understanding of geological systems. In ancient environments, such as the Cretaceous McMurray Formation that constitutes the oil sands of Alberta, Canada, little is known regarding the development of the past river system, mostly due to the complexity introduced at such a large scale (Hubbard et al., 2011; Musial et al., 2012). Consequently, my study area in False River was specifically chosen to represent a large-scale modern analogue to these ancient systems, specifically those of the Athabasca oil sands (McMurray Formation).

The objectives of this thesis are to (1) define the internal architecture of the False River Point Bar system in order to gain a better understanding of what processes controlled it's formation; (2) gain a better understanding of how sediment is transported through large meandering systems; and (3) provide a suitable and detailed analogue to ancient systems.

2. MEANDERING RIVER SYSTEMS

Sedimentary rocks deposited in fluvial settings comprise an important part of the fill of many sedimentary basins. These sediments tell us about environmental conditions at the time of sedimentation, but also reflect sediment production/erosion processes in the source regions, as well as the climate, speed and seasonality of sediment transport. Rivers tend to fall into either anastomosing, braided, or meandering systems and on low gradient coastal plains meandering rivers tend to dominate (Langbein, 1966; Reading, 1986). If we are to interpret the sedimentary geological record then we need to understand how sediment is transported through the river and how long it is stored and then reworked from point bar systems.

A meandering river is a river with sinuosity. A meandering river moves throughout an alluvial plain through time, with the area confined to movement referred to as a zone of river migration. Bounding each side of migration is a meander belt ridge, with a backswamp area lying to either side of this ridge (Reading, 1986; Fisk, 1947; Saucier, 1969).

The alluvial valley is defined as the valley through which a meandering river flows. Within it, there is a complex interaction of sedimentation and erosion distinctive to the slope, bank materials, and hydrologic factors within the alluvial plain and river (Gouw, 2007). Slope is one of the most important factors that contribute to the development of a meandering river, of which the other three are load, discharge, and the materials comprising the bed and bank through which the river is flowing (Fisk, 1947). Bed and bank materials are considered the primary factor in areas such as the Mississippi river because the river is presently ‘poised’. A river is considered poised if it has acclimatized to its slope, load, and bed materials, Thus, if a river is a poised, it reasons that the there would be little coarse-grained materials being fed into the river by its tributaries. Those coarse grains that are held within features such as point bars would be

periodically fed back into the river as migration occurs and the point bar is reworked, depositing again within a bar formation downstream (Reading, 1986; Willis and Tang, 2010)). This means that in places where bank materials are fine-grained and cohesive, the river migration is forced to conform by it's inability to impinge against them and erode the bank during migration, resulting in a diversity of meander shapes, such as that of False River (Fisk, 1947).

Early models of meander belts established simple mathematical relationships regarding slope, channel width, and curvature, concluding that in essence, rivers meander in order to reduce the shear and frictional properties caused when velocity reaches an unstable rate (Langbein and Leopold, 1966). According to Reading (1986), low slope is favorable over high slope in encouraging high sinuosity. Meandering tends to be more characteristic of rivers containing a greater amount of fine-grained sediments compared to coarse-grained. However, meandering itself is then responsible for the abundance of internal structures within the river and the resultant fluvial sediments (Reading, 1986; Saucier, 1969; Fisk, 1947).

Deposition and erosion both take place in each bend of a meander. Whether sediment is being eroded or deposited relates to the position of the thalweg, or point of highest velocity (Fisk, 1947; Gouw, 2007). The increased velocity at this point causes scouring within the river channel, and the formation of subsequent 'scour pools', which deepen with time. Owing to the geometry of the river channel, with the thalweg being closer in proximity to the outer (concave) bend, this causes erosion and eventual caving of the bank around the bend, and subsequent deposition on the (convex) bank where velocity slackens (Fisk, 1947). Because both erosion and deposition are both so closely tied to the velocity of the moving mass of water, they are both then closely tied to each other, and to the erodibility of the cutbank. In places where the cutbank is primarily made up of fine-grained alluvial material, the channel response is to deepen as a result

of increasing water velocity, while the presence of coarser materials would have the opposite effect (Gouw, 2007). However, while finer grained materials increase the velocity of the moving mass of water, channel migration flowing through coarser materials would have a larger zone of migration. Regardless of the bank material, it is the variability in the bank materials and the channels response to these materials that causes a change in position of the thalweg, and thus the migration/meandering of the river (Fisk, 1947). Thickness variations may then exist due to the constantly changing sinuosity of the river channel. As sinuosity increases, the depth of the thalweg scour is also expected to increase. Since the thalweg is deepest opposite the apex of the bar, the point bar should thicken in the direction of later accretion (Willis and Tang, 2010).

Bank caving is divided into two different mechanisms, sloughing and slumping, and these are the means by which the shoreline recedes (Fisk, 1947). This is because the river is constantly striving to reach a state of equilibrium, hence the constantly shifting position of the thalweg and river channel and the constant battle between erosion and deposition (Fisk, 1947; Saucier, 1969). In the case of the meander bends, the material produced by bank caving is deposited on the convex bank in the form of a point bar due to the surface flow being at the outer bank and the bottom flow at the inner bank (Fig. 2.1) (Langbein and Leopold, 1966; Reading, 1986; Willis and Tang, 2010). Moller (1993) described this process as a ‘sweeping’ motion towards the point bar from the thalweg, resulting in the laterally accreting units so characteristic of bars. More specifically, point bar deposition is attributed to the helicoidal flow of the moving water, which distributes the sediment with a pattern of fining upslope as well as downstream due to recirculation of the fines after passing around the apex of the bar (Reading, 1986; Fustic et al., 2012).

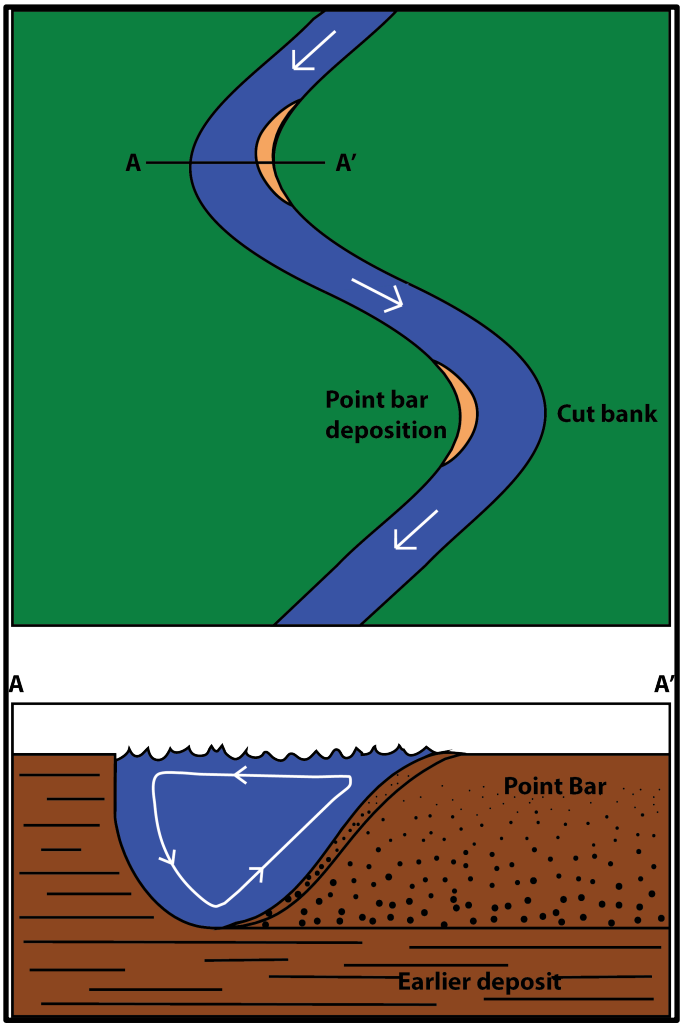

Figure 2.1. Simplified cross section (A-A') of a point bar in a meandering river channel. The white arrows indicate the direction the river is flowing.

Within a single bar different facies associations can be distinguished based on sediment grain size, assemblage of sedimentary structures and their position within the point bar (i.e., upstream or downstream). Three facies types are often deposited within a single phase of high water flow within the Mississippi (Davies, 1966). Point bars are noteworthy for their development of a ridge and swale topography, known as scrollbars, rather than a uniform flat surface (Hubbard et al., 2011; Nanson, 1980). One explanation for the presence of the scrollbars has involved the idea of current separation zones in which sediment is deposited against the convex bank while alternatively a bimodal size distribution in the grains within the bedload

could result in preferential deposition of coarse sediment near to, but not adjoining the convex bank (Bridges and Leeder, 1976). Alternatively, the role of dead trees acting as a nucleus of sedimentation on point bar platforms may be causing the localization of coarse sedimentation (Nanson, 1981). More simply put, Gibling and Rust (1993) theorized three main depositional styles that can result in scroll bars: migration of transverse sand bars, deposition during flooding events, and chute channel migration. This debate is important for understanding how sediment grain size is controlled during the construction of a point bar complex. Surface scroll bar expressions can be used for subsurface internal characterization, in which lateral vs downstream accretion is indicated based on scroll trajectories (Hubbard et al., 2011). Once the method of accretion is identified, inferences regarding channel width and heterogeneities are possible, which is especially useful in a reservoir setting where point bars deposited by downstream accretion would less desirable due to increased fine-grained strata (Hubbard et al, 2011; Smith et al., 2009).

A point bar, divided into its two most basic components, consists of a topstratum (the accretionary dipping units) and a substratum (lower bar sands), as defined by Fisk (1947). He further categorized these layers by the their alluvial grain size, with the topstratum, or upper bar, demonstrating a fining upwards gradation caused by the movement of the river and subsequent repositioning of the accretionary ridges away from their original position as the river changes the zone of active sedimentation, which migrates as the river migrates (Fustic et al., 2007; Fisk, 1947; Diaz-Molina, 1993). Cant & Walker (1978) described the facies sequence as a result of the lateral growth of the point bar combined with flood plain deposition, and the upper bar units were later categorized as inclined/interbedded heterolithic strata (IHS) by Thomas et al. (1987). These deposit overly the sands and gravels of the substratum. The topstratum IHS units, which

contain interbedded, dipping strata of sands, silts, and clays, have recently been established one of two characteristic and expected facies packages within a large-scale point bar system, with the other being the lower bar package of trough cross-bedded sands (Fustic et al., 2012; Musial et al., 2012).

From the proximal to the distal ends of the bar, the ratio of sand to IHS decreases. At the same time the heterogeneity at the downstream (younger) end is much great than that at the upstream end, where the lower bar is much thicker (Fustic et al., 2012). The lower bar dips parallel to the direction of river flow while the accretionary units of the upper bar dip perpendicular to that of river flow, with an average dip of 6-12°, and the contact between the upper and lower units dipping both in the direction of later and downstream accretion (Fustic et al., 2007; Fustic et al., 2012; Strobl et al., 1997).

Figure 2.2 demonstrates the concept of upward and downstream fining, as well as the accretionary dip of the upper and lower units with respect to a river channel. Though it does lack some of the structural complexities expected in a larger bar, such as erosional surfaces and mud drapes, it is a useful tool in visually understanding the wedged shaped geometries of the upper and lower units, as well as the ratio of IHS to the underlying sands. It was theorized that the pattern of downstream fining in a point bar is most significantly related to the change in current flow around the apex of the bar. As the helicoidal flow rounds the apex, the current may be appreciably reduced, promoting deposition of finer grained sediment due to recirculation after rounding the apex, as well as better preservation compared to upstream of the apex (Jackson, 1975; Paola et al., 1992; Willis, 1989). Larger clasts may also be broken down into smaller grains due to erosion. However, it is important to note that IHS represents an interbedding of silts

as well as sands, where the sand beds are deposited at times of higher energy and the silts during low discharge or slack tide (Labrecque et al., 2011).

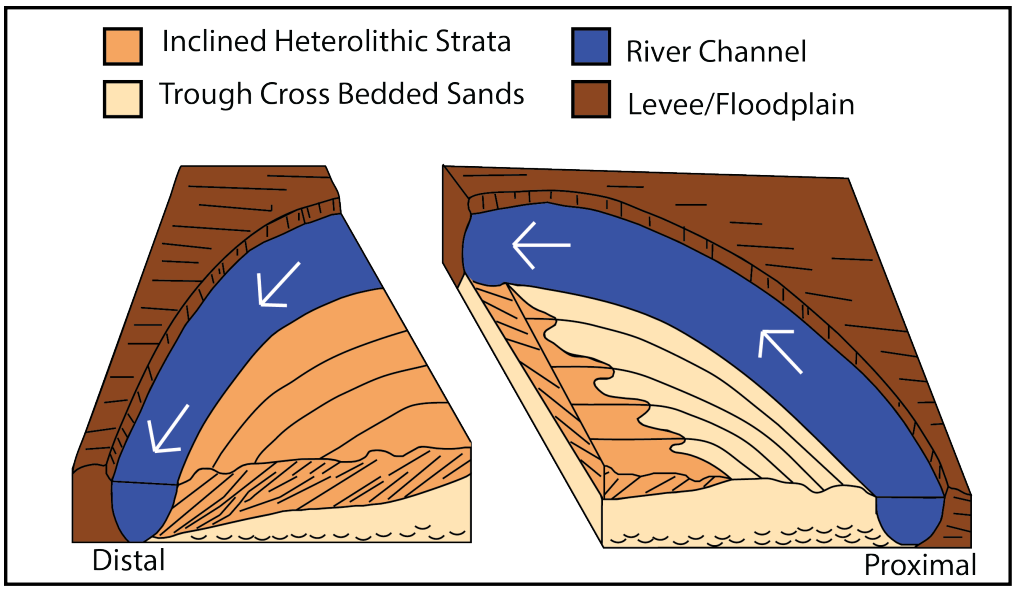

Figure 2.2. Cross sectional view and top view of a point bar featuring trough cross-bedded units in the lower bar and IHS in the upper bar. The ratio of IHS to trough cross-bedded sands increases downstream. Note the dipping strata of the upper IHS can be variable within the unit. Modified from Fustic et al. (2012).

Although Figure 2.2 depicts a strong boundary between the upper and lower units of the bar, this is due to a lack of continuity between the visual accretions of the IHS and lower sands, and should not be seen as a 'timeline boundary'. Ideally, a timeline would be able to be placed as a sinusoidal line of accretion from the top to the bottom of bar. However, this is not possible because of the trough cross-bedded nature of the sands, which do not record the accretionary angle of bar growth. Though a boundary does exist between the upper and lower bar, it is a facies boundary, not a timeline boundary (Musial et al., 2012).

Friend et al. (1979) further divided a point bar into storeys, which reflect the orientation of bar growth. In areas such as False River, where the shape of the point and orientation of the scroll bars in relation to each other are very asymmetrical, it would be expected that multiple storeys of inclined and fining upward sequences exist, at different angles and orientations to one

another due to seasonal flooding events which caused reorientations of the river channel (Blum et al., 2013).

In an ideal system with a single direction of point bar growth, one would expect to only see one storey of inclined heterolithic strata (IHS) topping the lower bar facies of trough cross bedded strata, demonstrating a bi-partite facies model (Reading, 1986; Fustic, 2007; Musial et al., 2012; Fustic et al., 2012). However, as a river experiences varying conditions during bar growth, the orientation of bar progradation may abruptly change, which is why more than one storey is common. As a result of this, what appears as one bar may actually be made up of several sets of accretionary units, divided by reorientation surfaces (Diaz-Molina, 1993; Jordan and Pryor, 1992).

Reorientation surfaces (Fig. 2.3) are considered to be first order divisions separating major phases of construction, but it is unknown exactly how/why they form, and what the complete stratigraphy throughout the units is. Without this understanding, difficulties arise in ancient systems when trying to map an entire forset, because it would be unclear where the new phase of construction is located (Brekke and Evoy, 2004). It is also unknown if each reorientation surface can always be expected to have fine grained clay/shale drapes across them, potentially hindering later fluid flow, and whether individual units have continuity across these surfaces (Musial et al., 2012). This is true both horizontally and vertically because of the variability of the inclined strata and the lack of understanding regarding the positioning of the reorientation surfaces. However, it is clear that each reorientation surface bounds individual lateral accretion sets, with variability from one to the next based on storm events or fluctuations within the river channel at the time of deposition (Fustic et al., 2007).

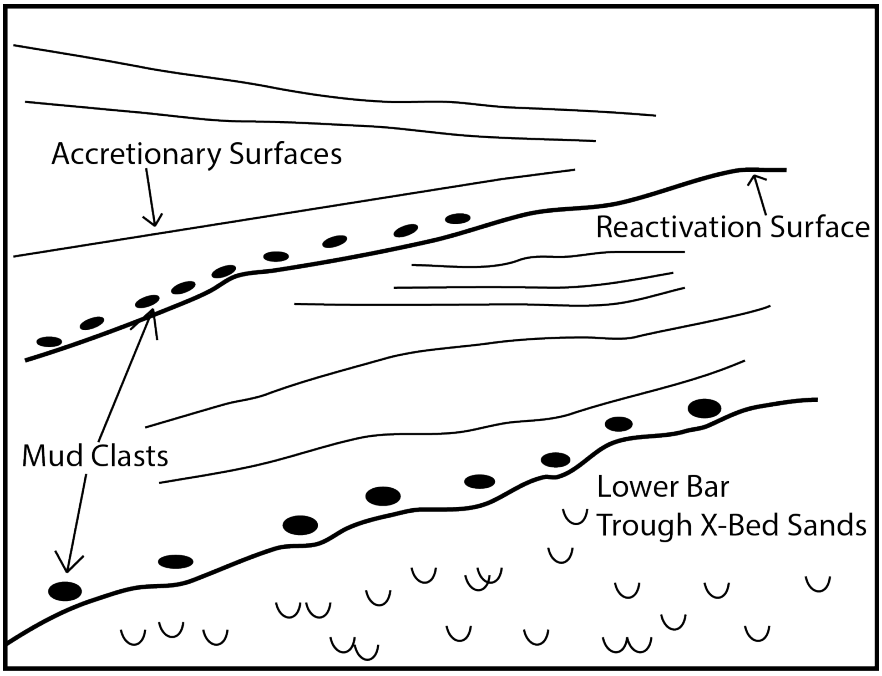

Figure 2.3. Stratigraphy of a point bar experiencing both tidal and fluvial inputs. Upper point bar accretionary surfaces are above lower cross-bedded sands, and divided by an erosional surface. This surface, as well as the upper erosional reactivation surface, is expected to be bound by mud clasts. Dipping accretionary deposits may also contain mud drapes. Modified from Musial et al. (2012).

Despite lacking a complete understanding of the mechanism of reorientation formation, especially in settings with variable fluvial vs marine influence, Jordan and Pryor (1992) noted that reorientation surfaces are simplistically erosional surfaces, contributing significantly to a decrease in permeability across the bed due to the deposition of fine-grained sediments. These impermeabilities become even more complicated when considering the fact that though accretionary units may be bounded by and contain thin mud laminae, grain variations exist in all cases, as well as discontinuities of the laminations (Musial et al., 2012).

Point bar strata characterization is important, because the sediment being fed into the bar (and thus eroded from the cutbank) plays a crucial role in the mechanism of cutoff, which essentially isolates the bar and leaves it secluded from the main channel of the river (Zinger et al., 2011). Neck cutoff occurs when the opposite banks of a meander begin eroding towards one

another (Saucier, 1994). Changes in alignment of the upstream arm of the meander are converted downstream into the downstream arm. The upstream arm will eventually catch up to the downstream, as the upstream arm is moving through sandy point bar material while the downstream arm is encountering more cohesive, less easily eroded materials, potentially culminating in cut-off (Fisk, 1947). While periodic flow eddies may sweep sediment into the abandoned channel, these areas are eventually plugged, preserving the structure of the point bar (Reading, 1986) (Fig. 3). Within this model, there are also opposing opinions on the rate that the actual cut-off progresses. In one scenario, cutoff is abrupt and the ends are rapidly plugged, while in the other scenario cut-off is regarded a gradual diversion (Willis and Tang, 2010).

This type of cut-off differs from chute cutoff, in which it forms as a mechanism for the river to straighten its flow during high water levels by reducing the amount of flow in the main channel and feeding it into the chutes (Zinger et al., 2011)(Fig 2.4). Because the flow is directed across the surface of the bar, cut-off will occur along this channel, rather than create a new (and straighter) channel like that of neck cutoff. However, though differences exist in the transition from flow being focused and stable in the main channel to complete cutoff, the oxbow lakes formed in either circumstance are bounded by both the outer erosional surfaces of the past river banks and the inner inclined strata of the point bar (Reading, 1986; Saucier, 1994).

Chutes can also occur along the surface of a point bar without leading to cut-off. Furthermore, the scrolls deposited by chutes can have very similar properties to main-channel scrolls, and yet rework the stratigraphy of the bar top sediments as they migrate across the surface. As a result, chutes are poorly understood, and due to the lack of knowledge regarding their behavior stratigraphers have run into problems when seeking to build geologic models of point bars and the role that chutes play (Reading, 1986; Musial et al., 2012).

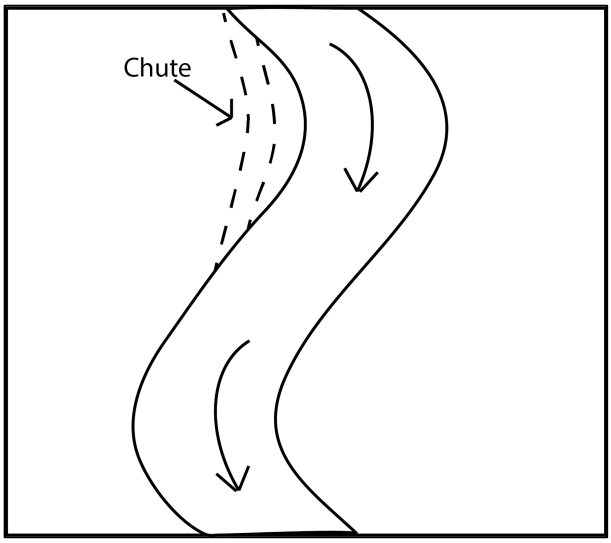

Figure 2.4. Diagram of a generic meander loop with a chute cutting across the surface of the point bar. Depending on different variables, chutes may or may not develop into a cut-off.

When a river cannot accommodate the high level of water caused by flooding, water overflows the banks and spills onto the flood plain. This progression builds natural levees, and beyond that sedimentation occurs in the floodplain areas. Levees, by nature of grain deposition, fine outwards towards the toe due to the coarser sediments depositing first, forming the characteristic ridges of a levee (Fisk, 1947).

Once a meander loop is cut-off from the river and an oxbow lake forms, flow is diverted from the abandoned channel, and the upstream and downstream arms of the bar will begin to infill with sediment, eventually forming clay plugs that cut off all flow during normal water levels (Fisk, 1947). Saucier (1994) theorized that these areas would form natural levees as the river began to migrate back towards the abandoned channel, infilling certain areas and essentially sealing off that portion of the river as a path for drainage, dramatically reducing the volume of sediment accumulation. This supports Fisk's (1947) observations that sand deposition exceeds no more than one third of the length of the meander loop from the upstream arm, where coarse materials are introduced directly following cutoff, after which it is covered with silts and clays

(Blum et al, 2013). However, because the rate of accumulation within a channel is dependent on the rate of cut-off, it is important to note that the extent of sand deposition may be different for other river systems outside of the Mississippi, which was the area of study for both Fisk and Saucier. Nevertheless, once the path of drainage via the meander arms is hindered or blocked, in most cases flood drainage will exit onto the floodplain (Saucier, 1994). This results in predominantly fine grained sedimentation within the abandoned channel, where the appearance of clay plugs is a common occurrence, especially in fluvially influenced meander systems where mud accumulation is cyclically interrupted by seasonal flooding events, in which case silty layers may deposit (Musial et al., 2012). However, Fisk (1947) noted that the rate and grain size of sediment accumulation is dependent on the rate of cut-off, and that a large proportion of abandoned channels in the Mississippi are primarily silty sands and clays, not clay alone (Jordan and Pryor, 1992).

Backswamp deposits, which are a feature of the floodplain, are formed along river systems following periodic flooding mostly during times of sea level rise, and as a result are made up of mostly fine-grained sediments (Gouw and Autin, 2008). In river systems with an extensive history, such as the Mississippi, which has experienced multiple episodes of sea level fluctuation, backswamp deposits can become quite thick. Thickness, as measured from borings by Fisk (1947), increases from north to south along the river, and varies from 7.6 to 42.7 meters in Louisiana, with the average near our study area being above 18 meters. Yet despite the occurrence of thick deposits, backswamp deposition is not found in every location along the present course of the Mississippi River. In regards to this particular river, scouring caused by river meandering is prevalent in areas with high sinuosity, where the river cuts into the backswamp deposits as erosion occurs and replaces the deposits mostly with point bar deposits

(Gouw, 2007; Saucier, 1969). Farther south, especially in Louisiana, there is an interplay between deltaic and floodplain deposits (Fisk, 1947).

Though False River is geographically above any direct tidal influence, point bars can be formed in areas affected by both tidal and slack water flow, especially during seasons correlated to a higher tidal current strength. In areas that do experience a strong tidal effect, the internal structure of point bars have been shown to contain many erosional reactivation surfaces draped by small mud clast breccias (Fig. 6) (Musial et al, 2012; Labrecque et al., 2011). Regardless of the cause of these surfaces, reactivation surfaces are expected to appear in both fluvial and tidally influenced point bars, with the main difference being that accretionary sets are more easily recognized in point bars which have predominantly fluvial input due to a thicker occurrence of mud drapes deposited when the water level is low. In contrast, point bars receiving a strong tidal influence will be more affected by high vs low tide, hindering at times a thick deposition of mud drapes (Musial et al, 2012). In addition, though many similarities regarding discharge and migration rates exist between the fluvially influenced point bars of the Mississippi River (the study area) and the tidally influenced point bars discussed by Musial et al. (2012), it was noted that the point bars of the Mississippi predominantly follow the bi-partite facies model due to a less common occurrence of tidal influencing, with clean sands in the bottom of the bar and IHS in the upper.

This is important when considering ancient point bars, which are usually classified as tidal or fluvial based on fossil analysis and geomorphology. Debates currently exist in areas such as Athabasca, where fossil indicators point to a marine depositional setting, despite the presence of fluvial geomorphology (Hubbard et al., 2010; Musial et al., 2012). As a river reaches the coast and its ability to carry sand diminishes, large sweeping river meanders like those of False River

cease to exist, making the sinuous nature of a channel indicative of a fluvial setting (Fisk, 1947, Gouw, 2007). Because of this, a study of a large-scale bar formed in a purely fluvial setting is a much needed clarification and analog in order to classify ancient systems.

Although braided stream and deltaic plain deposits do not have any direct bearing on the sedimentary structure of the Mississippi River being considered in this study, it is still important to note that these deposits do make up a portion of the fluvial river system of the of the Mississippi as a whole, though the in the case of the braided stream deposits they may be covered by younger backswamp and natural levee deposits (Farrell, 1987). In a simplistic manner, visible braided stream deposits can be found farther north of False River, Louisiana, in Mellwood, Arkansas, and deltaic plain deposits farther South of Donaldsonville (Fisk, 1947). Braided streams were prevalent in the Lower Mississippi River Valley during the cyclic glaciation of the Pleistocene and early Holocene, and most likely represent the sediment underlying our study area. However, the point bar at hand is of Holocene age (Saucier, 1969).

3. STUDY AREA AND HISTORY

The False River point bar system is located roughly 48 kilometers north of Baton Rouge, in the parish of Pointe Coupee of Southern Louisiana, within the Lower Mississippi Valley (south of Cairo, IL) (Fig 1.2). Though much research has been conducted on the history and evolution of the Mississippi River, a scarcity of data exists regarding the large and complex point bars formed by the meandering nature of the river. False River itself has been included in numerous books and papers as a representation not only of the size of the Mississippi River, but also as a classic example of crevasse splay topography and neck cutoff. However, though False River is prevalent in many studies, and has been researched specifically by Fisk (1947) and Saucier (1969; 1974; 1994), an in-depth analysis of the mechanisms of formation and the complex heterogeneity of the bar remain to be discussed.

3.1 Mississippi River Valley Evolution

The Mississippi River originates in Minnesota and terminates in southern Louisiana, at the Gulf of Mexico. As summarized by Fisk (1944; 1947) and Saucier (1969; 1974; 1994), the Mississippi River Valley is essentially the product of cyclic glaciation throughout the Quaternary following the deposition of preglacial sands and gravels, known as the 'graviliferous blanket'. This cycle, repeated 5 times across 1.5 million years, consisted of five major glacial stages and 5 major interglacial stages (including the Holocene), though these stages have been broken down into smaller, more detailed events when necessary (Blum and Roberts, 2012; Rittenour et al., 2007).

Most importantly, though the ice sheets themselves did not extend past southern Illinois, glaciation cycles produced meltwater and outwash as the result of climactic changes, resulting in erosion and deposition during waning and waxing ice sheets (Blum et al; 2012; Saucier, 1994).

River slope was highly affected by glaciation, as gradients increased in response to a seaward receding shoreline and caused entrenchment as far north as Vicksburg, Mississippi (but no farther north than Alexandria, LA in the last glacial stage). Wind action and rainy conditions were also theorized by Saucier (1974) as important geologic controls on valley formation. Wind formation would have been responsible for loess deposition in upland areas after being removed from braided-streams, while pluvial conditions caused valley lowering as well as the formation of terraces.

The first glaciation, known as the Nebraskan Glacial Stage, began roughly 2.48 million years ago and created the southward flowing trend of the Mississippi River and what is referred to as the 'Ancestral Mississippi Valley' (Saucier, 1974). Following this stage was the Aftonian Interglacial Stage, during which waning ice sheets caused an expected infilling of the previously eroded valleys. However, sedimentation did not reach the previous level of the graviliferous blanket (Saucier, 1994).

The cyclic waxing and waning of glaciation proceeded for the next million years, first with the Kansan Glacial Stage and the Yarmouth Interglacial Stage. Resumed valley cutting and entrenchment by streams were seen during glaciation, which degraded and removed much of the sediment laid down during the Aftonian. The Montgomery Terrace, built during the Yarmouth Interglacial Stage, was later eroded by the next stage of glaciation, the Illinoian Glacial Stage. Succeeding the standard of 'erosion, entrenchment, and degradation' during glaciation was the Sangamon Interglacial Stage, which lasted for roughly 200,000 years. (Saucier, 1994).

The Early Wisconsin Glacial Stage began 195 kya. Due to a large drop in sea level, increased erosion was seen in the lower portion of the Lower Mississippi River Valley and braided streams were predominant in the upper portion (Fisk, 1947).

Conversely, by the Mid Wisconsin Interglacial Stage, 125 kya, the peak of glacial withdrawal had been reached and the subsequent meltwater created the Prairie Terrace (Blum and Roberts, 2012). It also began what Blum and Roberts (2012) referred to as the beginning of the construction of the present-day alluvial-deltaic system. While at this stage the river was meandering in nature, this would only continue until the Late Wisconsin Glaciation 80 kya, in which the river changed to braided.

The late Wisconsin Glacial stage (80-11 kya) was comprised of two glacial maxima separated by a smaller glacial-period fall in sea level (Blum and Roberts, 2012). Identified by their marine isotope data, these are also called MIS 4, 3, and 2, respectively. During MIS 4-3 (80 26 kya) major channel belt formation occurred, followed by valley incising and deposition during the last glacial maximum and subsequent deglaciation during MIS 2 (20-11 kya) (Blum and Roberts, 2012; Saucier, 1974).

Overall, though rainy conditions led to some meander belt formation on some of the tributaries, glacial debris and seasonal discharge variations resulted in the river remaining braided, with major channel belt formation occurring 80-26 kya (Blum and Roberts, 2012; Saucier, 1974). After this, incision and deposition occurred until 11 kya and meandering began again by ca. 10 kya within the Holocene (Blum and Roberts, 2012; Saucier, 1974; 1994)

The history of the Mississippi following the appearance of man 12 kya is more difficult to discern than would be assumed. The onset of the Holocene is marked by notable changes in floodplain level, as well as in the major tributaries. Meander belts, river diversion, and changing discharge all occurred within this time, and connections between different processes can be difficult to make (Saucier 1969; 1974). Currently, the major tributaries of the Mississippi River are the Ohio and the Missouri Rivers. Draining the Appalachian Mountains, the Ohio River

contributes most of the water in the lower Mississippi. The Missouri River, draining from the Rocky Mountains, contributes more sediment (Blum and Roberts, 2012).

In summary, Pleistocene and Holocene deposits consisting primarily of sand and gravel due to widespread continental glaciation were deposited on top of a graviliferous blanket, resulting in an unconformity dating from late Tertiary/early Pleistocene. Entrenchment due to the following glaciation cycles created what is now known as the Mississippi River Valley, with aggradation beginning in the southern area of the valley about 8000 ybp (Gouw and Autin, 2008) . Holocene aged meander belts have predominantly replaced the Pleistocene and later Holocene aged braided river system, with sediment grain type/ sizes of both system being documented by both Fisk (1944; 1947) and Saucier (1969; 1974; 1994).

3.2 False River Point Bar

False River represents a meander loop cut-off from the Mississippi River that occurred around the year 1722, with deposition estimated to have occurred between 1200 and 400 years before present, though after cut-off deposition of channel fill continued to occur (Sternberg, 1956). Neck cutoff was determined as the means of abandonment by Fisk from an aerial photographic of the river in 1947. His images show that the oxbow lake is bounded on one side by the accretionary point bar, and on the other by a natural levee (Fig. 3.1). This is in sharp contrast to that of chute cutoffs, which are generally poorly defined and have shorter lengths. Figure 3.2 depicts a bar and oxbow lake created by neck cut-off as defined by Fisk's study, further backed by the fact that the meander was cut off relatively recently, with the presence of the 'long, arcuate lake' being further evidence for neck cut-off (Fisk, 1947).

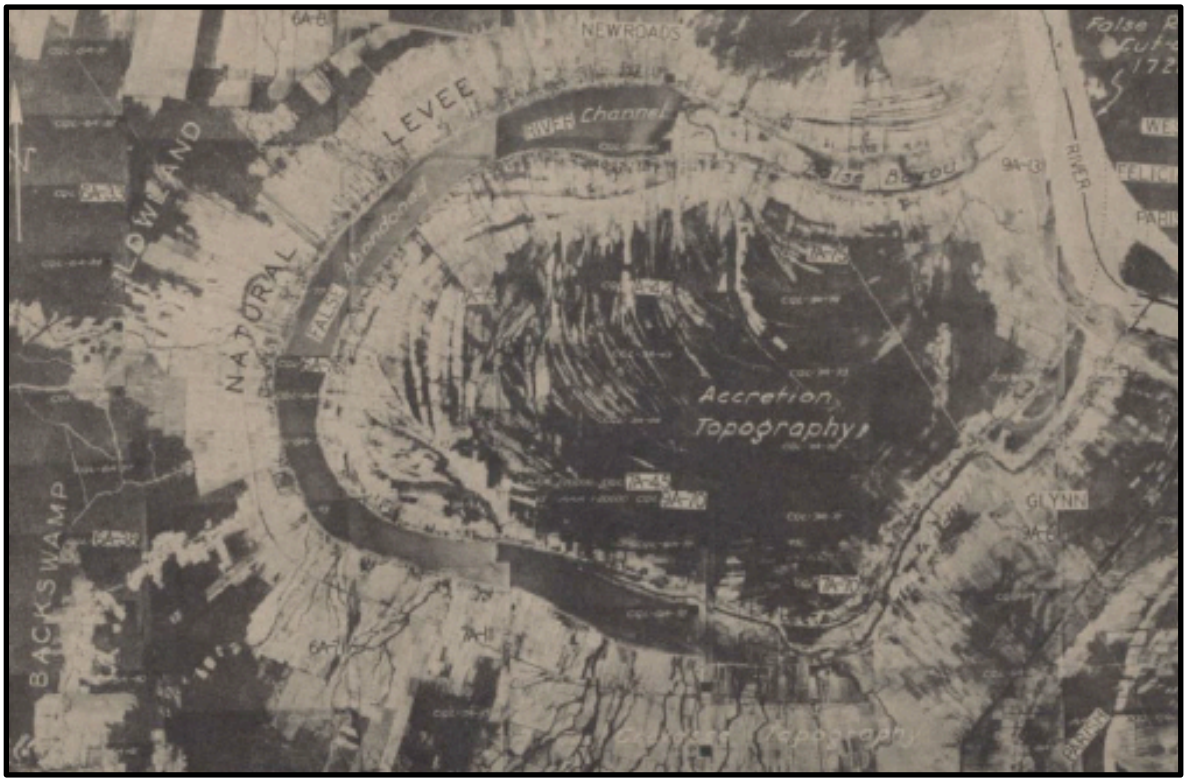

Figure 3.1. Aerial photograph of False River. Image taken directly from Fisk (1944).

The sediment of the False River point bar is of Holocene age, unconformably overlying the sands and gravels of the early Pleistocene (Coleman, 1966; Blum et al., 2013). As seen in Fig. 3.3, through the cross section of Fig. 3.4, inclined point bar sediments underlay levee deposits and sit on top of what Saucier considers undifferentiated meander belt deposits and substratum deposits, with sharp boundaries between these sediments and the abandoned channel fill on either side (Saucier, 1969). However, as shown by this early model, though there is a division between the inclined upper bar and lower 'undifferentiated' deposits, Saucier does not fully recognize the stratigraphic complications between the upper and lower bar, as he groups the lower bar sand package within the substratum deposits, nor does he recognize the fining downstream trend relating to heterogeneities in the distal part of the bar, as shown in later models (Fustic et al., 2012).

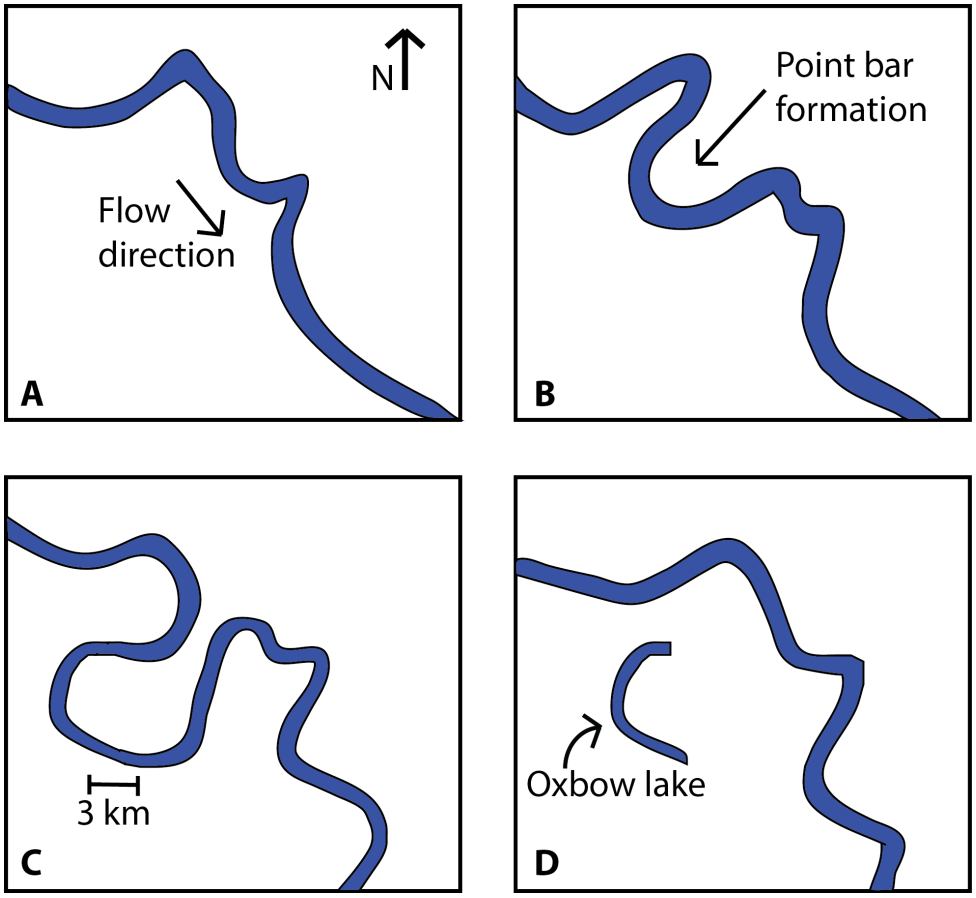

Figure 3.2. Evolution of False River, demonstrating point bar formation through neck cutoff. A) Mississippi river approximately 1200 ybp. Flow direction is to the southeast. Meander bends are present in the study area, and the point bar has begun forming B) River approximately 900 ybp. C) River approximately 500 ybp, with complete cutoff occurring 400 ybp. D) The False River oxbow lake at present, completely cut off from the current Mississippi River to the northeast. Approximations based on data from Fisk (1947).

This cross section also over-simplifies the division and unconformity between the base of the point bar and the sands and gravels related to cyclic glaciation of the Pleistocene, which should be relatively equal in depth to the thalweg of the channel at the time of formation (Fisk, 1947). Instead, the Holocene aged trough cross-bedded sands of the lower bar are grouped with the Pleistocene glacial sands and gravels as a 'substratum', which Saucier recognizes as a fining upwards sequence from coarse sands and gravels to fine sands.

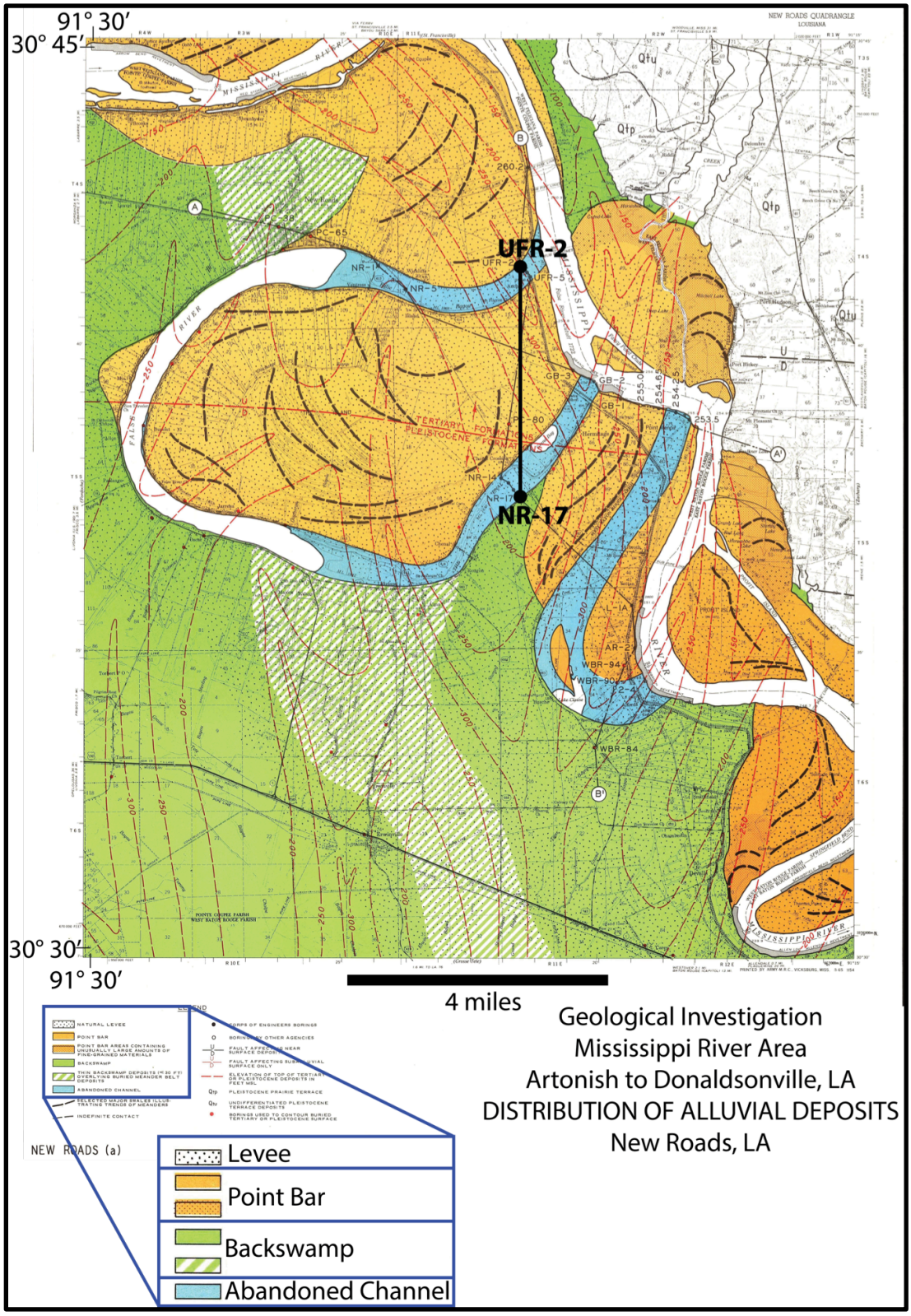

Figure 3.3. Geologic map of the False River oxbow lake and point bar, modified from Saucier (1969). The cross section indicated by the black line is shown in Fig. 3.4.

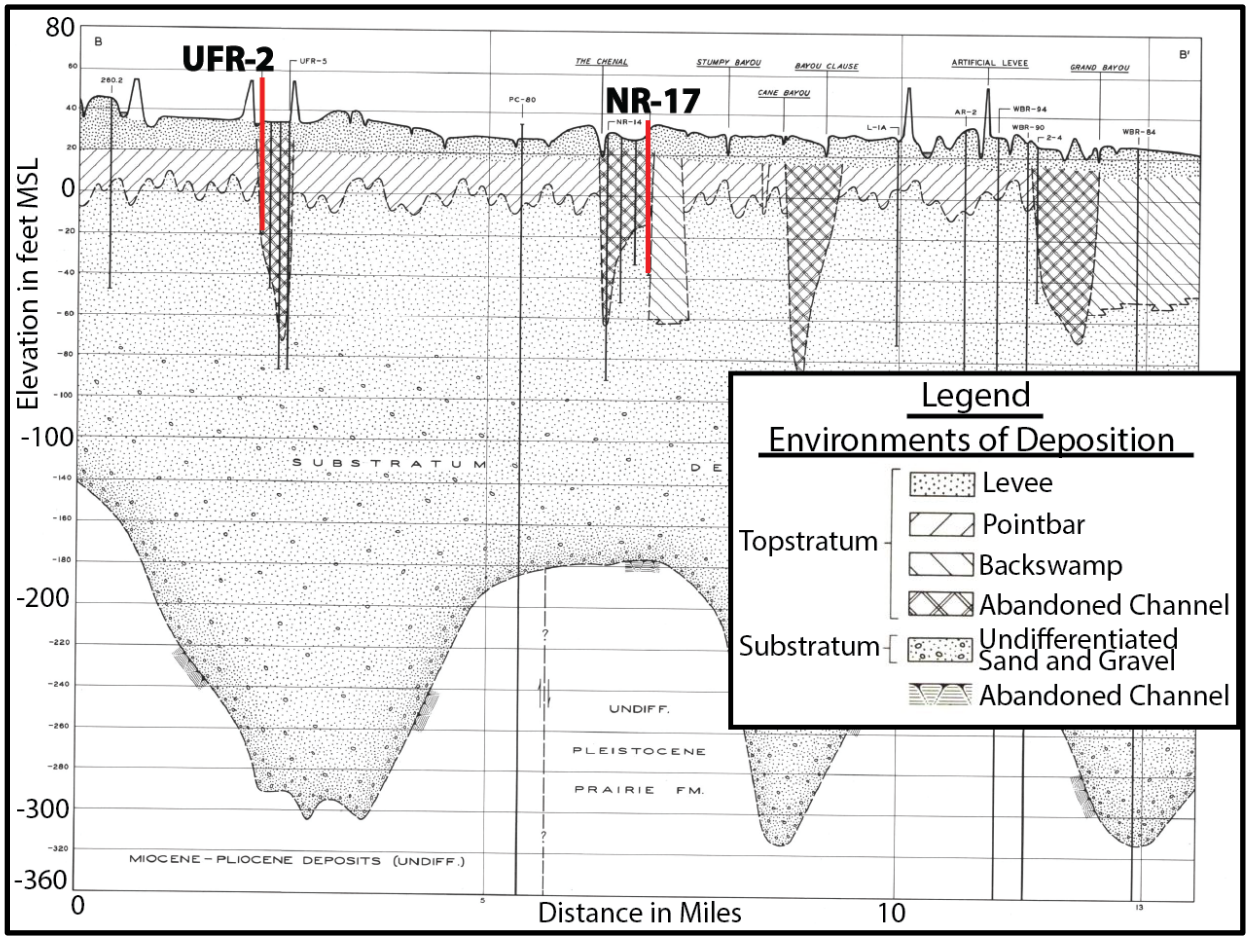

Figure 3.4. Cross-section through the False River point bar from Figure 3.3. The red lines indicate the well location and depth. As indicated, the lower point bar units are grouped together with the Pleistocene sands and gravels as a 'substratum' unit. Modified from Saucier (1969).

However, despite not having a clear division between the substratum units, the coarser glacial deposits appear to be begin at a depth relative to the depth of the channel deposits as indicated by the cross sections, and a division between the two deposits is discussed within the text. Overall, Saucier (1969) noted the first appearance of gravel between a depth of 75 and 150 feet (22.9- 45.7 m) throughout the Lower Mississippi Valley, and it is only those substratum deposits that occur below a depth of 80 to 100 feet (24.4- 30.5 m) that indicate the Pleistocene braided deposits of the Mississippi River. Substratum deposits above this interval are considered meander belt deposits, though it should be noted that these would only be lower point bar units

as the upper accretionary units are recognized in their own category. In other words, though Saucier grouped the lower Holocene point bar units with the coarser Pleistocene sands and gravels, he did recognize that a division existed at a relatively accurate depth as shown by the cross sections.

Based on this original data from Saucier (1969) and recent developments regarding large-scale point bar systems, it is expected that the stratigraphic packages within the False River point bar would match those discussed within the introduction of this paper. These facies packages are the IHS (inclined/interbedded heterolithic strata), which Saucier depicts as the dipping point bar sediments within Figure 3.4, and the trough cross-bedded sands of the lower bar, which Saucier had previously grouped within the substratum units (Fustic et al., 2012; Musial et al., 2012; Saucier, 1969).

As recognized by Fisk in his 1947 paper, there are sharp boundaries between the channel belt sands and the floodplain clay rich sediments. There is also a well-developed crevasse splay developed on the southern side of the meander loop (Farrell, 1987). Migration of the False River point bar towards the southwest has resulted in a coarsening upwards within the overbank deposits and the development of surficial splay deposits (Fig. 3.4), which also show a coarsening upward pattern internally. These in turn fine upwards after each splay is abandoned (Sternberg, 1956). Although there are fewer abandoned channel fillings in this section of the river, which is characteristic of the young age of this portion of the Mississippi, thickness of the filling was recorded at 38 meters thick, compared to 27 meters in the north and 43 meters farther south (Fisk, 1947).

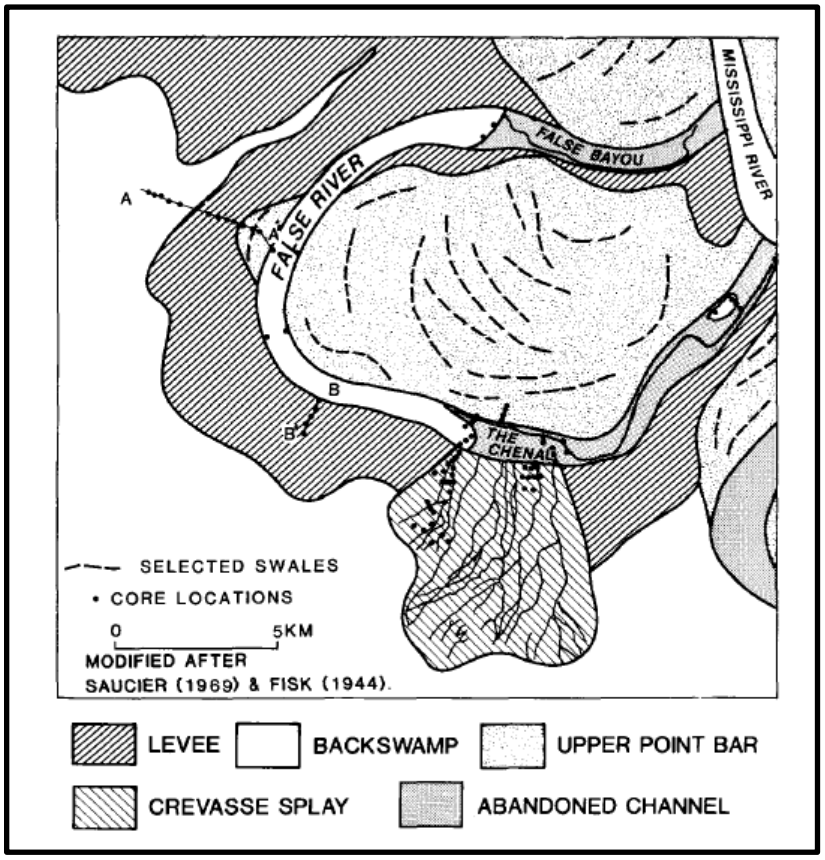

Figure 3.5. Overbank and sub-environments of False River. Notice the crevasse splay in the lower bend of the river channel. Figure taken directly from Farrell (1987).

Fisk (1947) defined the perfect meandering stream as "one in which bends develop to a uniform size and shape and maintain a constant rate of downstream migration". In order to achieve this, the elements which contribute to the meandering of the stream would have to be in perfect equilibrium, with the valley slope being constant and no resistance being offered by the materials of the river. The closest example of ideal meandering in the context of our study area would be south of Donaldsonville, Louisiana, in the deltaic plain. Deltaic plain deposits are considered to be relatively uniform, with meander migrations being relatively slow. This is not the case with meanders north of Donaldsonville (such as False River) in which no regularity between loops can be tracked, with the loops themselves being irregularly large compared with those to the south.

The irregularities seen in the Mississippi meander loops can be explained by the greater sediment heterogeneity in certain portions of the river where surface slope is low, with average being about 0.15 m/km. In areas where major tributaries join the main channel, a steeper slope can be expected, while in other areas, such as basins and the central and southern parts of the Mississippi Valley, slope is comparatively low (Fisk, 1947; Saucier, 1974). Resulting in heavy scouring, this heterogeneity causes a relatively deep channel cross section as compared to those observed in the north. When encountering hard points formed by fine materials, the river adjusts itself by deepening and modifying it's cross section in relation to the areas where erosion is hindered, sometimes eroding more vulnerable areas downstream. Thus, the abundant irregularities in grain size and bank materials affect not only which stretches of the river are eroded, but also the flow velocity and channel alignment. This continues to lead, and has led, to the unusual shape of meandering throughout the valley and to the asymmetrical bar of False River, because the system is constantly in flux (Fisk, 1947).

This prevalence of fines also leads to a higher occurrence of slumping, as opposed to sloughing, when defining bank caving (Fisk 1947). Recognizing the mechanism of bank caving is a useful tool regarding meandering systems, as it points to the level of cohesiveness of the sediments, and would further confirm that the unusual shape of the False River point bar is caused by the presence of fine-grained alluvial sediments.

In the case of False River, the irregularity of the original channel and size of the current point bar introduces complexities not yet fully understood. In a smaller, simpler system, such as the Brazo- Trinity Rivers, the velocity and position of the thalweg changes between bends as the helicoidal flow of the river changes it's sense of rotation, and results in the basic model outlined above (Bernard and Major, 1963; Connolly and Mazzullo, 1986). However, in more complicated

systems erosion can be influenced by factors such as the presence of floodplain silts and clays, non-uniform river flows, seasonal variability in terms of discharge, and reworking of the sediments by chutes. These factors introduce heterogeneity into the units, especially down stream where it is expected that the upper units contain Interbedded Heterolithic Strata (IHS) of sands, silts, and muds, within laterally accreting units. (Fustic et al., 2011).

4. METHODS

In this study I used a variety of methods in order to try and understand how the point bar system at False River was constructed, with particular reference to analyzing the reorientation surfaces that form the primary boundaries between different components of the point bar. The methods breakdown into those used for regional surveying and the targeting of critical areas and those that are designed to look at specific areas and aspects of the point bar system.

4.1 Study Area and Location Tools

The map used to direct and design this study is the Light Detection and Ranging (LIDAR) Digital Elevation Model (DEM) shown in Figure 4.1. LIDAR is an acquisition tool that, when collected, yields data corresponding to latitude, longitude, and height. This is done by aiming a laser scanner at the ground surface by use of an aircraft, which produces a point cloud of data in accordance with the difference in time for the pulsed light to return (Gestch et al., 2002). A three dimensional digital elevation map (DEM) is created using the values provided by the LIDAR. The data, which was public, was downloaded from the USGS at http://earthexplorer.usgs.gov/. The raw data were loaded into ER Mapper where the data was enhanced, colorized and shaded. When evaluating the accuracy of the vertical scale, it is more important to take into consideration how the elevation is being determined rather than considering the laser tool, which is in most cases the most accurate component (Renslow, 2012). The National Elevation Dataset (NED) was used and created by the USGS, and serves as a public database for mapping. Resolution is 1/9 arc-second (3m cell size) (Gestch et al., 2002). Because of the high accuracy inherent in LIDAR, the digital elevation map of False River was a useful tool in targeting field locations for the purpose of reaching reorientation surfaces at depth. The DEM image was sufficiently high resolution to be able to see the ridges and swales that

comprise the primary surface topography of the point, i.e., the scrollbars. It is offsets in this topography that helped me identify the surface manifestation of the reorientation surfaces which I believe to be consistently dipping towards the West and Southwest based on the location of the oxbow lake and the convex-west shape of the scrollbar topography, which record the direction of lateral migration of the dipping units (Labrecque et al., 2011) .

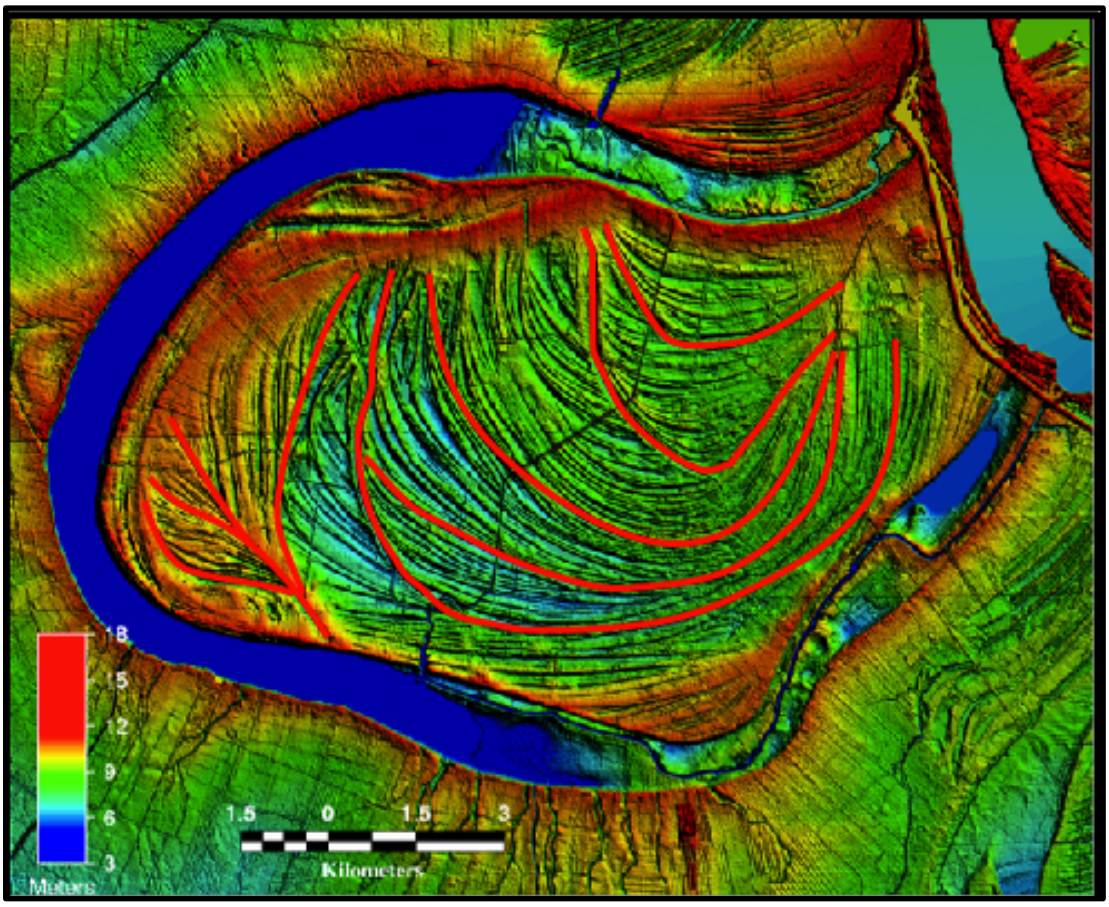

Figure 4.1 LIDAR DEM of False River with assumed reorientation surfaces drawn in red. Reorientation surfaces were chosen based on scroll bar truncation expressions on the surface of the bar.

Using basic trigonometry and an assumed accretionary angle of 6° as discussed in the Introduction Chapter, I chose coordinates 95 meters away from where the reorientation surfaces intersected the ground level as a means to capture the strata at a depth of 10 meters in a borehole or geophysical log. Because of potential disruption in the shallow subsurface, for example

because of agricultural activities, it was important to try and sample these critical boundaries at a depth where their natural state might be preserved.

Study locations (Fig. 4.2 and Table 4.1) along the False River point bar were chosen based on their proximity to reorientation surfaces expressed on the surface, with the intention of sampling or measuring the properties of these surfaces at depth. These locations were dispersed throughout the head, tail, and apex of the bar as a means to identify different facies associated with different stages of the bar formation, especially those of the reorientation surfaces. Existing models suggest that there should be substantial differences in grain size between the coarser, sandier units in the upstream, northern part of the system, whereas in the southern downstream part fine-grained facies would be expected (Fisk, 1947).

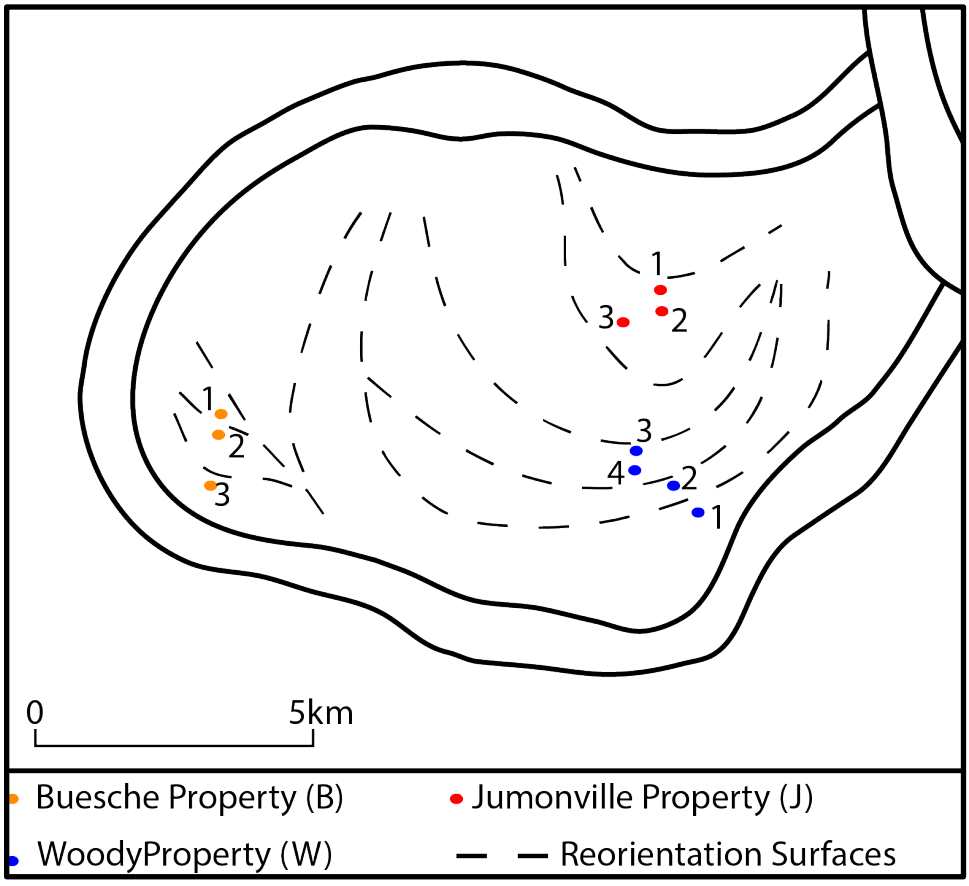

Figure 4.2. Sample locations at False River. The landowner initials (B, W, and J) correspond to the location numbers. These can be matched to Table 4.1.

Table 4.1. Field locations from Fig. 4.2 and tests conducted at False River on three properties: Woody (W), Bueche (B), and Jumonville (J). EC refers to sediment electrical conductivity and HPT is sediment hydraulic profile tooling.

Location	Coordinates	Data acquired by LSU	Data acquired by Protech
W1	30°37'29.10"N 91°23'3.02"W	-	Spot core, EC, HPT, gamma
W2	30°37'39.25"N 91°23'15.59"W	-	Spot core, gamma
W3	30°37'55.49"N 91°23'39.12"W	-	Spot core, EC, HPT, gamma
W4	30°37'46.80"N 91°23'34.86"W	EC 3	-
B1	30°37'56.34"N 91°27'49.98"W	-	Spot core, gamma
B2	30°37'49.80"N 91°27'51.54"W	EC 4	Spot core, EC, HPT, gamma
B3	30°37'42.71"N 91°27'57.24"W	EC 5	Spot core, EC, HPT, gamma
J1	30°39'31.12"N 91°23'22.29"W	-	Spot core, EC, HPT, gamma
J2	30°39'21.86"N 91°23'23.77"W	EC 1	Spot core, EC, HPT
J3	30°39'19.21"N 91°23'48.03"W	EC 2	Spot core, EC, HPT, gamma

In order to gain access to the land within the study area, I used an online tool, the Pointe Coupee Parish Assessor, which contained a digital map of the parish. Each property was defined, with landowner names and addresses given. Through use of this facility I was able to contact landowners on an individual basis to acquire access permission on three different properties. I then utilized my access of the properties to conduct research on multiple areas of each premises, as shown on Figure 4.2. Work was undertaken both using equipment owned and operated by Louisiana State University and also using a privately hired company, Professional Technical Support Services (Protech), based out of Baton Rouge who had similar or slightly more capable equipment, as well as professional crews who could gather more core or geophysical information quickly. Table 4.1 and Figure 4.2 show the distribution of tests conducted throughout the False

River point bar. Because I wanted to know about whether reorientation surfaces are associated with a change in lithology I chose to collect natural gamma and electrical conductivity logs that would be sensitive to grain size variations, as well as continuous and spot cores.

4.2 Geoprobe Machines

All intrusive data collection was completed using a shallow environmental geologic coring unit: either a Geoprobe 6610DT Direct Push machine (Fig. 4.3A), or a larger, more powerful Geoprobe 8040DT Advanced Direct Push machine (Fig. 4.3B). In each case, the machine functions by advancing the tooling into the subsurface by static (push) force, which is essentially a function of the weight of the vehicle. This is then combined with percussion (hammering) as the force needed to advance the tooling increases.

While each Geoprobe can have their own unique set of tooling, the mechanism for attaining depth was essentially the same for both machines, in that each functions by pushing sections of steel rods of specific lengths. As each successive rod that makes up the entire tool string reaches ground level, the head of the Geoprobe is lifted and another rod is attached into the one below it, lengthening the tool string and allowing deeper penetration. Rods for the Geoprobe 8040DT had a 2.25 inch outer diameter, while rods for the 6610DT had an outer diameter of 1.5 inches. The Geoprobe coring rigs were used both for extracting sediment samples from the subsurface and for deriving geophysical data from the same or adjacent intervals. Coring itself is a much slower process than collecting subsurface geophysics. Consequently, sampling of sediment itself was restricted compared to the larger number of geophysical logs that I was able to collect in a single area, and which provided a wider aerial coverage that could be ground-truthed at those location where both sets of data were collected.

Figure 4.3 A) Geoprobe 6610DT being operated by myself and two field assistants at Site J3 for sediment EC testing. B) Geoprobe 8040DT at Site J1, being operated by a Protech employee. Machine was used for borehole creation for gamma logging.

4.3 Geophysical Logs

Subsurface geophysical data acquisition was done through sediment electrical conductivity (sediment EC), hydraulic tooling profiling (HPT), and gamma logging paired with discrete coring and identification. Acquiring geophysical data was an important aspect of this project because of the incompleteness inherent in core capture. It is difficult to get a 100% recovery rate for sediments in core, especially in areas where the strata are extremely sandy, such as a point bar. The lack of cohesiveness causes the sediments to flow out of the bottom of the core barrel, even in areas where there are less permeable layers and a core catcher is used. By collecting geophysical data, I was able to acquire complete logs at every location without the loss of recovery seen in core.

Tool diameters vary between different Geoprobe models as a result of the variations in energy exerted by each machine, and which function the machine is performing. For the gamma logging, a PVC pipe was inserted inside the rods for use as a guide, requiring a larger diameter of 2.25 inches and thus a larger, more powerful machine. The depth reached was also greater (by 12 to 6 m) for gamma logging than for any of the other geophysical logs, because the Geoprobe 8040DT is capable of reaching greater depths than the smaller Geoprobe 6610DT, which uses smaller rods. The Geoprobe 6610DT is ideal for tooling/logging of sediment EC and HPT. Each has a probe of 2 inches in outside diameter, which attaches to the 1.5 inch rods with a 'percussion tolerant' adapter rod. These probes characteristically reach shallower depths than expected from a larger machine and require the use of a rig such as the Geoprobe 6610DT, because a larger machine would cause damage to the tool string and instrumentation.

4.3.1 Sediment Electrical Conductivity

Sediment electrical conductivity (sediment EC) (Figure 4.4) is a measurement of the ability of the grains (and pore fluid) to carry the flow of an electric current. As ions conduct electrical current more efficiently, sediments with a high ion conduct will have a higher EC value, such as clays (Revil and Glover, 1998). In contrast, coarse-grained sediments such as sand will have a much lower value. Because of this, sediment EC is a useful tool for detecting lithology (by means of fluid and matrix), especially in areas where multiple sites can be sampled, allowing for horizontal correlation (McCall, 1996). Most importantly, sediment EC is a cost effective means to study the lithology of a site without the need for an initial borehole, and with the added benefit of being in direct contact with the sediment. This ease of use also means that multiple logs can be run in one field day.

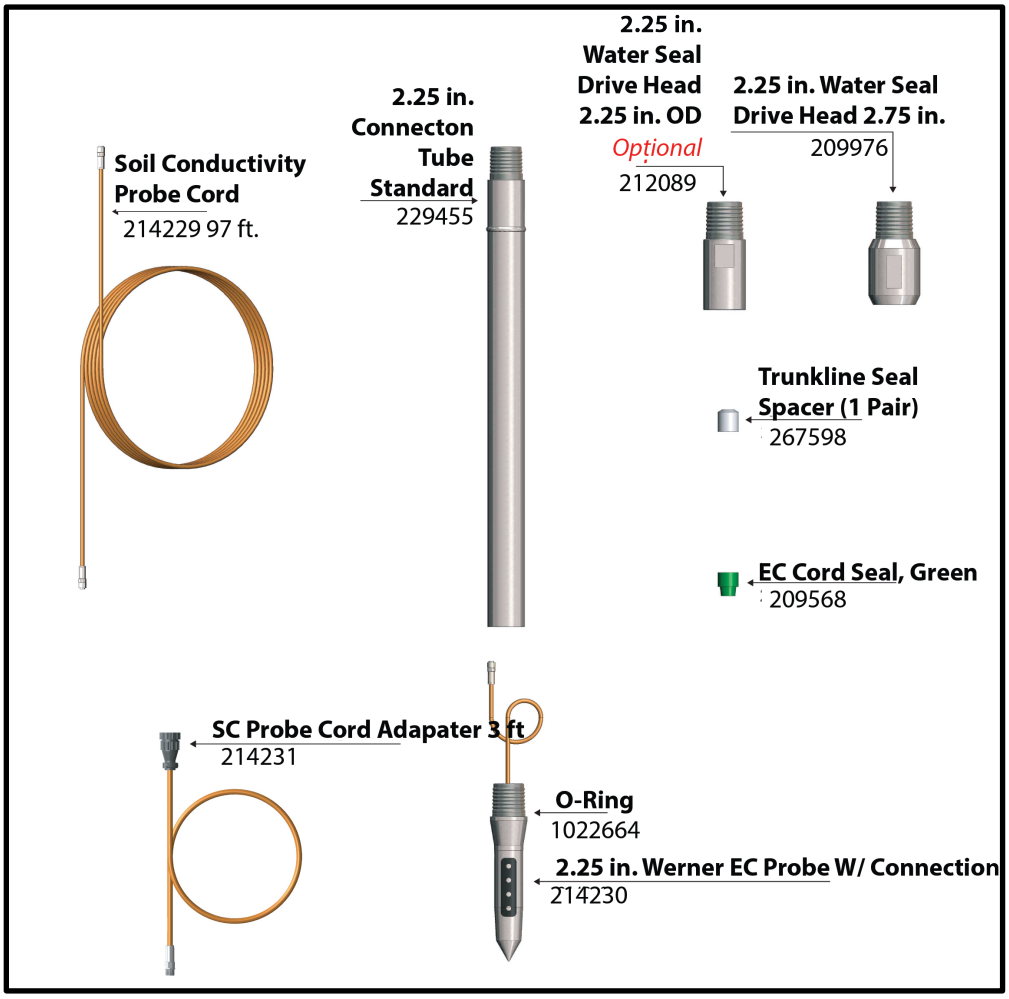

Figure 4.4 Direct Image® Electrical Conductivity (EC) System

The sediment EC measurement rig (Figure 4.5) consists of a probe (Fig. 4.6), a trunk line, string pot recorder for depth (Figure 4.7), and display equipment, paired with the basic Geoprobe rig equipment. The EC probe measures electrical conductivity through a Wenner dipole array (Figure 4.6), which is pushed through the formation. The probe relays the data in real time via the trunk line wire seen in Figure 4.4, which is connected to the tail of the probe and threaded through the rods, terminating in the port of the FI6000 Field Instrument (fig. 4.5). The data can then be viewed using DI Acquisition software from Geoprobe on a laptop during connected to the FI6000. All data are automatically recorded and saved in a folder created before probing commences, and can be viewed during both real time acquisition and a later time.

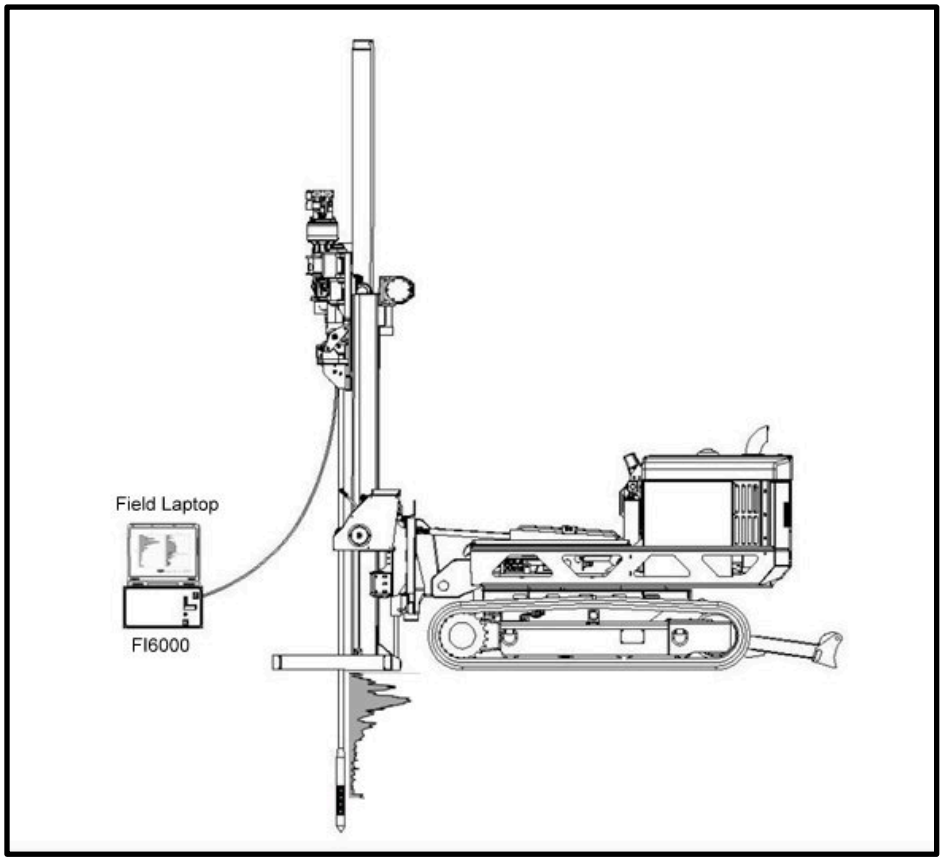

Figure 4.5 Schematic diagram of Geoprobe connected to the FI6000 field instrument via the trunk line.

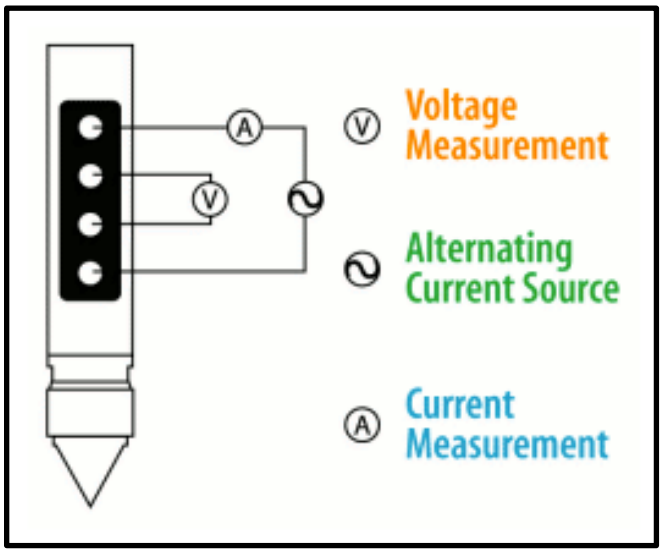

Figure 4.6. Direct Image® Electrical Conductivity (EC) probe diagram. Both the EC probe and HPT probe heads have the EC conductivity dipole array seen here.

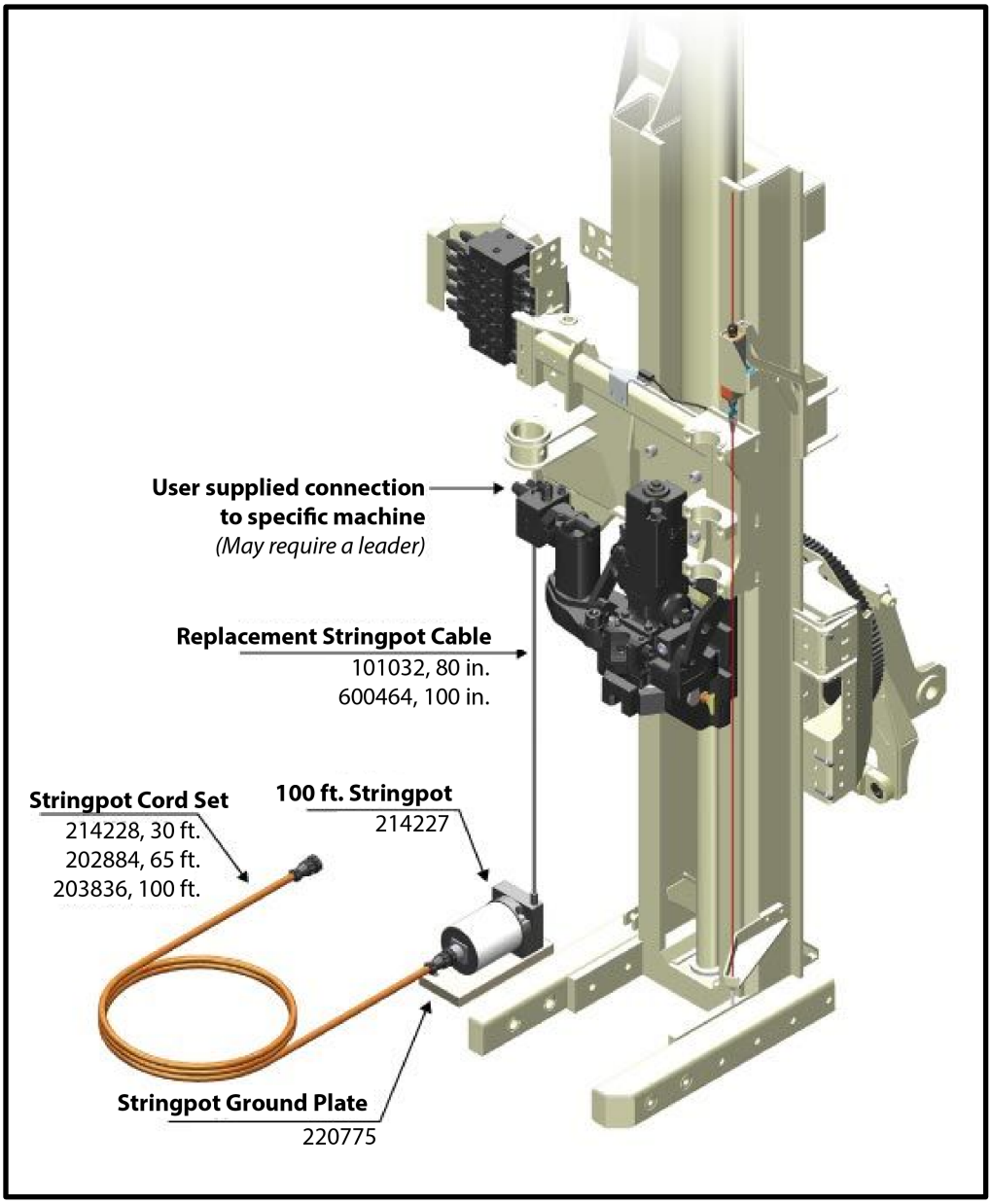

Figure 4.7. String pot connection diagram from Geoprobe Systems®

4.3.2 Sediment Hydraulic Profile Tooling

Hydraulic profiling tooling (HPT) (Figures 4.8 and 4.9) works in a similar manner to the sediment EC. One primary difference is the introduction of water into the borehole. In addition to a sediment EC dipole, the HPT probe also has a screen, which transmits water into the adjacent sediments and is connected to a downhole pressure transducer within the probe that

measures the pressure required to inject water into the sediments. In this way, HPT pressure can be recorded (at the centimeter scale) and related to the permeability and hydrostratigraphy of the formation. The advantage of this probe is that in addition to the HPT log, it also logs sediment EC simultaneously, as well as flow rate of the water being pushed through the screen and rate of push (ROP) of the probe.

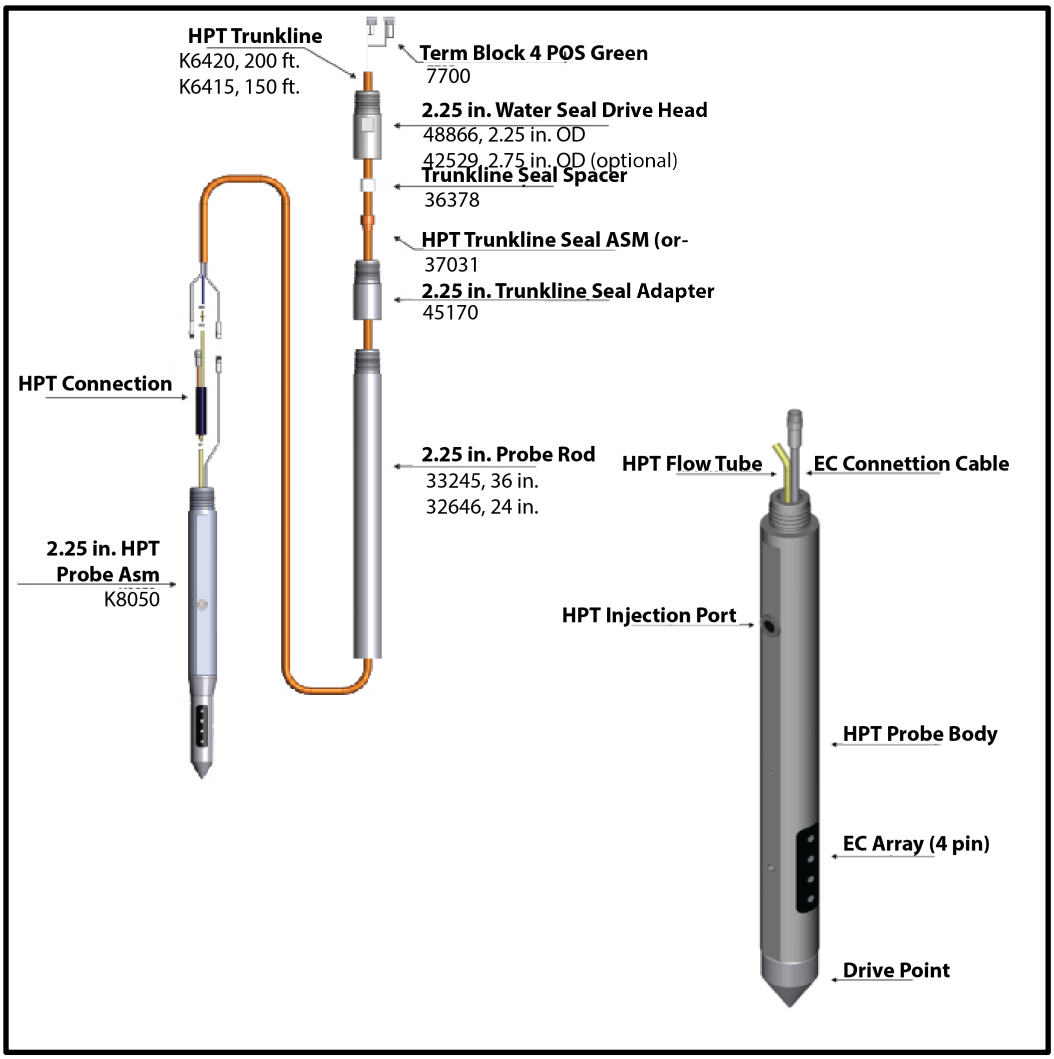

Figure 4.8. Direct Image® Hydraulic Profiling Tool (HPT) System from Geoprobe Systems®

In this way, direct comparisons can be made between the lithology shown by the sediment EC and the permeability recorded by the HPT, as coarser grained sediments would be expected to correlate to lower HPT value and finer-grained sediments with a high HPT value.

This makes sediment HPT an especially useful tool in strata where the permeability recorded by the sediment HPT does not predictably match that of the flow rate or the sediment EC. For example, one would expect for a low sediment EC to correspond to a coarse-grained sediment, such as sand. This should then be reflected in the sediment HPT log as a correspondingly low value (low injection pressure), relating to higher permeability, and thus a higher flow rate compared to that of a silty sediment. However, in an area where the flow rate is lower than expected, an anomaly exists that would need to be inspected in the core (McCall, 2011).

Though mud layers and early cementation would be expected as the cause for anomalies in a younger system such as False River, ancient systems may also be affected by diagenesis (Musial et al, 2011). This system of quality checks is why the combination of sediment EC, sediment HPT, and core analysis are so effective at revealing lithology in the sub-surface. Not only are the probing tools cost effective, but this further translates into the viability of spot coring, where intervals in some cases need to be chosen in the same day in real time.

Figure 4.9. Professional Technical Solutions Services company conducting soil HPT testing at Site J2.

4.3.3 Natural Gamma Logging

Gamma logging (Fig. 4.10) is an important tool and bridge-across to the sediment EC and HPT logs, and can often be deployed using Direct Push Technology (Geoprobe) to deeper depths than either the sediment EC or the sediment HPT. This is because the gamma tool is inserted within a tool string that is forcefully hammered into the formation prior to the gamma probe being introduced. Because the gamma probe is delicate and must be lowered at a constant rate via a downhole wire, a PVC pipe is inserted within the tool string rods once the rods have reached the depth required so no damage comes to the gamma probe. In contrast, sediment EC and HPT can be hammered directly into the ground without a prior borehole being created, but not to the same extent due to the probe being attached during hammering.

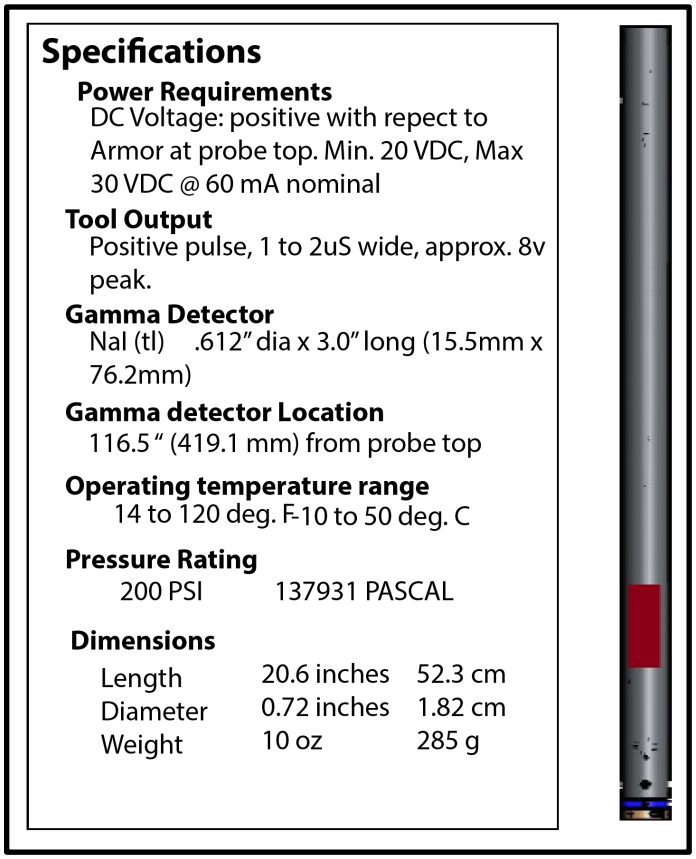

Figure 4.10. Tool specifications and probe drawing for the 2GA-1000 ultra slim natural gamma tool (Mount Sopris).

Additionally, gamma is a relatively quiet tool once the tool string has been put in place, allowing for multiple runs in the same borehole with minimal additional time or money investment (Fig. 4.11). Moreover, the measurements taken tend to provide unique information concerning the different lithologies that might be present in the borehole. For example, natural gamma ray tends to be high in fine-grained, clay- rich sediments because clays tend to be enriched in radioactive elements such as potassium, and therefore emit more natural gamma radiation (Howell et al. 2014). In the absence of complete core recovery, gamma ray logging can provide an approximation of the lithologies encountered at that depth.

Gamma logging was done through the use of a Geoprobe 8040DT paired with a Mount Sopris 2GA-1000 ultra slim gamma tool (Figure 4.10). An initial borehole was created using the 8040DT, which pushed the rods in place to a depth of 30.5 m. A PVC liner was inserted inside the rods, and both were left in place for the remainder of the gamma logging. Dampening of the gamma signal may have occurred due to measurements being taken within the PVC liner as well as the rods, but this was a relative effect since all measurements were taken using the same technique. The gamma tool, which provides natural gamma measurements via a Sodium Iodide crystal, measured at a rate of 1.5 meters per minute in the up-hole direction. Two logs were taken at each location for quality comparisons. The probe was lowered and raised by using an MX Series Winch, manufactured by Mt. Sopris (mountsopris.com). The winch allowed for speed to be regulated in both directions, and connected the information relayed by the probe head to the surface instrumentation, which in this case was a laptop displaying a graph of the data in real time.

Figure 4.11. Gamma downhole logging by Professional Technical Support Services using the Geoprobe 8810DT.

4.4 Coring

Fieldwork began on May 5th 2014, with continuous coring (FR-2) followed by another continuous core (FR-3) at a separate location,, seen in Fig. 4.12. Though FR-2 was obtained at the same coordinates as Site J1, different names were used to avoid confusion between the continuous core (FR-2), and the interval cores. A Geoprobe 8140LS Roto-Sonic Drill Rig was used to collect the two sections to a depth of 36.5 m, which was the expected depth to Pleistocene aged sediments (Saucier, 1969). Using the rotary capabilities of the rig, a sonic dual tube 45 sampling system was paired with the machine in order to simultaneously case the hole and sample the soil. The soil samples were collected in clear PVC liners in increments of 1.5 m,

with a diameter of 7.7 cm. Labeling and recovery analysis were done on site. Once both coring locations were completed, the cores were transported to the lab at LSU for further analysis.

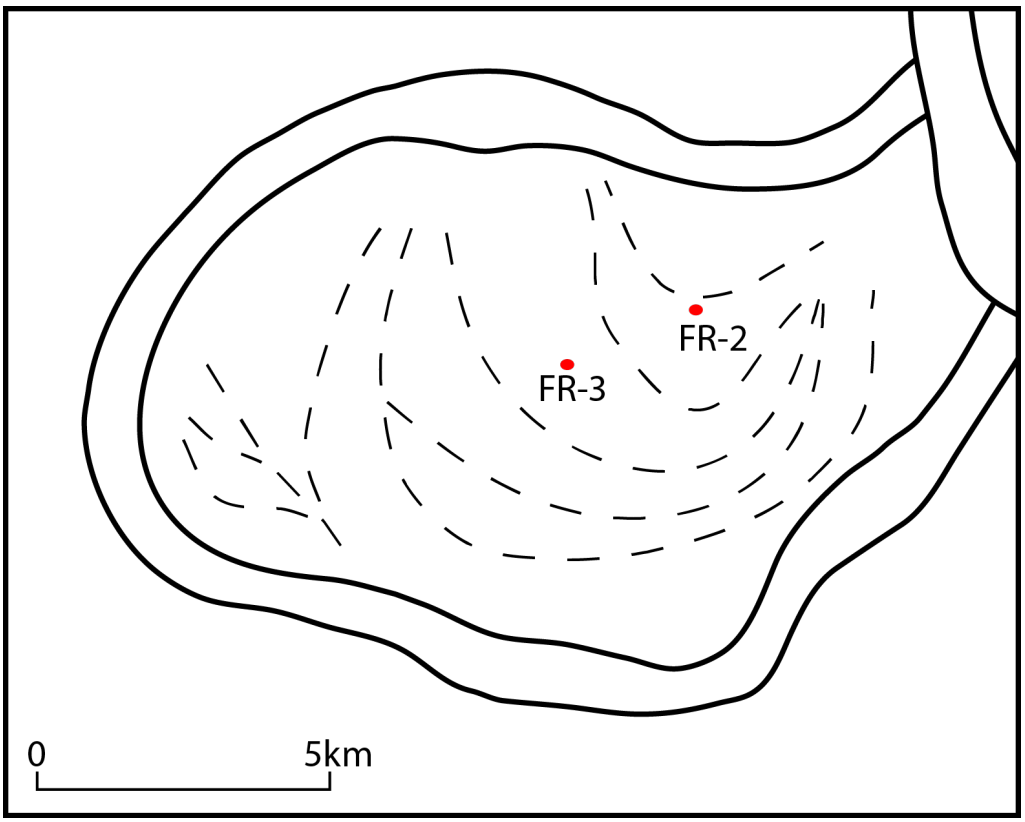

Figure 4.12. Field locations of continuous core samples. FR-2 was taken at the same location as the J1 cores. FR-3 was taken at a separate property, and was not sampled further.

Interval coring was done at the locations listed in Table 4.2. Intervals for coring were chosen on-site based on the real time data shown by the gamma logs, and represent areas of either higher heterogeneities or anomalies, or a section that would be easily correlated to the logs for gamma value identification. All interval cores were obtained using the Geoprobe 6610DT, and thus were a smaller diameter of 3.81 cm. With the exception of core W1, which was logged for correlation purposes, these cores will be split by the following researcher conducting the second half of this project.

Table 4.2. Intervals cored for each Site. The Sites not listed did not have coring perfomed.

Field Site	Core Intervals (m)
W1	0-22
W2	0-13.4
W3	0-22
W4	NA
B1	0-13.4, 19.5-22
B2	0-9.8, 13.4-19.5
B3	0-12.2
J1	0-36.6
J2	0-13.4
J3	0-13.4

4.5 Data Loading and Quality Checks

All geophysical data were first viewed in the Geoprobe Systems® Direct Image® Viewer 2.0 software. This software was a valuable tool as the data collected in the field could be directly loaded into the program without any reformatting. Within the program logs could also be displayed in different formats for quality analysis or further calculations.

For example, hydraulic conductivity (K), which measures how well a fluid moves through sediment (McCall, 2011) was found by inputting the static pressure values (stabilized formation pressures) collected in the field and creating an absolute hydrostatic pressure line over the HPT pressure log. This line was then used to create a corrected HPT pressure plot that accounts for the additional hydrostatic pressure with depth, after which the hydraulic pressure plot was run. The depth to the water table is reflected as the inflection point on the absolute hydrostatic pressure line where the pressure exceeds that of atmospheric pressure. An example of this process can be seen in figure 4.13. The EC, HPT Press. Avg, and HPT Flow Avg. graphs are automatically generated by the field data and displayed upon opening the file. After this, the Abs. Hydrostatic Pressure line can be generated, followed by the Corr. HPT Press graph and the Est. K. The units are also automatically chosen, as Direct Image® operates in a depth of ft. This

should be taken into account when comparing the units between the x axis and the y axis, as EC is in millisiemens/meter while the depth, HPT, flow, and K are in ft. The importance of these graphs will be explained in further detail within Chapter 6.5.

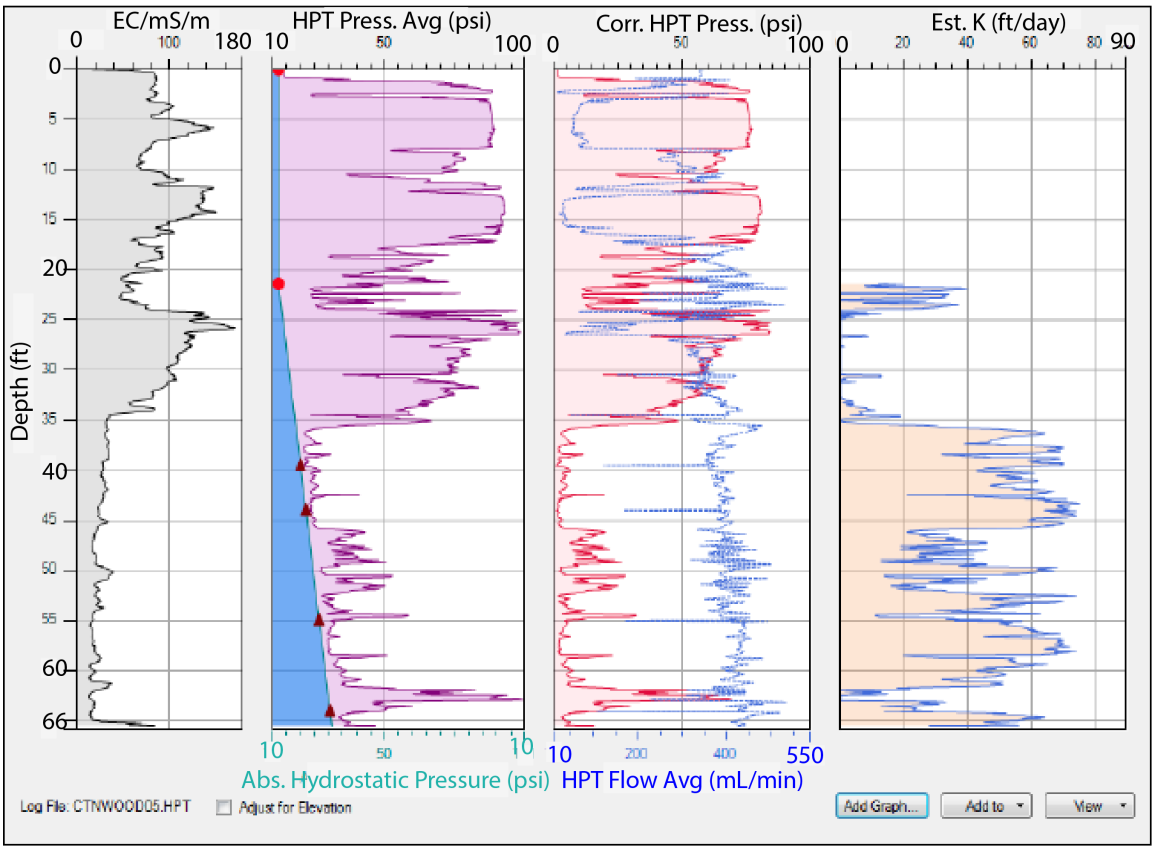

Figure 4.13. An example of a hydraulic conductivity plot (far right) created from values from the HPT and flow plots within the Direct Image® Viewer 2.0 software. Image courtesy of Geoprobe Systems®.

Further interpretations were done using the Petrel 2014.5 E&P software platform and the geoscience core, facies modeling, and well correlation modeling packages within the software. Because the EC and HPT data were originally recorded in the Geoprobe Systems® Direct Image® software, they had to first be loaded into the Direct Image® Viewer 2.0 software and then exported to a .dat format for loading into Petrel for analysis. The gamma logging software was Mt. Sopris Advanced Logic Technology (ALT). ALT produced the data in comma delineated .dat files, which I loaded into Petrel for comparison alongside the EC and HPT logs.

5. RESULTS

Within Petrel, the geophysical logs were scaled (same scaled based on logging type), adjusted to elevation using the elevation data provided by the DEM, and three well tops were created based on interpreted facies packages. Though the figures within this section contain the tops of these interpreted facies packages, why the interpretations were made will not be explained within this chapter, and can instead be found within the Discussion.

Regarding any anomalies seen within the logs, there are a number of possibilities as to why these might occur, and unless specified they should be treated as real and not technical errors, because equipment QC (quality check) was conducted in the field before, during, and after acquisition. Though EC is considered a reliable indicator of the lithology of the sediments, there are a number of factors that can affect the values given, especially in relation to clay. One example is a low EC value corresponding to a (much) higher value on the HPT, such as in Figure 5.1. In this example, EC is relatively low compared to the rest of the log, and decreases within the 40-50 ft section. Conversely, HPT increases up to 50 psi. This could demonstrate that the sediment is actually much more clay rich than originally thought, with the low EC values being caused by dissolution of ions within the sediment. This may be further verified by viewing the flow rate at the observed interval, which would be expected to decrease. The opposite is also possible within the logs, and variations between these extremes can exist as well (McCall, 2011). As discussed, dissolution is a large factor, and is especially applicable within our area due to the high level of the water table.

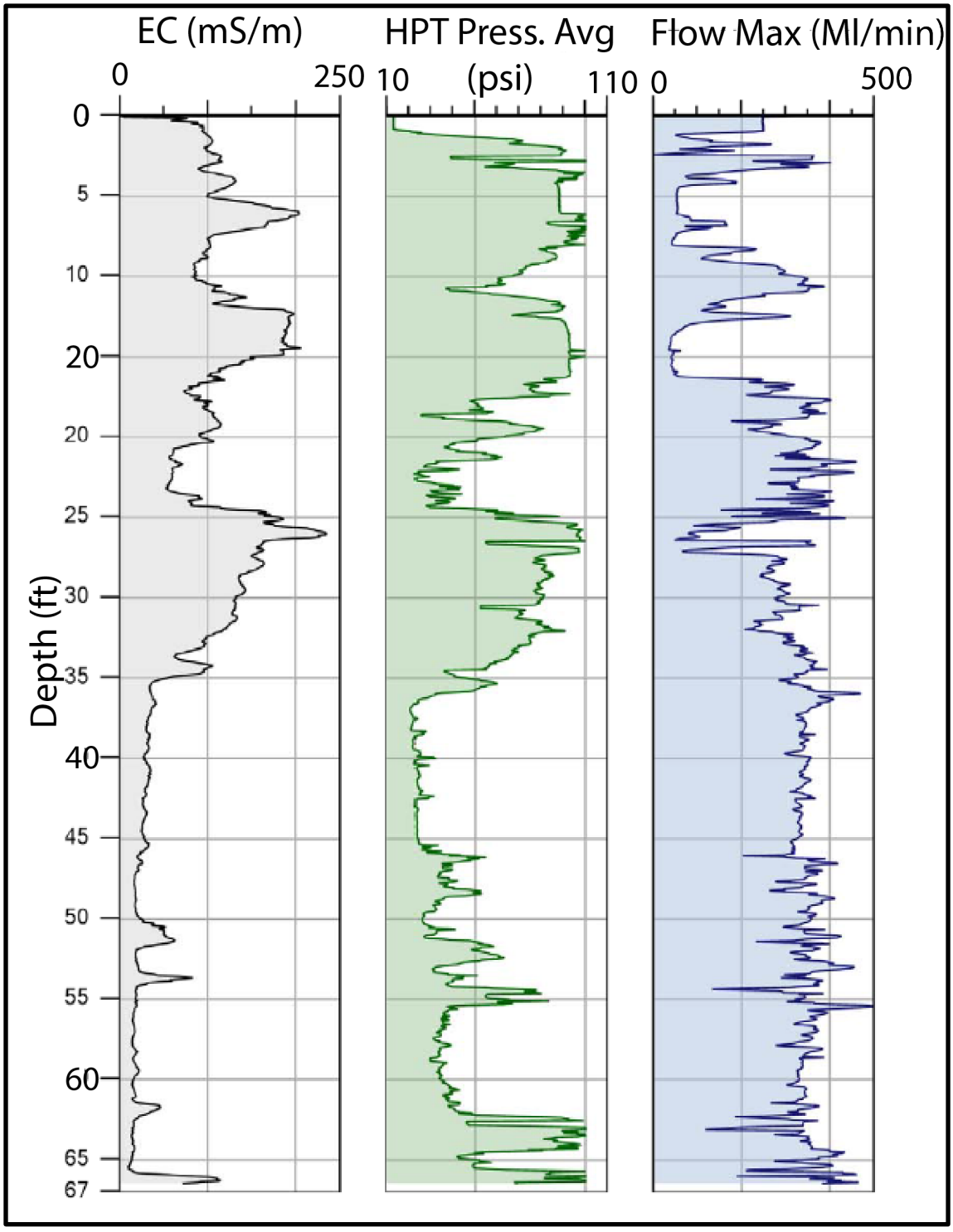

Figure 5.1. An example of compiled EC, HPT logs. Image modified from Geoprobe Systems® (McCall, 2011).

5.1 Jumonville Area (Early Upstream Apex)

The Jumonville geophysical logs (Figures 5.2-5.4) contain the least overall variability when compared to those of the other two properties. Gamma, electrical conductivity, hydraulic profile tooling, flow rate, and ROP were all logged within each Jumonville borehole. J1 shows varying degrees of change within the first 3.5 m, after which the lithology appears to fine with depth. An abrupt change in EC and gamma occurs at about 9 m in depth, after which the EC values remain between about 15 and 30 mS/m. J2 contains a lower package within the logs that a show a consistent gamma and EC from the base of the log up to 11 m. Above this, from 11 m to the surface, the values of the gamma, EC, and HPT become much more variable. In comparison, thought the J3 log does contain some variability within the top portion of the logs, the values (especially those of the EC) are lower than those within the J2 log. However, the same consistent trend of EC is also present in the lower portion of the J3 logs as seen in J1 and J2.

The most obvious anomaly within these locations is between 26 and 28 m at Site J1, where the flow rate drops significantly (Fig. 5.2). This should be ignored, as a technical difficulty occurred which caused the water to become blocked within the tool string. However, the anomaly at Site J3 (Fig. 5.4) at a depth of 23 m cannot be attributed to a technical error. The HPT jumps and the flow rate decreased as expected due to the decreased permeability, with a decrease in gamma as well. Unexpectedly, the EC doesn't appear to increase as significantly as the HPT until below this interval. Because the EC was logged simultaneously and with the same probe as the HPT, this anomaly cannot be attributed to depth errors.

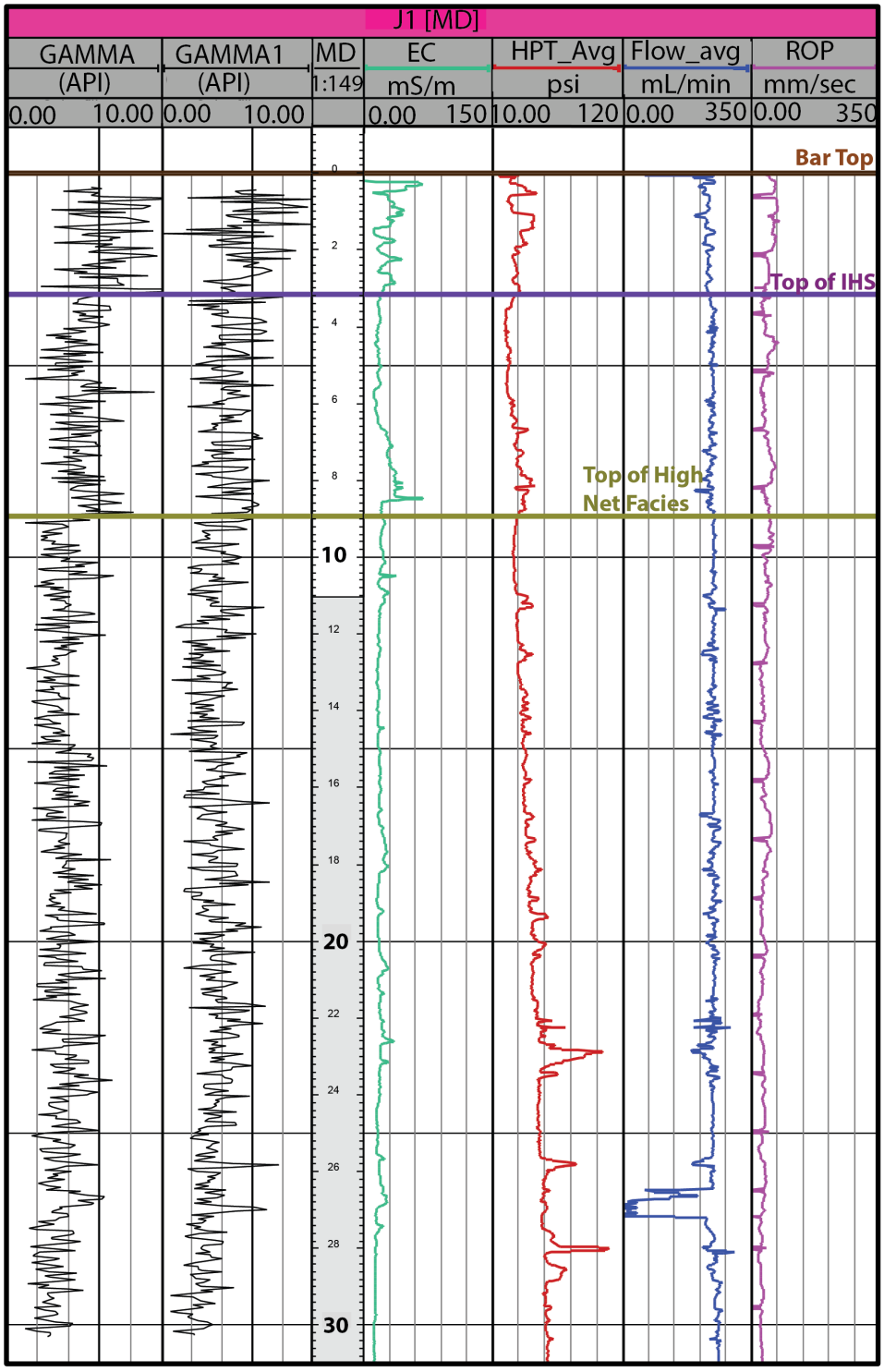

Figure 5.2. Compiled geophysical logs from Site J1. From the left, the logs are: gamma (2 runs), the measured depth (MD) in meters, EC (green), HPT (red), flow rate (blue), and ROP (purple). The well tops represent the top of each interpreted facies. The high-net facies package is another name for the trough-cross bedded sands facies. All facies package interpretations are explained within the Discussion chapter.

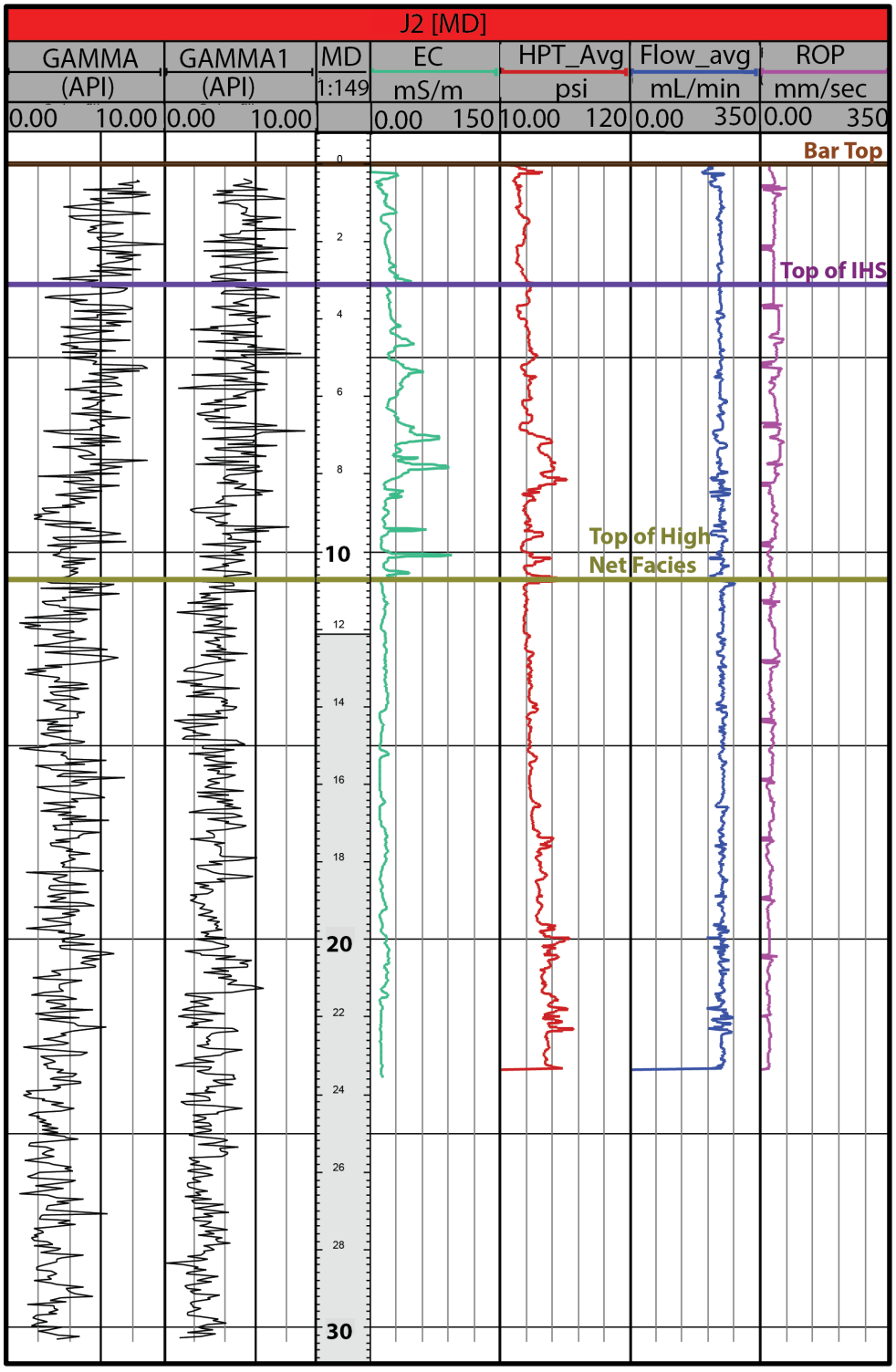

Figure 5.3. Compiled geophysical logs from Site J2. From the left, the logs are: gamma (2 runs), the measured depth (MD) in meters, EC (green), HPT (red), flow rate (blue), and ROP (purple). The well tops represent the top of each interpreted facies. The high-net facies package is another name for the trough-cross bedded sands facies. All facies package interpretations are explained within the Discussion chapter.

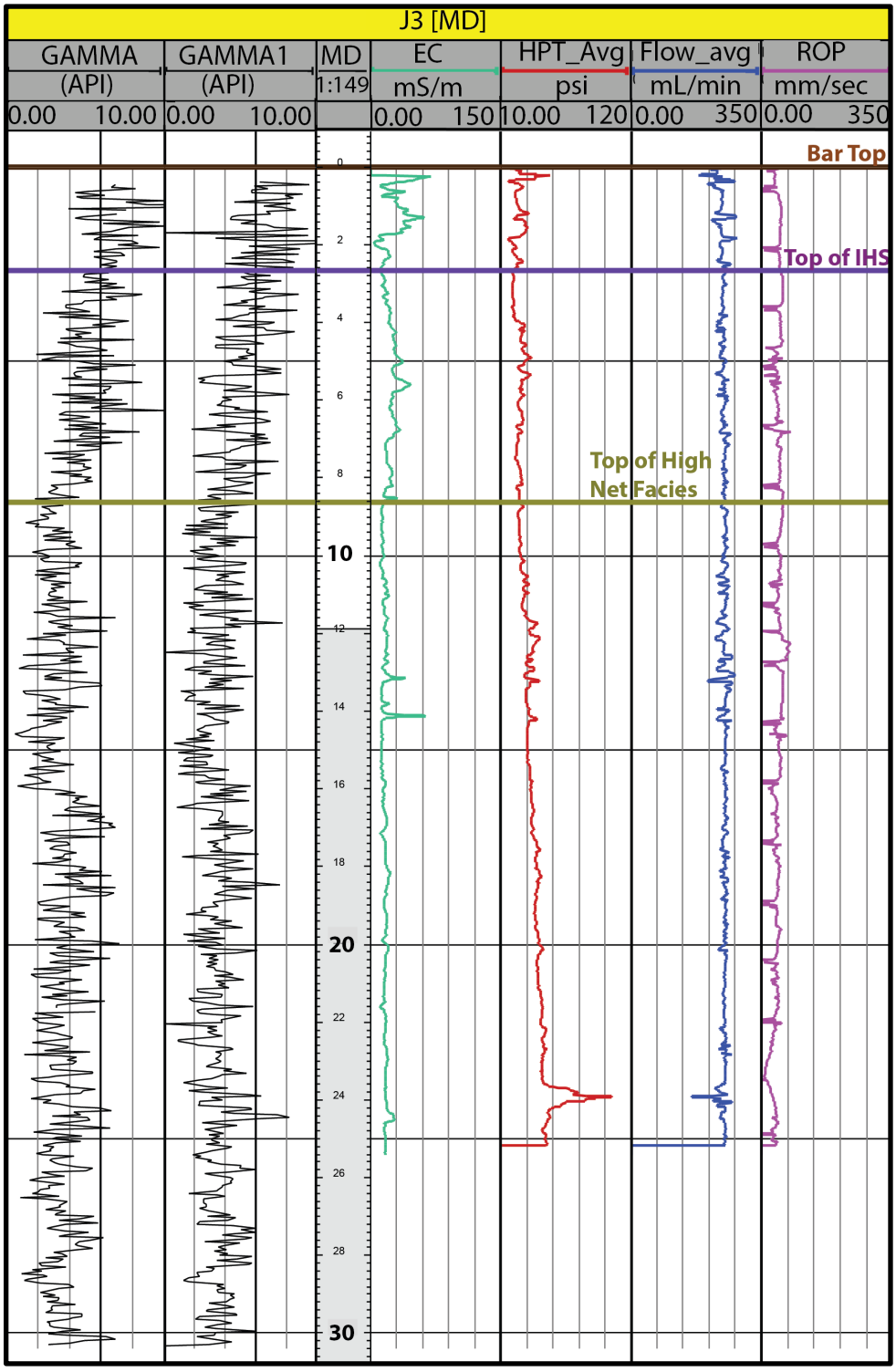

Figure 5.4. Compiled geophysical logs from Site J3. From the left, the logs are: gamma (2 runs), the measured depth (MD) in meters, EC (green), HPT (red), flow rate (blue), and ROP (purple). The well tops represent the top of each interpreted facies. The high-net facies package is another name for the trough-cross bedded sands facies. All facies package interpretations are explained within the Discussion chapter.

5.2 Bueche Area (Mid Outer Bar)

The Bueche geophysical logs (Figures 5.5-5.7) contain more variability in comparison to those of the Jumonville logs, and especially in comparison to each other.

Gamma, EC, HPT, flow, and ROP were logged within Site B3. Shown in Figure 5.7, B3 is clearly the most heterogeneic, and contains the highest EC values of any of the Bueche sites. Specifically, EC values were well above 30 mS/m in most of the log, with the exception of a lower value of about 10 mS/m from the surface to 2 m. An anomalous 'step like' pattern is also visible in the HPT log of B3, and is mostly likely due to increased pressure being exerted from the HPT probe. When comparing this HPT pattern to that of the rate of penetration (ROP), each decrease in HPT is consistent with each new rod addition to the tool string, and is caused by transmitted water from the probe exceeding the lithostatic pressure of the formation during the temporary cease in probing.

The B2 logs (gamma, EC, HPT, flow, and ROP) are visibly much different than those of B1 and B3. The electrical conductivity does exceed 30 mS/m in any portion of the log, and shows little variability. The gamma also shows a consistent trend throughout most of the log, with the exception of a strong change at about 5.5 m. Below this, EC remains mostly steady, but HPT experiences an increase between 6.5 and 10.5 m. However, though the EC doesn't increase as much as would be expected by the increased permeability trend present in the HPT, the gamma values are reflective of a coarser section fining downwards (as indicated by a trend from lower to higher values) from the surface to 10.5 m, below which the section becomes more heterogeneous. Interestingly, if I use an angle between 6 and 10 degree for a reorientation surface, this is the depth interval at which I would predict the reorientation surface to lie. Notably in this interval, there are two small increases in EC at 14.7 and 15.9 m, though only the increase

at 15.9 m appears to be anomalous, because the flow increases instead of decreases. There is also an anomaly at a depth of 20 m with a very strong increase in HPT and a decrease in flow below 20 m. The gamma and EC responses do not match at this depth. The gamma suggests small variations in grain size, but nothing great enough to predict such a large pressure increase. The EC in contrast appears to actually decrease from 20-21.5 m.

Site B1 (Fig. 5.5) could be considered intermediate between Sites B2 and B3 in relations to the variability within the log. Strong peaks in the electrical conductivity occur at 0.8, 2.3, 14.7, 18.3, and 19.8-20.2 m in depth. There is also an abrupt increase in EC at about 4.46 m, followed by both an overall increase in value we well as more variability within the logs. Only gamma and electrical conductivity were logged for this location.

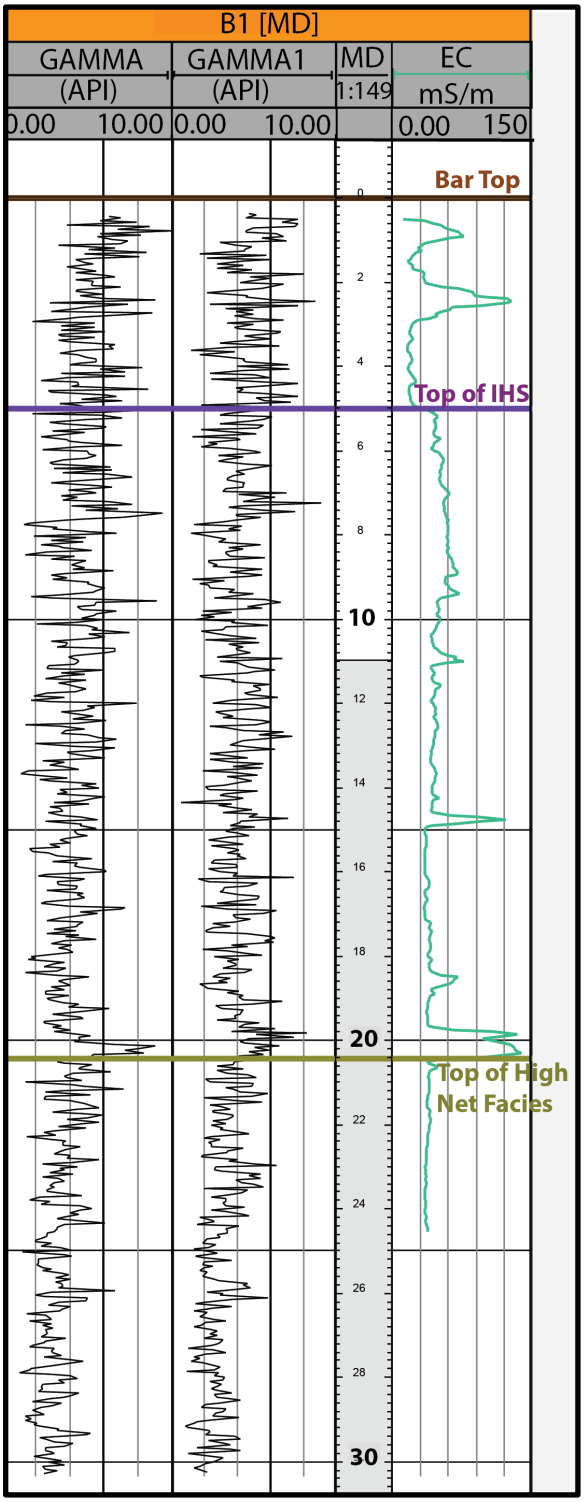

Figure 5.5. Compiled geophysical logs from Site B1. From the left, the logs are: gamma (2 runs), measured depth (MD) in meters, EC (green), HPT (red), flow rate (blue), and ROP (purple). The well tops represent the top of each interpreted facies. The high-net facies package is another name for the trough-cross bedded sands facies. All facies package interpretations are explained within the Discussion chapter.

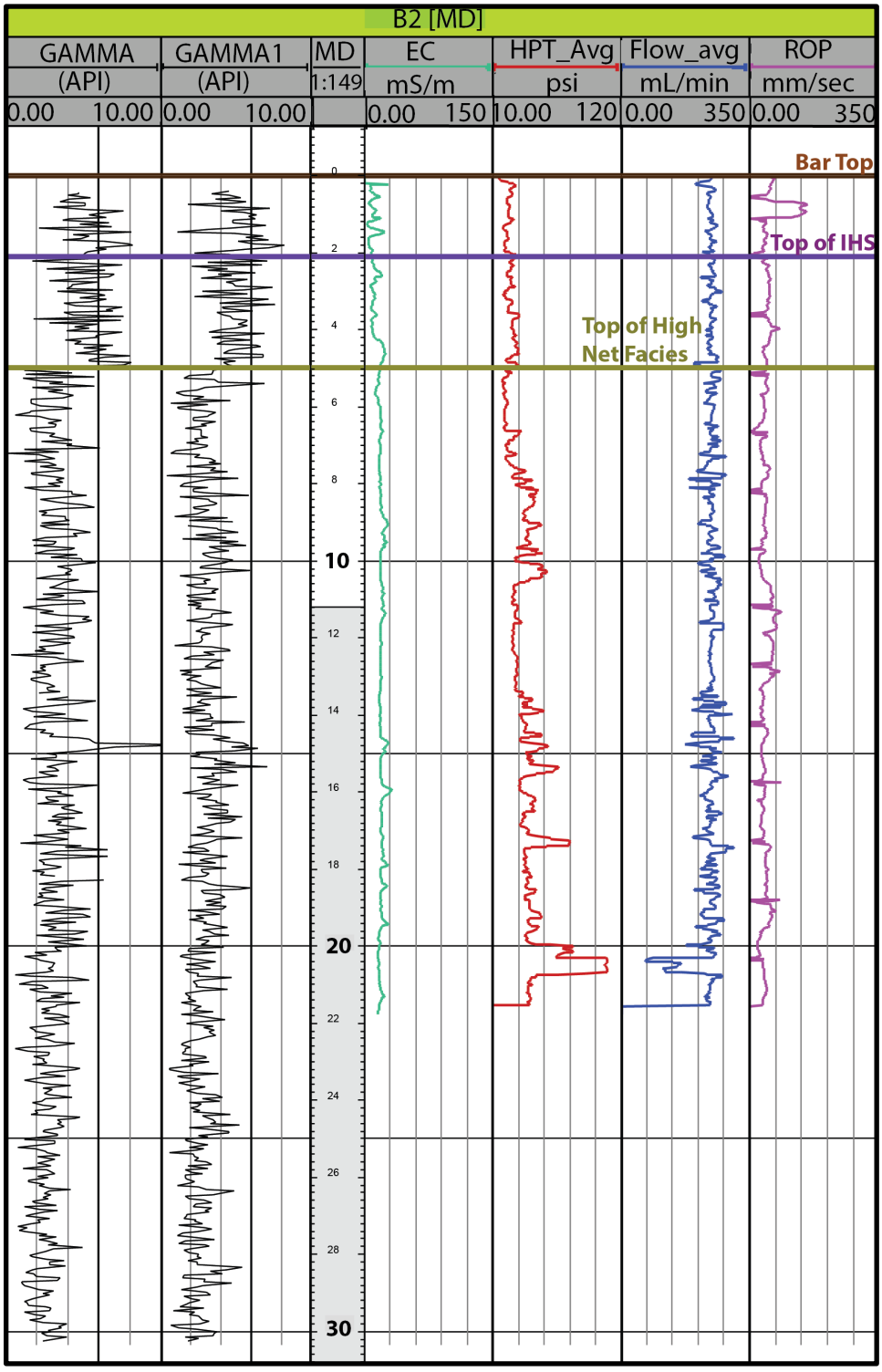

Figure 5.6. Compiled geophysical logs from site B2. From the left, the logs are: gamma (2 runs), measured depth (MD) in meters, EC (green), HPT (red), flow rate (blue), and ROP (purple). The well tops represent the top of each interpreted facies. The high-net facies package is another name for the trough-cross bedded sands facies. All facies package interpretations are explained within the Discussion chapter.

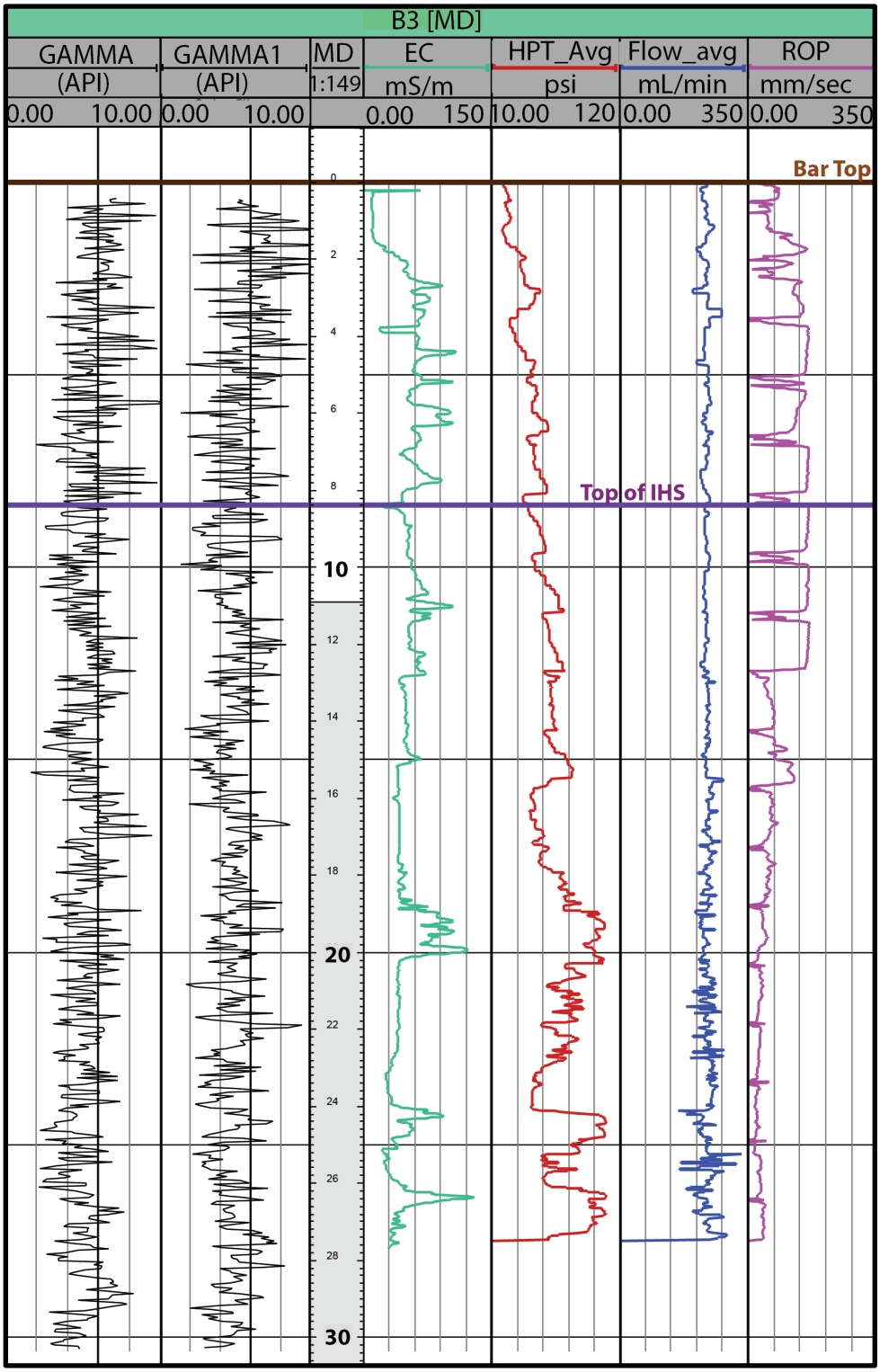

Figure 5.7. Compiled geophysical logs from site B2. From the left, the logs are: gamma (2 runs), measured depth (MD) in meters, EC (green), HPT (red), flow rate (blue), and ROP (purple). The well tops represent the top of each interpreted facies. The high-net facies package is another name for the trough-cross bedded sands facies. All facies package interpretations are explained within the Discussion chapter.

5.3 Woody Area (Bar Tail)

The Woody geophysical logs (Figures 5.8-5.11) are the most bar-tail area sampled. Though geophysical data was obtained at each location within this Site, each location does not always contain all of the geophysical logs listed in the Methods section. Gamma, EC, HPT, flow, and ROP were all logged at W1, with 3 gamma logs at this location as opposed to 2 at all of the other locations. Though W2 does contain 3 gamma track as well, the third track was not logged as deeply. W3 also has an absence of any HPT, EC, flow, or ROP data. W3 has logs for gamma, EC, HPT, flow, and ROP. W4 only contains electrical conductivity data.

The most apparent feature at Site W1 (Fig. 5.8) is visible in the logs at about 19.8 m. Not only is there is a strong change in the overall values, but the observed variability above this point decreases significantly below this depth.

Because the W2 logs only contain gamma data, which is inherently noisy due to the nature of the tool, specific changes are less easily identified. However, there is a general decreases in values with depth. At about 1.9 m there is also a change from high gamma (an average of 9 API) to lower gamma values (about 7.5 API).

W3 exhibits a decreasing trend within the gamma and EC logs with depth, although there are some smaller intervals within this trend that stand out. From the surface to about 1.8 m the electrical conductivity spikes up to about 60 mS/m, after which it drops again to about 15 mS/m. Below this the values spike intermittently through about 12.2 m. Below 12.2 m the logs show less variability than above, with one spike in EC at about 18.4 m.

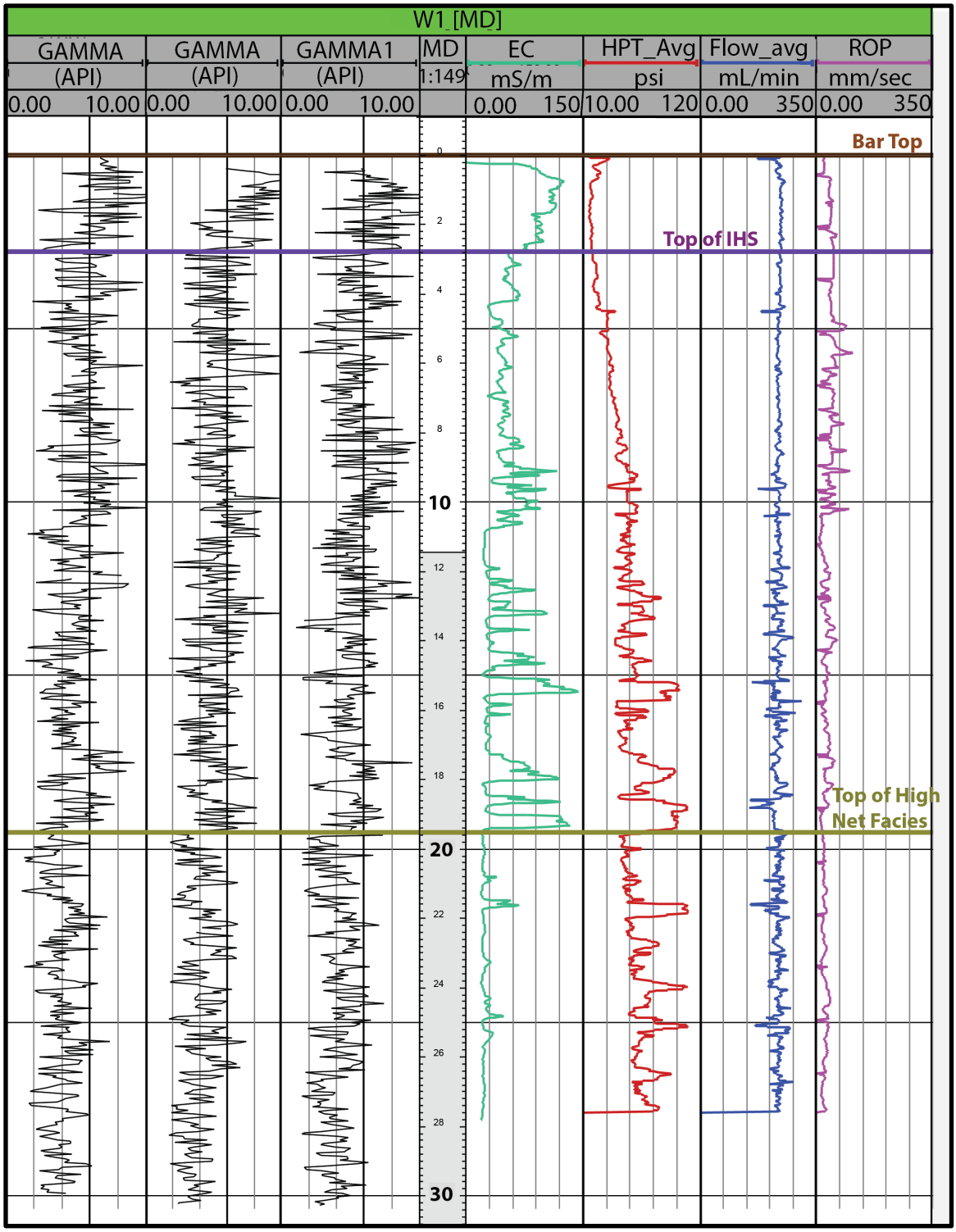

Figure 5.8. Compiled geophysical logs from site W1. From the left, the logs are: gamma (2 runs), measured depth (MD) in meters, EC (green), HPT (red), flow rate (blue), and ROP (purple). The well tops represent the top of each interpreted facies. The high-net facies package is another name for the trough-cross bedded sands facies. All facies package interpretations are explained within the Discussion chapter.

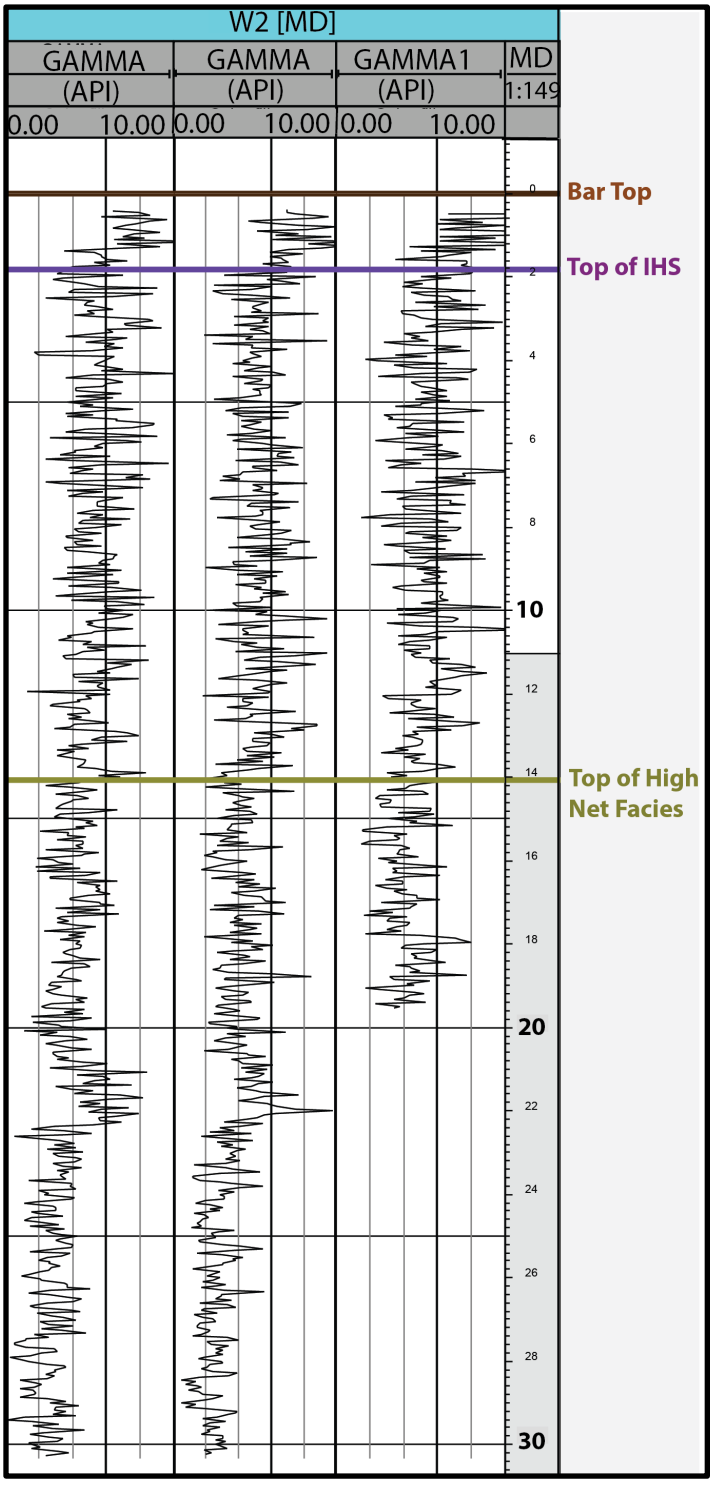

Figure 5.9. Compiled geophysical logs from site W2. From the left, the logs are: gamma (2 runs), measured depth (MD) in meters, EC (green), HPT (red), flow rate (blue), and ROP (purple). The well tops represent the top of each interpreted facies. The high-net facies package is another name for the trough-cross bedded sands facies. All facies package interpretations are explained within the Discussion chapter.

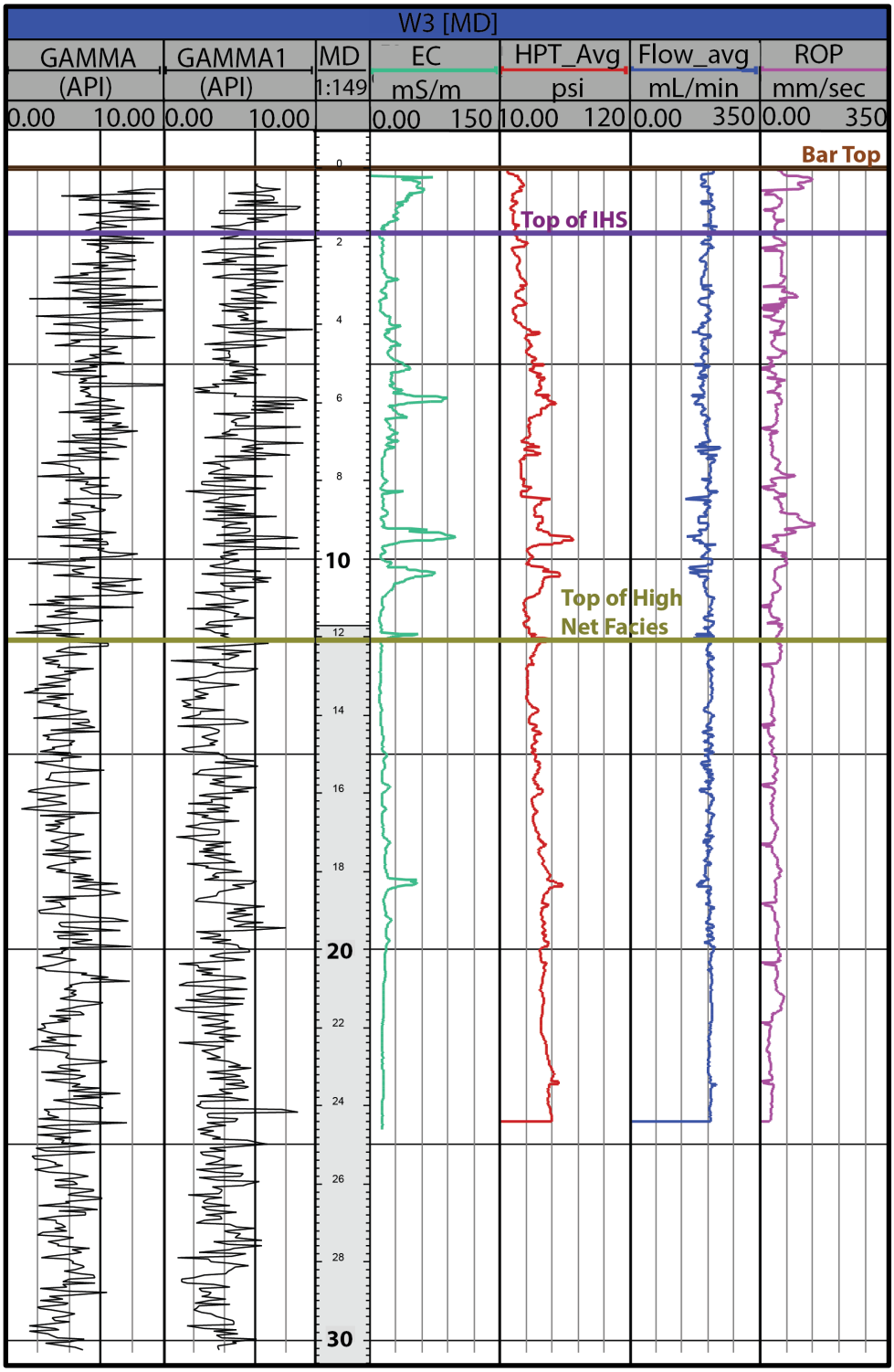

Figure 5.10. Compiled geophysical logs from site W3. From the left, the logs are: gamma (2 runs), measured depth (MD) in meters, EC (green), HPT (red), flow rate (blue), and ROP (purple). The well tops represent the top of each interpreted facies. The high-net facies package is another name for the trough-cross bedded sands facies. All facies package interpretations are explained within the Discussion chapter.

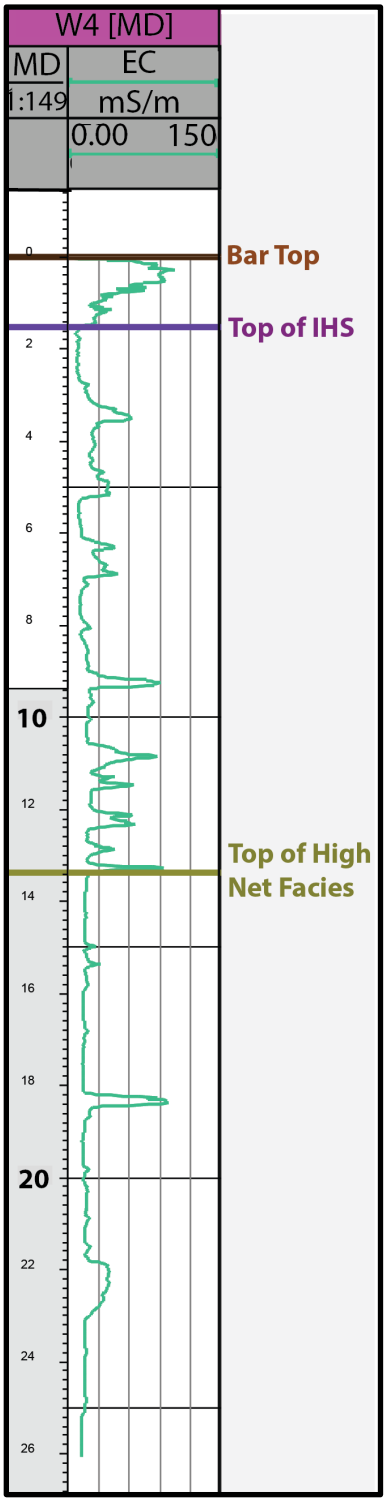

Figure 5.11. Geophysical EC log from site W4.The well tops represent the top of each interpreted facies. The high-net facies package is another name for the trough-cross bedded sands facies. All facies package interpretations are explained within the Discussion chapter.

Figure 5.12. Photograph of Core W1, section 3, 39-62 cm. The boundary at 54 centimeters is the division between the Bar Top deposits and the lower IHS units.

5.4 Modeling

A 3D subsurface model (Fig. 5.13) (Appendix A) was created in Petrel by first defining lateral and vertical boundaries. The DEM served as the lateral boundary (x,y) and top layer for the model because it contains elevation data across its entire surface, allowing for an accurate surface topography. The base of the model was chosen at a depth of 35 m and was contained within the same x,y space as the DEM. This depth was chosen from cores FR-2 and FR-3. Both cores contained a gravel base at an average of 35 m, which is expected to be the base of the point bar and the boundary between the bar and the Pleistocene sediments below (Saucier, 1969). As discussed in the introduction, bar thickness is expected to increase with increasing sinuosity and thalweg scour depth, but due to a lack of widespread depth data, this thickness variation was excluded from the model.

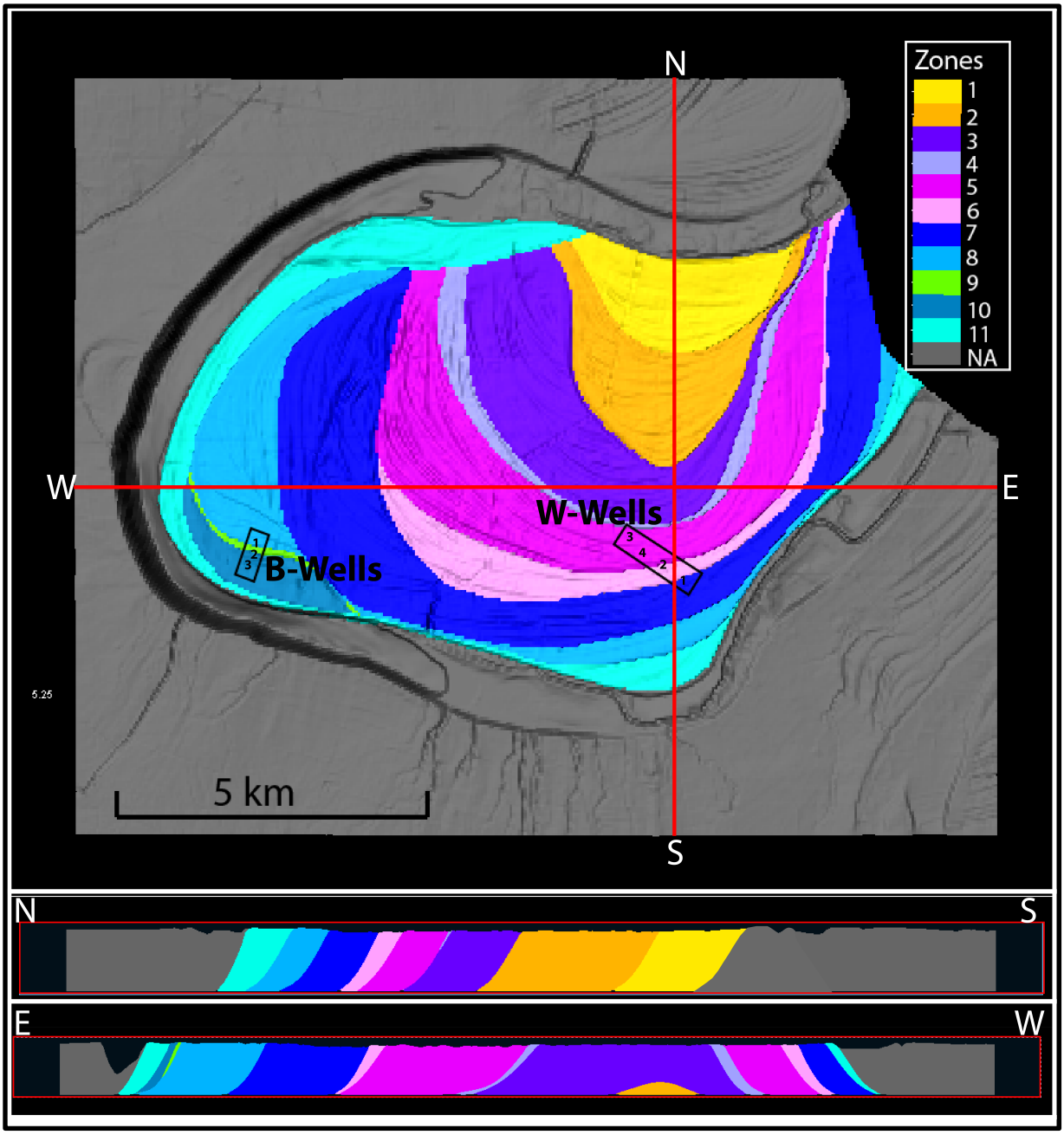

Figure 5.12. Petrel model containing zones bounded by reorientation surfaces. Zones represent new phases of construction in the growth history of the bar. The grey zone is the channel and surrounding backswamp deposits. The black squares around the well are the boundaries of the sector model. The cross section locations are indicated by the red lines along the model. Vertical exaggeration is 20.

An abandonment slope profile was used to approximate the dip of the surfaces in the model (Fig. 5.14). Because of changes in grain size throughout the bar, this approximation of dip

was more appropriate than estimating an average dip for the entire bar, especially when considering that no dip data from seismic imaging was available. Using this dip, 3D reorientation surfaces were created that started at the surface of the DEM and terminated at the 35 m base (Fig. 5.14). These surfaces were chosen based on the surface expression of the reorientation surfaces as apparent on the DEM and were bounded by its border (Fig. 5.14A). Figure 5.14B also shows an example of one of the dipping surfaces before it was input into the larger 3D grid. The model, which was essentially a grid model, was made up of individual cells that were 50 m by 50 m laterally, and had a thickness of 5 m.

Smaller sector models within the larger 3D framework were created at the Bueche and Woody areas (Figures 5.15 and 5.16). Each sector model contains the zones bounded by the reorientation surface boundaries and the boreholes for that property. A facies property (Appendix A) was also created within the sector models on a purely qualitative basis to demonstrate the general trends seen within the logs (Appendix B). The sand facies was created using the sand trend property within Petrel, and the percentage of fines (labeled silt) within the sand was input from estimations based on the logs. The facies were then oriented to dip parallel to the reorientation surfaces, though the dip within any lower sand facies should be ignored as it would not be visible due to the cross bedded nature of the lower high-net package. Cell size was much smaller for the sector models as the ability of having well control within these smaller models allowed for a finer scale model. As such, cell size was 5x5 m, and with a vertical thickness of 0.2 m. Lengths and widths of the sector models were large enough to include all of the logs within that area, but small enough to allow justification of the facies as interpolated from the logs to the boundaries of the sector. Data from these areas were not interpolated throughout the rest of the model due to the large scale of the bar and the lack of data between the sector model locations.

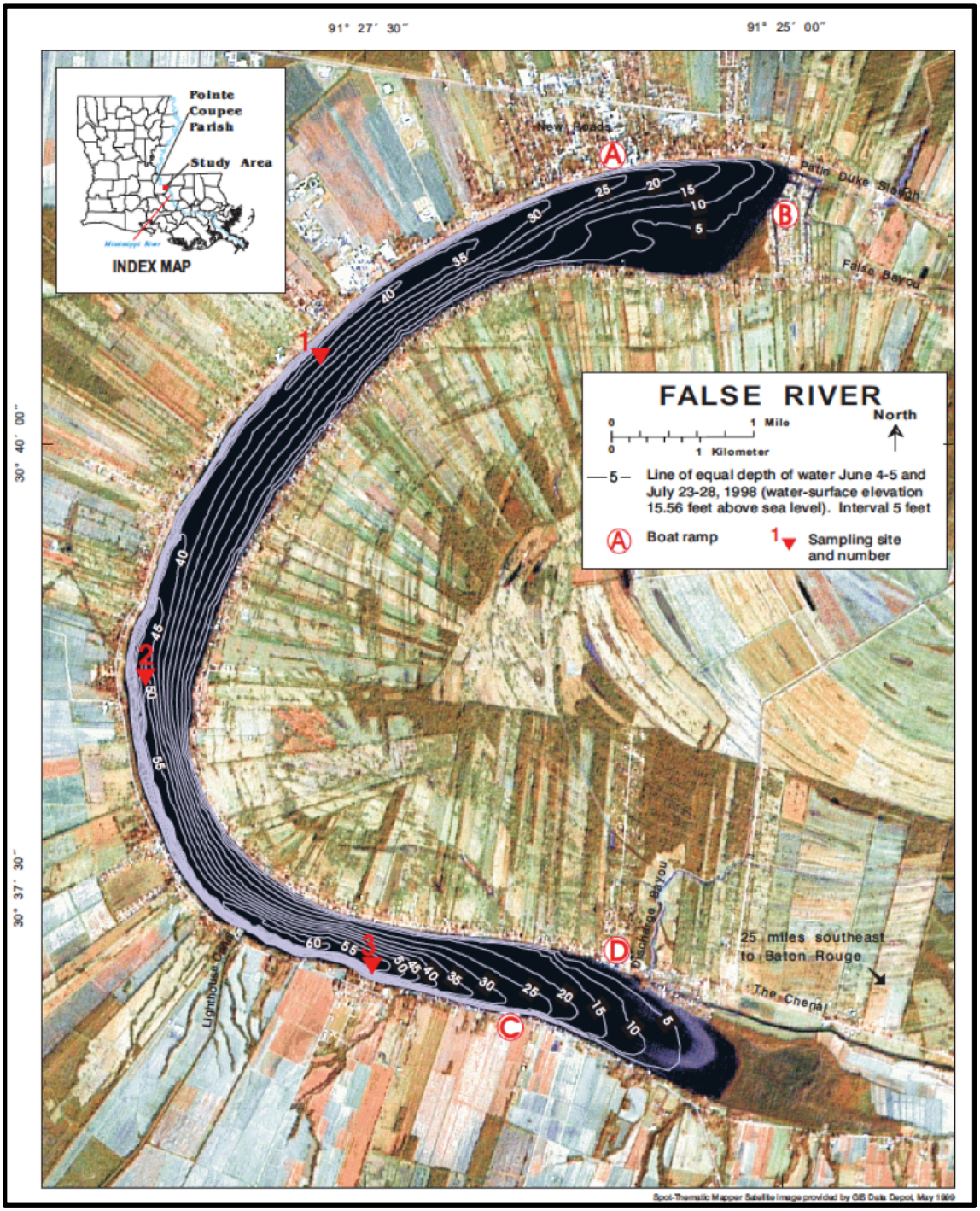

Figure 5.13. Bathymetry of False River, June 4-5 and July 23-28, 1998. Values depicted were used to approximate the dip of the surfaces used in the 3D subsurface model of False River (Ensminger, 1998).

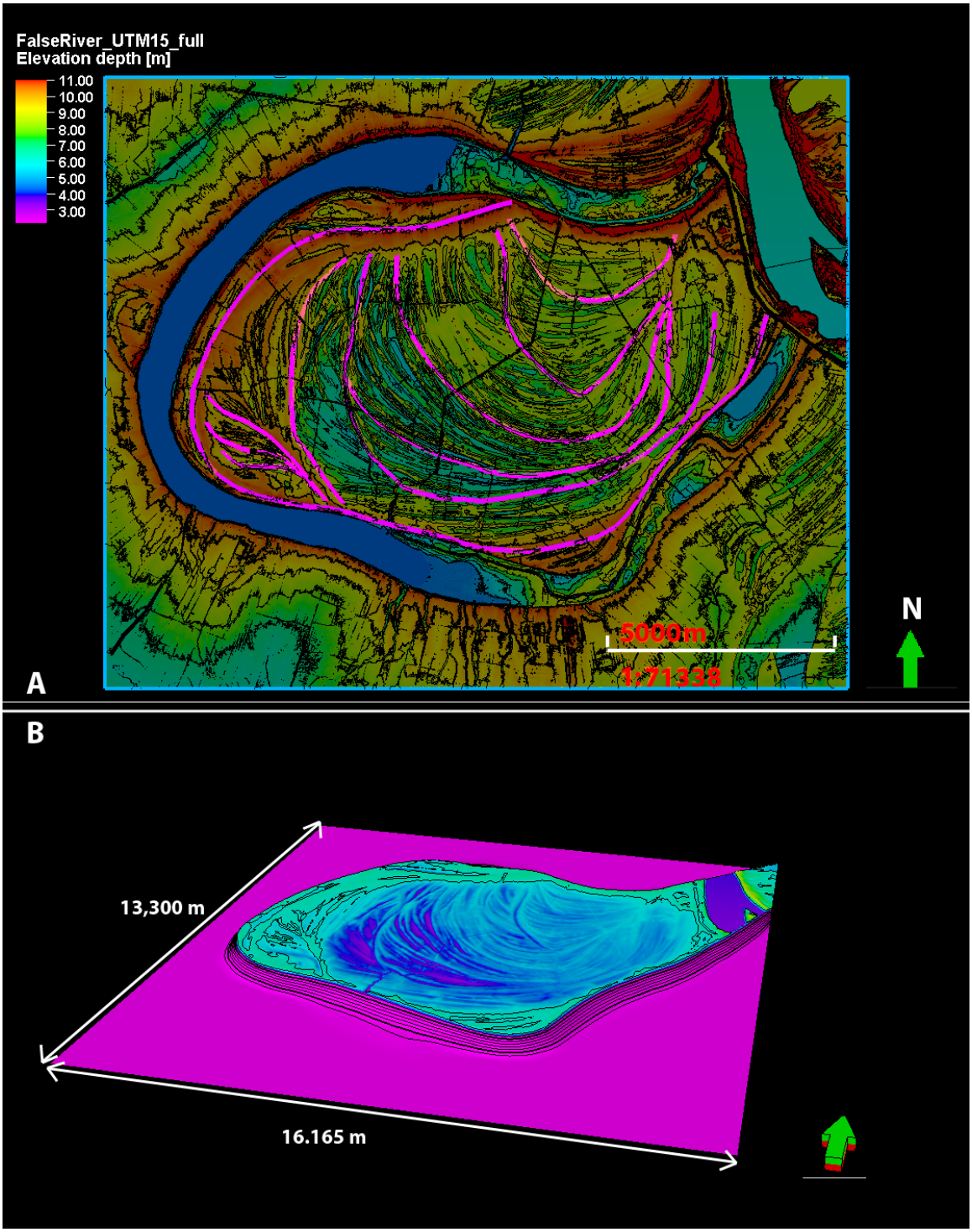

Figure 5.14. A) DEM of False River loaded into Petrel and used as the top layer of the 3D model. Reorientation surfaces were drawn according to their expression in the DEM. The DEM is at 50% opacity and the reorientation surfaces were colored pink for visualization (color does not match scale bar). B) An example of one of the reorientation surfaces in a 3D window with a vertical exaggeration of 10. The pink surface represents the base at -35 m RSL, and is the same size as the DEM. Vertical exaggeration is 10.

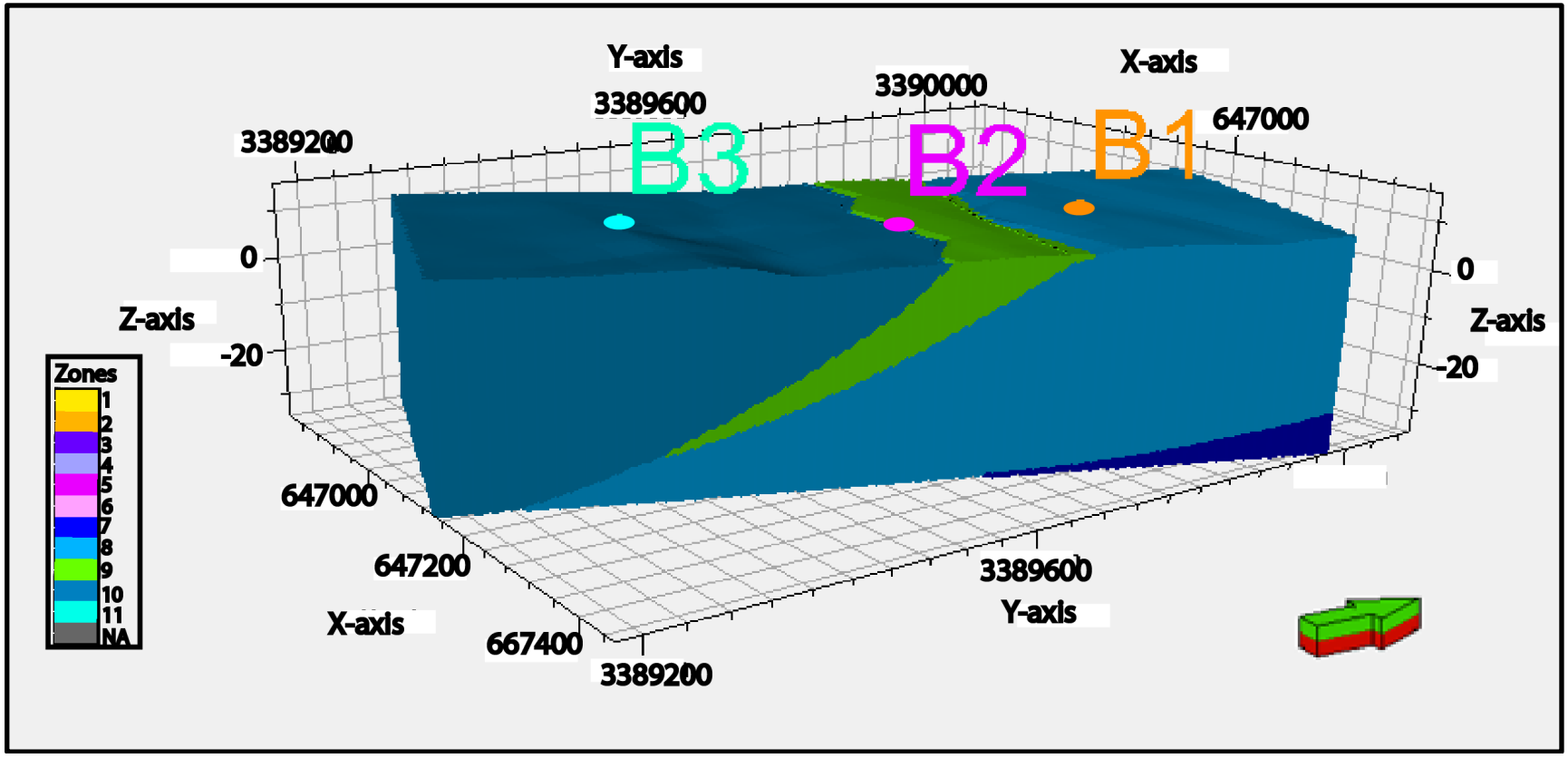

Figure 5.15. Sector model from the Bueche property. The borehole location are indicated on the top of the model. The colored circles are the tops of the boreholes, and extend vertically down. The arrow points north. Though Zone 9 appears to pinch out, this is a false characteristic due to the cell size of the model being too large to account for boundaries this close to each other. Vertical Exaggeration is 5.

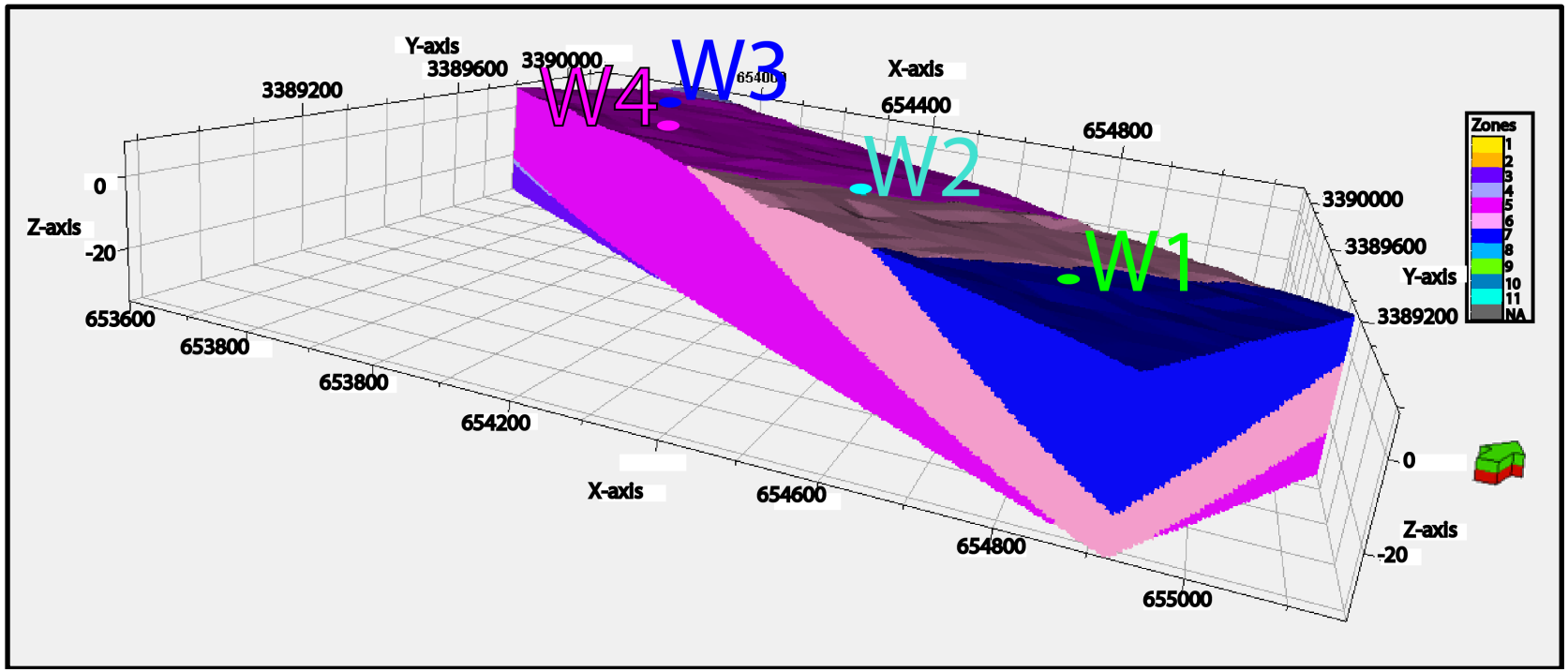

Figure 5.16. Sector model of the Woody property. The borehole locations are indicated by the lettering on top of the model. The colored circles are the tops of the borehole, and extend vertically downwards. The arrow points north. Vertical exaggeration is 5.

6. DISCUSSION

Position within any given point bar is an important factor when considering heterogeneity of units. This applies not only to stratigraphic continuity, but also to the lithology within each area and the ability to predict how sediment is distributed between times of major growth and reorientation events. When comparing the results of this study to that of a simple model that predicts that a bar should 'fine upwards and downstream', I concluded that this was an insufficient statement, because this explanation lacked an understanding of the true boundaries between surfaces and the variations between events in different depositional localities across the bar. Without that understanding, building a model for a large point bar at the facies and bed-scale would not only have been impossible, but inaccurate. This was critical when considering a large scale point bar like False River, where the compound nature of the bar and obscure geometry prevent predictions from being made regarding constructional history and facies stacking patterns.

6.1 Log Interpretations

Though exact numerical values could not be used to determine facies cutoff within the data, three distinct packages of facies were chosen: 'bar top sediments', 'interbedded heterolithic strata', and 'high net facies'. These were chosen based on the standard stratigraphic packages within large-scale point bars, as discussed in the Introduction section of this paper. The high net facies package is equated to what has otherwise been referred to as lower bar cross-stratified sands (Fustic, 2007; Fustic et al., 2007; Hubbard et al., 2011), but a unique name was chosen to avoid any confusion related to a name that indicates a spatial placement, such as 'lower bar'. Because the occurrence of these packages has previously been established, and general trend for electrical conductivity and HPT are known, interpretations were made by examining the trends

of the log data in relation to each other and the expected stratigraphy.

The shallowest deposits, labeled the bar top sediments, are the sediments deposited by periodic bar top flooding, and will always be present as a top surface of a point bar unless physically removed by outside means. Because of this, and based on confirmation from each landowner that no surface sediments had been physically removed by them, it was assumed that bar top sediments would be present in every log. Due to this assumption, only the base of this package needed to be found in order to assign the package to each log. This base, which is the boundary between this package and the IHS, was interpreted by looking for an abrupt change in sediment lithology, usually from higher to lower EC and gamma values due to the inherently low energy of the system after cutoff (Labrecque et al., 2011). This assumption was further confirmed from Fig. 5.12, which shows this boundary within the core sample.

Beneath the bar top units are the inclined/interbedded heterolithic strata (Fustic et el., 2012; Labrecque et al., 2011; Musial et al., 2012). This facies was characterized by packages within the logs that were highly variable at a small scale, which points to interbedded strata of different grain types and sizes. Because interbedded heterolithic units would inherently have variable log values, matching the numerical values of the logs to a set ‘standard’ was unnecessary as the trend of the logs within this package is more important. Variability within the units that can be equated to varying sediment types is visible in the logs regardless of what exact range of values correspond to sand in comparison to those of silts and clay. Thus, this facies package was identified in logs by first assigning the base of the bar tops units and then verifying that the units below it was variable in nature. The base of the IHS was then placed where grain size (from the gamma and EC) and permeability (as indicated by the HPT) increased, indicting a grain coarsening, and/ or the heterogeneous nature of the IHS package ceased.

The lower bar sands, which characterize the lower portion of all point bars within the past and recent literature referenced for this study, were identified within the logs over an interval from the base of the log upwards by looking for low gamma and EC values in comparison to those of the bar top and IHS packages. As discussed, because interpretations were made in a relative sense and based on an already established facies package of point bars, it was less important to assign exact values to these packages as the trends within them were the most important. However, based on the core section from W1, it was assumed that any electrical conductivity values below approximately 30 mS/m were sand of varying grain sizes, though some logs did contain sand packages with slightly larger values. Also, all lower bar sands are considered to be consistent with the literature and thus trough cross-bedded nature.

6.1.1 Jumonville Log Interpretations

Easily definable facies boundaries are visible within the Jumonville area logs (Figs. 5.2-5.4). Overall, they exhibit a fining upwards sequence, with some small peaks in the HPT and EC logs, interpreted as periodic fine-grained, less permeable layers. Bar top deposits characteristic of the top surface of a point bar were expected to be present in each location, and sit above the interbedded heterolithic strata (IHS). The boundary between these units was placed when the trend of the logs changed, and was not based on a high vs low value. Since bar top units are essentially sediments deposited during flooding events, depending on the energy of the event and the location of the borehole within the point bar, these deposits could have a wide range of sediments types. Within J1 and J3, this boundary was placed because of a change from higher, more variable values to lower, more consistent values, indicating two separate packages. Within J2 the boundary was placed at a point between a fining downwards interval and a lower, more heterogeneous interval.

The lower bar trough cross-bedded sands represent the largest portion of each log, and though the logs cut off above the base of the point bar, this facies is expected to extend to that depth as well. Though this package was visible in each of the Jumonville logs as established by low gamma and EC trends, the boundary between this and the upper IHS units was clearer in some boreholes than in others. Specifically, the top of the sands was identified in J1 and J2 where the gamma and EC values abruptly changed from a lower value in the sands package to a higher value within the IHS. However, the J2 log was more difficult to interpret due to the less variable nature within the gamma and EC logs. Because of this, HPT was a used to located the depth at which the sediments were indicating a better permeability, which indicate a sandier unit. As a quality check, the depth of this interpreted boundary was then compared to those within J2 and J1, as each should occur at a relatively similar depth.

6.1.2 Bueche Log Interpretations

Unique, individual trends are very apparent within each of the logs from the Bueche area (Figures 5.5-5.7). While all exhibit general fining upwards trends, strong boundaries representing characteristic intervals like those seen at the Jumonville property are not apparent.

Site B3, shown in Figure 5.7, is clearly the most heterogeneic, and contains the most fine-grained sediments of any of the Bueche sites. Because of this heterogeneity, clear intervals of floodplain deposits, upper bar, and lower bar are not determinable, although the top of the log appears to have geophysical characteristics that indicate that it is finer and less permeable than the lower half of the section. Between about 1.6 m and 12.8 m the electrical conductivity, though variable, has an overall high trend with the gamma showing characteristics indicative of there being many fine-grained strata interbedded with various coarse-grained layers. Below 12.8 m the overall facies seem to be coarser than those above. There are, however, very high values in the

electrical conductivity and hydraulic pressure logs (HPT) relating to relatively thick, impermeable layers at 18.5-20.1 m, 24-25 m, and 25.5-26.6 m.

Site B2 has a very visible boundary between what I interpret to be an upper fine-grained section and a lower coarse-grained section at 4.95 m. Within the top unit, an IHS boundary has been defined, but is only a small section of the over log.

Within the B1 logs, (Fig. 5.5) the interval between the surface and 2.26 m contain two sharp peaks representing the presence of fine-grained sediments, underlain by a coarse-grained interval from 2.26m to 4.46 m. Below 4.46 m the sediments yield geophysical responses that are indicative of relatively coarser sediment, with many thin silt drapes. A boundary characterized by a small layer of fine-grained sediment is present at a depth of 20 m. Some fine-grained drapes can be interpreted throughout the log, but nothing indicating anomalous behavior such as at Site B2.

6.1.3 Woody Log Interpretations

Overall, the sediment surveyed at the Woody property (Figs. 5.8-5.11) consists of a coarsening downwards trend, with a greater amount of fine-grained intervals than what is seen in the Jumonville property (early bar). Although the Bueche property at Site B3 does contain a high percentage of fine-grained sediments, the sediments sampled and logged at the Woody property exhibit a greater overall percentage of fine-grained strata throughout each log, compared with at just one location in the Bueche area. There are also a higher amount of jumps in EC values within the logs, which appear at smaller intervals than at the other properties.

The W1 borehole (Fig. 5.8) is closest in proximity to the abandoned river channel and demonstrates geophysical logging responses indicative of a fining upwards trend. Two distinct boundaries have been placed at 2.75 m and 19.5 m and represent the intervals of top bar deposits

(Fig. 5.12), IHS, and deeper sand-rich strata, and placed due to the visible difference within each portion. Though some small mud drapes are present in the sand-rich facies, it is the upper portion of top deposits and IHS that dominate these logs. The upper portion of the section from the surface to 3 m depth is interpreted as a mostly impermeable muddy layer, coarsening progressively down into IHS below. Regarding the IHS, it is much thicker in this location than any of the other boreholes on the Woody property, and is very heterogeneous. Within the HPT log the values are also much higher than within the others, even within the sand.

Though W2 (Fig. 5.9) only contains gamma data, facies boundaries were still interpreted at this location. The boundary between the bar top package and the IHS, at about 1.8 m, was picked because of the decrease in gamma. The top of the trough cross-bedded sands was also chosen for the same reason.

The facies boundaries within W3 and W4 were chosen on about the same basis in relation to each other. Within the logs at each location the gamma and EC values decrease to the base of the bar top units. After this, variability consistent with a homogeneous sediment package occurs until the lower bar sands are reached.

6.2 Facies Interpretations

Geophysical data from Sites J1, J2, and J3 confirm that the upstream sediments deposited early during bar formation deposits are indeed sandier and less heterogeneous. As expected, there are larger portions of the lower bar trough cross bedded sands with few fine-grained drapes. The HPT and flow rate logs also indicate that there are fewer boundaries to impede fluid flow in the upstream part of the bar. This stratigraphy is attributed mainly to the position within the bar, as these sediments were deposited early during construction.

The accretionary strata within the Woody property (downstream) appear to have been deposited before cutoff and during normal mid stage bar growth based on the occurrence of upper and lower bar deposits within all of the logs and a lack of levee deposition as would be apparent on the DEM. Additionally, there is a consistent fining outwards trend in the sense that the sequence at Site W1 contains a larger thickness of IHS, with the IHS decreasing away from the abandoned channel. Within the lower sands heterogeneities do exist, and can most likely be attributed to the position of these locations at the time of deposition, which would have been downstream of the apex. Because of this, the high energy periods needed to deposit the sands would have periodically fluctuated enough to allow finer sediment to settle.

Figure 6.1 shows that the IHS and lower sand-rich (high net) facies all dip consistently towards the abandoned channel. This means that had these boreholes been closer together, individual strata could have ideally been mapped within the interbedded units. Knowing where this can be done in a point bar is important, as low net (clay–rich), bar tail, heterogeneous strata have never been quantified. This is also definitive proof that even in complex point bar systems accretionary migration directions in the subsurface do match the surface scroll bar topography.

Also of note in the geophysical logs from the Woody area are responses indicative of the presence of fine-grained strata in the lower portions of the high net (sand-rich) facies. Because these are in the lower bar, they cannot be correlated on a timeline basis because the boundaries of the accretionary layers are not visible in the sands as they are in the upper bar. However, when considering their deposition within a migrating river channel, it is reasonable to presume that each may have been deposited by similar formational events, resulting in possible mud rip-ups or fine grained settling of fine-grained sediment at equal positions in the river channel at different times.

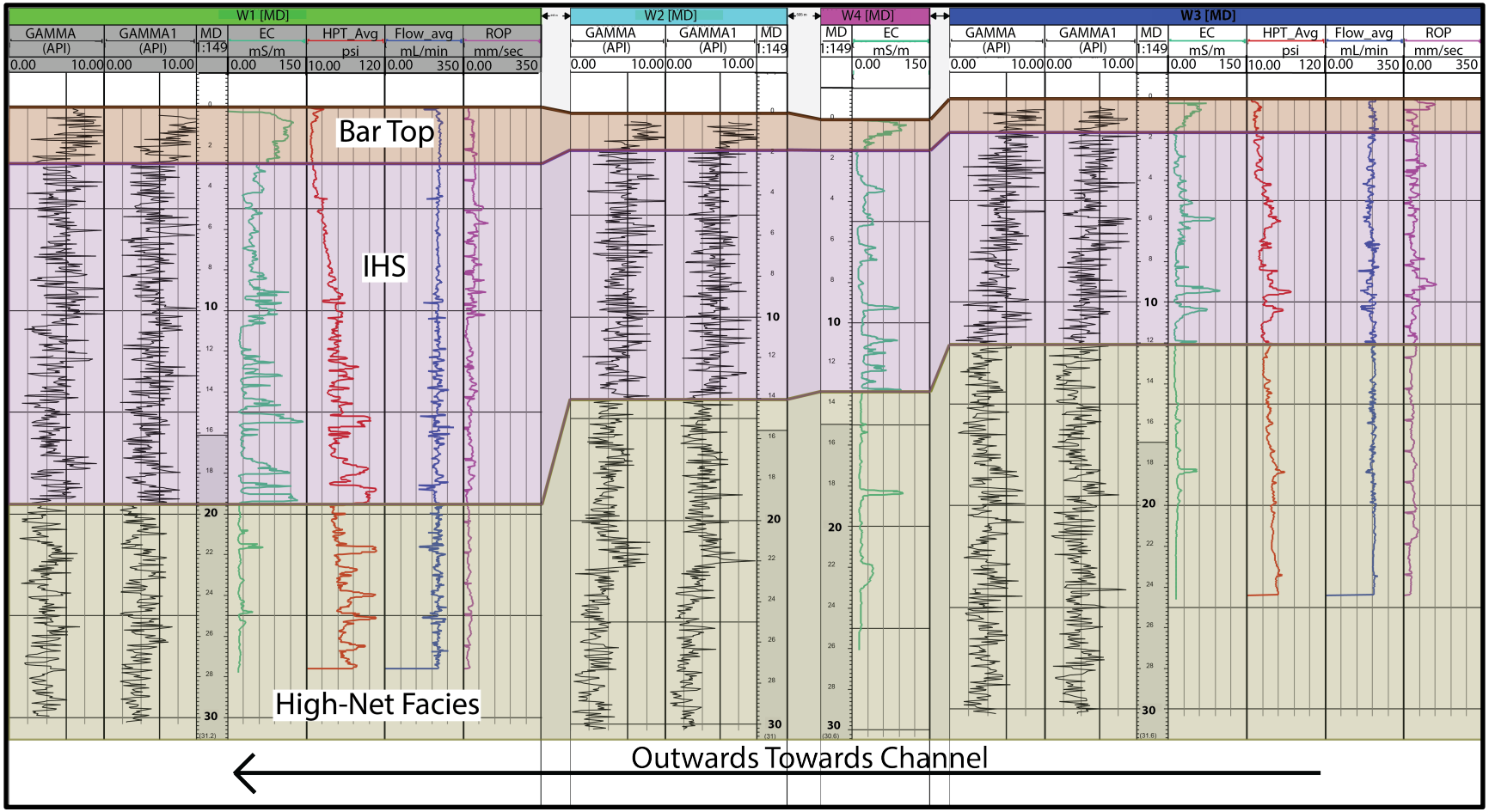

Figure 6.1. Compiled cross section of the Woody geophysical logs, demonstrating a consistent dip from the inner bar towards the outer channel. From left to right, the logs are: W1 (green), W2 (light blue), W4 (pink), and W3 (dark blue).

Sediments surveyed at the Bueche property contains both extremes: a log with a very large section of lower bar deposits, and a log entirely containing higher net, sandy interbedded heterolithic strata and inner bar levee deposits. Though high net sands are seen in the lower bar at Sites B2 and B1, Site B3 is missing this facies entirely. It is also likely that sands are present in the lower part of the bar that was not recorded in the logs, as seen in other point bar models (Fustic, 2007; Fustic et al., 2007; Hubbard et al., 2011).

When viewed from the surface there appears to be accretionary surfaces cutting between each of the borehole locations, though it is more likely that the surface between Sites B2 and B3 is actually a reorientation surface. This is most obvious when viewing the logs in cross section (Figure 6.2). Because of the differences between the logs from Sites B2 and B3, it was necessary for them both to be within different zones of accretion by placing a reorientation surface between them at a steeper angle than in the rest of the bar. This steep angle, coupled with a different 'rhythmicity' around the apex near Sites B1, B2 and B3 than farther around the bend, points to differences in shear stresses and deposition here than elsewhere in the bar. Considering the position near the apex of the bar and within the inner levee deposits, and the fact that the Site B3 log contains no high net sands, a balance between vertical aggradation versus lateral accretion due to decreasing energy after B2 must also be considered. This leads to my interpretation that the logs from Sites B1, B2 and B3 are most likely recording insipient or active abandonment from the main river channel.

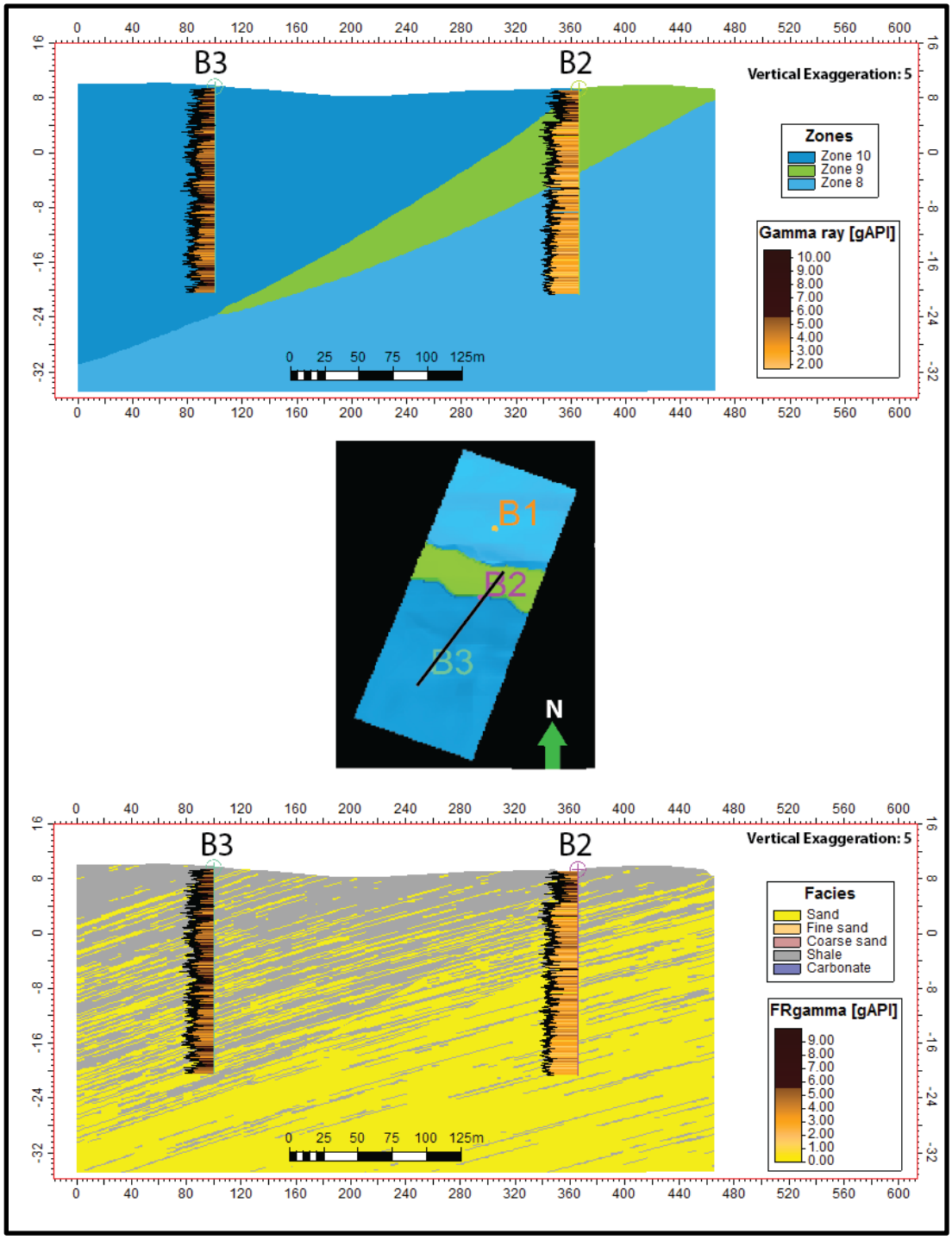

Figure 6.2.Intersection through Sites B3 and B2. The steep reorientation between Zones 9 and 10 was required in order to match the different facies packages of the logs. Though Zone 9 appears to pinch out before reaching the bottom, this is a false artifact due to the cell size of the model, and the zone should reach the base of the cross section. Vertical exaggeration is 5.

6.3 Bar Constructional History

The evolution of the False River point bar can be grouped into three first- order stages (Fig. 6.3), based on changes in depositional style as evidenced by the reorientation surfaces. While the point bar is in a broad sense one unamalgamated bar that grew over a broad time frame, the large scale and inherent complexity of formation require that more care be taken into understanding the system and the control over the system through time as sediment distribution may change between long-lived growth periods and reorientation events.

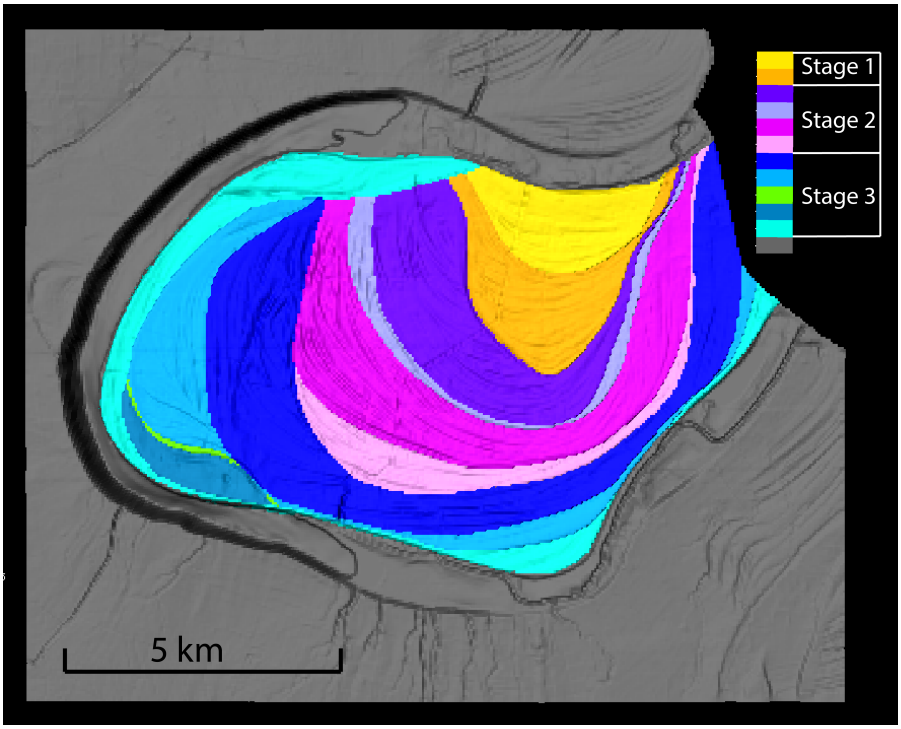

Figure 6.3. 3D model showing the zones grouped into overall growth stages. The stage one bar was simple, the stage two bar was a transition from simple to asymmetrical, and stage three represents compound apex bar growth.

Early stage bar growth was simple and relatively symmetrical. Although the earliest stage appears to no longer be present/preserved, the most headward part of the bar would likely have extended past the present channel and into the opposite bank, where a newer (younger) bar now exists as an outcome of channel migration (Fig. 6.4). Although the Jumonville boreholes (J1-J3),

which are the most headward boreholes sampled, appear to be in the actual head of the bar, the area should in fact be classified as more apex than bar head, because of erosion during bar development that may have eroded earlier portions of the bar northward of Sites J1-J3. Thus, Sites J1-J3 were actually formed at the apex during early bar formation, when it was a simple bar (single half ellipse curvature).

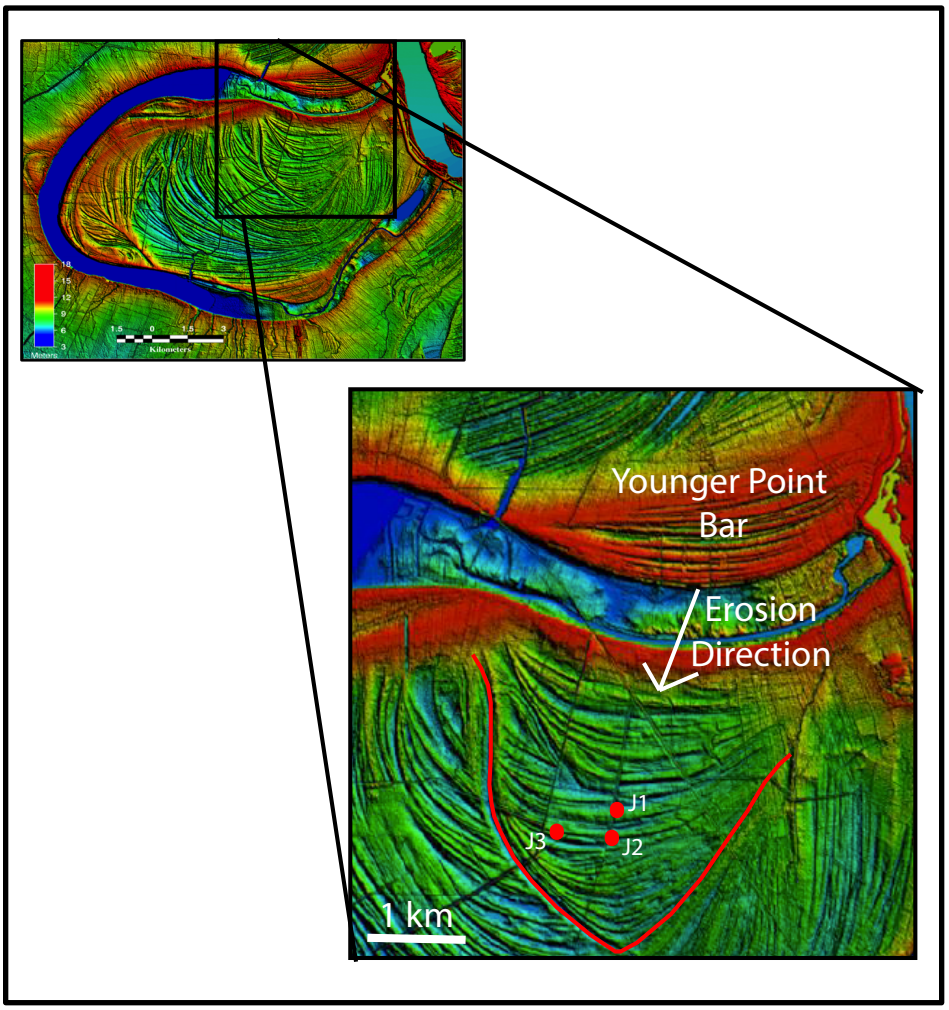

Figure 6.4. Zoomed in section of the DEM. Notice the younger point bar to the North of the abandoned channel which formed and eroded into the older head of the stage one bar.

Though early stage bar growth can be classified as a simple bar and comparable to a basic model of a point bar, the mid stage bar growth was more complex. After the reorientation surface which bounds Zone 2 the apex of the bar began to migrate west, and as the bar grew through

Zone 6, a transition from a simple to an asymmetrical point bar is visible on the DEM. Sites W1-W4, which are located in the tail of the bar slightly downstream of the western apex, sit within the later part of this transitional bar stage (W4, W3, and W2), and in to the early compound bar stage (W1). As discussed, these logs follow the expected pattern of accretion direction and facies changes. Based on this, I concluded that although complex bars may have obscure growth patterns, the transitional periods between simple bar growth and asymmetrical bar growth do not necessarily create unpredictable subsurface accretionary sets.

Stage 3 growth continued in an asymmetrical pattern (Fig. 6.3), but with time also began to develop meanders within its meander as a result of the large scale of the system. Essentially, as sinuosity within the meander increased, the river channel began to erode back into the southwest portion of the bar created earlier during Stage 3 growth (Fig. 6.5), possibly due to the increasingly low gradient of the channel, creating an apex downstream of the mid apex site while also creating one upstream. This resulted in the multiple apexes seen in the current system, and the compound nature of late stage bar growth.

The geophysical logs from Sites B1-B3, which are located in a near-apex area of the bar, recorded the late portion of the compound growth stage and sit distinctly within inner levee deposits formed slightly downstream of the western apex. At some point in the evolutionary time-line between B1 and B4, lateral accretion began to stall and the bar was eventually cut off, which limited the supply of sand into the river channel. As a result of a decrease in lateral accretion, I infer that vertical aggradation would correspondingly begin to increase, leading to the deposition of inner levee deposits around the outside perimeter of the bar.

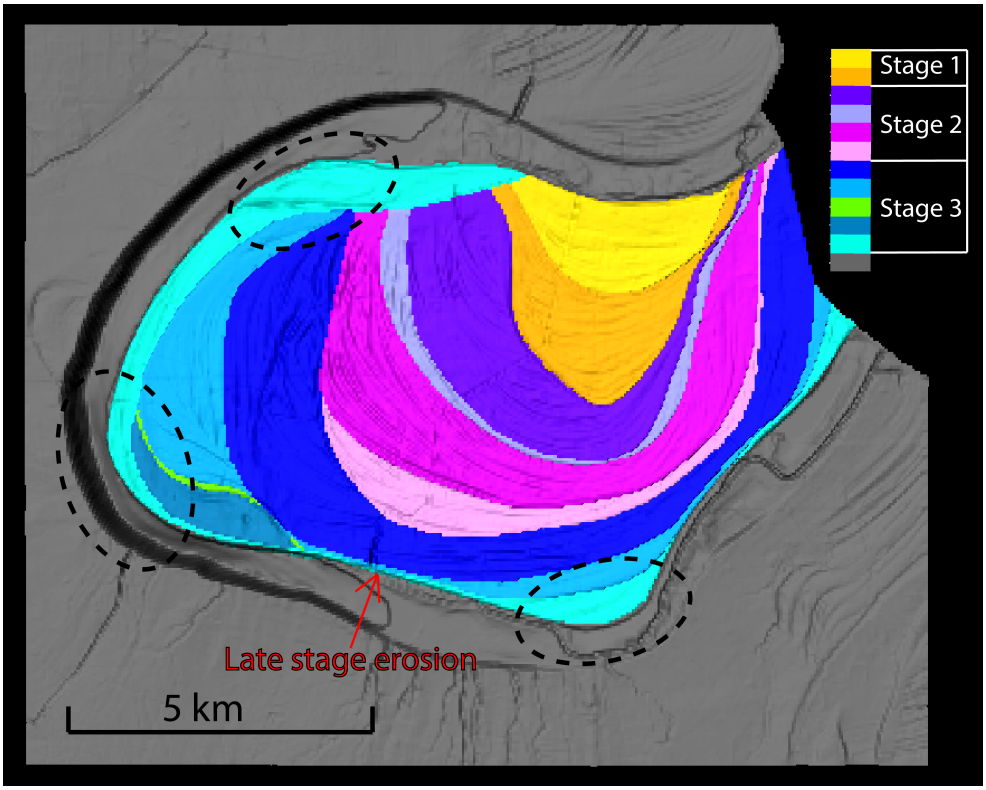

Figure 6.5. 3D model from Figure 6.3 with the three late stage compound apexes in dashed circles. The location of late stage erosion is indicated by the red arrow.

Though some models of point bar cut-off argue for a swift timeframe and depletion of sands being introduced into the channel, data from Sites B1-B3 support the opposite model of cut-off, which developed much more slowly. It is evident from the logs from Site B3 that flooding events and times of active deposition were still occurring during abandonment, and were recorded in this section as intervals of higher net facies bounded by thick sequences of interbedded, fine-grained strata. As abandonment progressed, fining upwards within the section was prevalent, with a thick section of inner levee deposits topping the section in this area. These levee deposits, though present all around the outer portion of the bar, were greatest and most laterally continuous at the apexes of the bar where the velocity abruptly changed, creating ideal conditions for dumping sediment and allowing slow lateral accretion even after cut-off began.

My interpretation of a cut-off event being recorded in the Bueche geophysical logs was further supported by the uncharacteristic trend of thickening outward versus thickening towards the head. As the bar grows in a simple system natural levee deposits are expected to accumulate at the head and build outwards towards the channel (Gouw, 2007). This would result in a wedge shaped deposit that thins towards the channel. However, in the False River system only Zones 1-7 appeared to demonstrate this trend, in sharp contrast to the thick deposits around the perimeter of the bar and accumulated at the late stage apexes.

6.4 Reorientation Surfaces

Reorientation surfaces were a particular target of this study and for modeling because they change the accretionary angle, direction of lateral accretion, and the means by which the point bar is progressing. Essentially, each time the point bar reorients, the entire geometry of the point bar is reset. This non uniform pattern is problematic because it creates an even greater complexity in relation to large scale bars, especially if these events can be linked to facies changes and stacking patterns. Because these surfaces effectively bound phases of construction within which the upper and low bar units accrete, they must be understood if the continuity of the fine-scaled heterogeneities is to be determined.

6.4.1 Identification in Logs

Continuity through the bar and across reorientation surfaces were assessed on the basis that dip could be variable throughout the bar. This was because not only was the true dip still unknown, but an asymmetrical bar that also displays numerous reorientation surfaces would be expected to have variations, not a constant angle everywhere throughout the bar. As can be seen in Table 6.1, the presence of reorientation surfaces was evaluated at three different dip angles: 6, 8, and 10 degrees. These were chosen based on previous studies discussed in the introduction.

Table 6.1. Depth of reorientation surfaces in each borehole calculated based on assumed angle and a known distance from the surface expression as viewed from the LIDAR image in Figure 4.1.

	Distance from reorientation surface (m)	Depth of reorientation with prograding dip of 6°	Depth of reorientation with prograding dip of 8°	Depth of reorientation with prograding dip of 10°
Location				
B1	NA	NA	NA	NA
B2	59.00	6.20	8.29	10.40
B3	98.00	10.30	13.77	17.28
W3	129.00	13.56	18.13	22.75
W2	73.00	7.67	10.26	12.87
W1	82.00	8.62	11.52	14.46
W4	400.00	42.04	56.22	70.53
J1	33.00	3.47	4.64	5.82
J2	320.00	33.63	44.97	56.42
J3	625.00	65.69	87.84	110.20

Figures 6.6-6.8 show the interval between 6 and 10 degrees that the reorientation surfaces are expected to occur within. Based on this, the expression of the reorientation surface in the logs was not possible without having an exact dip angle. Each interval looks relatively different for each location, especially because the reorientation surfaces can occur both within the upper and lower bar facies. If the surfaces were expressed in the logs, their expression did not seem to vary dramatically from that of the basic heterogeneity inherent in the bar. This was complicated further because although they had been characterized in the literature as being draped by mud, it is not clear if the reorientation surfaces would be sand on sand, mud on mud, or a sand on mud boundary because during each reorientation the head of bar begins to be cannibalized, leaving an uncertain facies boundary (Musial et al., 2011)

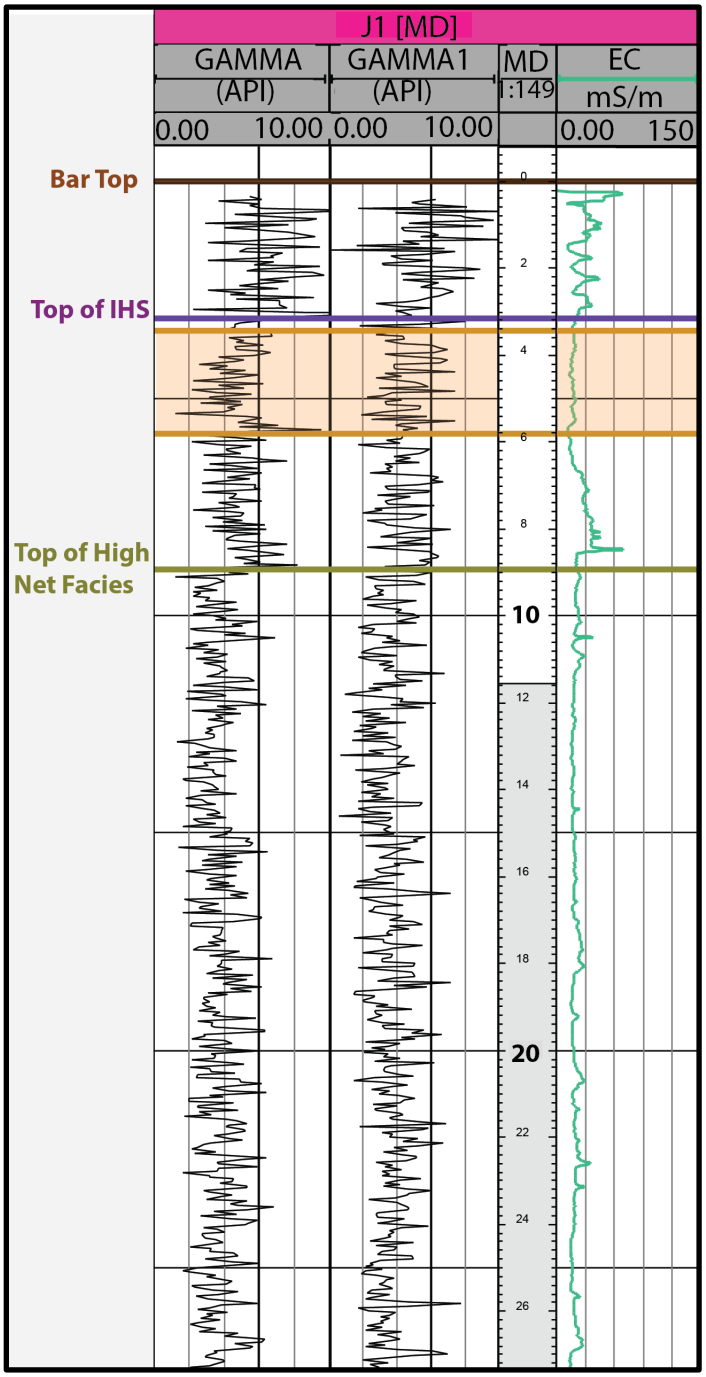

Figure 6.6. A portion of the Site J1 borehole section. The shaded section represents the interval where reorientation surface could occur if dipping between 6 and 10 degrees. Sites J2 and J3 do not contain an interval within the logged section. The measured depth (MD) is in meters.

Knowing the angle of the reorientation surfaces is critical in order to place them within the logs and the subsurface. Considering that these surfaces are erosional in nature and can reach

steep dips, finding the dip angle is required in order to know with greater accuracy how far the accretionary layers of the subsurface are extending, and if the dips of these surfaces can be predicted based on their surfaces expression and/or bar location. This is of even greater importance when applying this information to ancient system in which predictions must frequently be made.

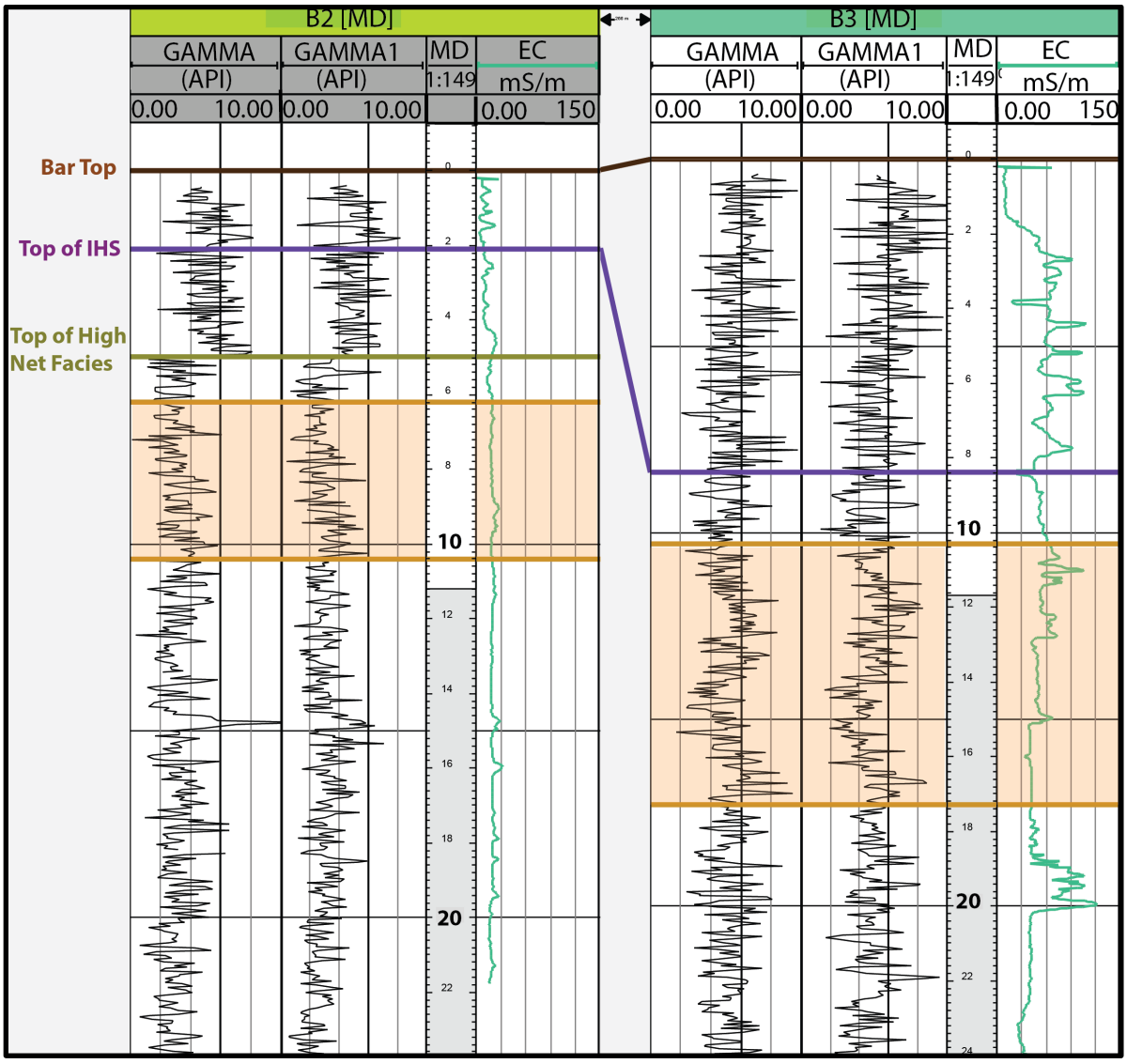

Figure 6.7. Portions of logs from Sites B2 and B3. The shaded section represents the interval where the reorientation could occur if dipping between 6 and 10 degrees. Site B1 does not contain an interval within the logged section. The measured depth (MD) is in meters.

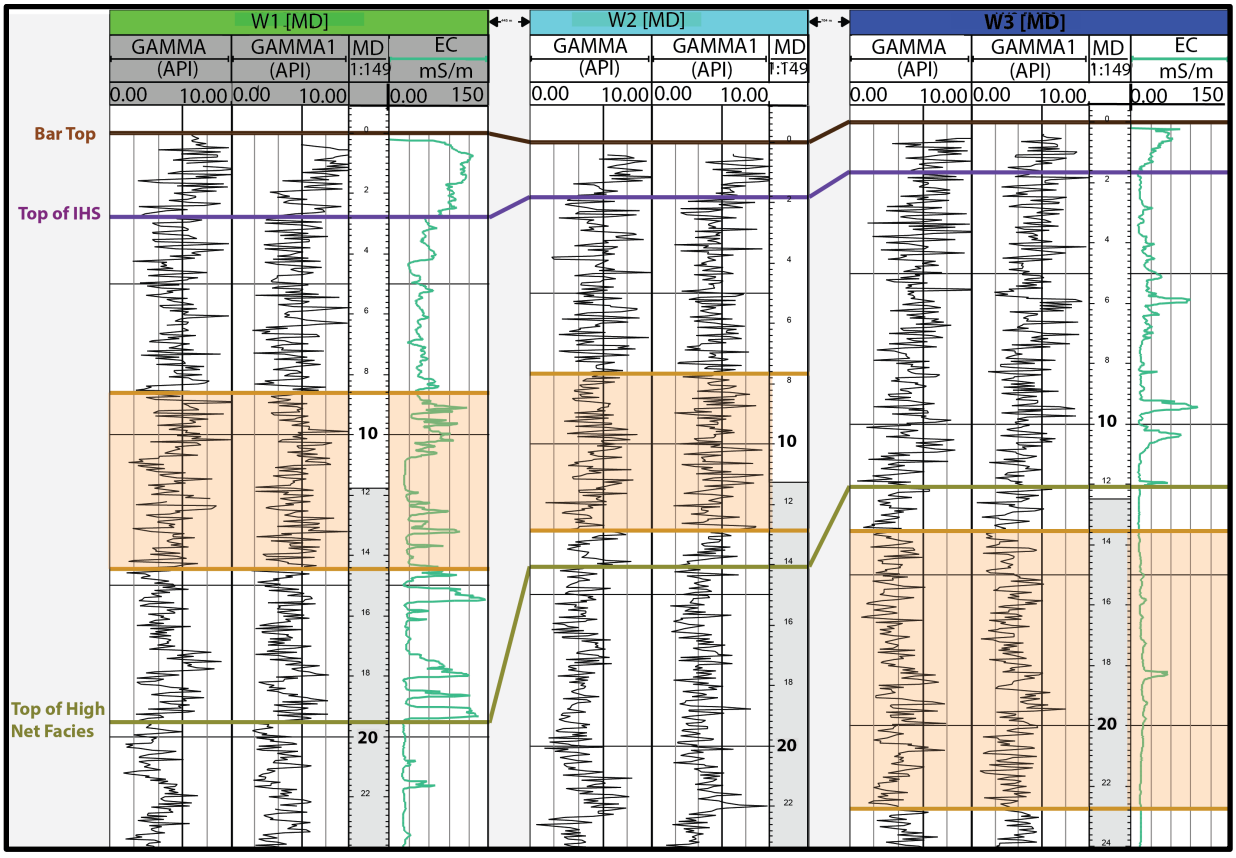

Figure 6.8. Portions of the logged sections from Sites W1, W2 and W3. The shaded section represents interval where the reorientation could occur if dipping between 6 and 10 degrees. Site W4 does not contain an interval. The measured depth (MD) is in meters.

When assuming average accretionary and reorientation dips, care should always be taken to account for the differences within each system. Though dip may be consistent in most areas, prevalence of the reorientation surfaces is indicative of high energy events, especially where the head of the bar has eroded back. In addition, it can never be assumed that the dip of the accretionary surfaces is consistent with that of the reorientations bounding it, as demonstrated by the Bueche sector model (Fig. 6.2). Although a high-energy event resulting in steep reorientation clearly occurred here, the resulting accretionary surfaces deposited after reorientation must dip at much lower angles (approximately 2.5-5.0 degrees) as averaged from the slope abandonment profile due a general decrease in energy. One should also never assume that a dip pattern seen in

one growth stage of the bar can be applied to another, as each stage is the consequence of different depositional factors.

6.4.2 Chute Deposits

While for the purposes of the this study all of the offsets visible in apparent map view have been classified as reorientation surfaces, the abrupt onlap of scroll bars against the reorientation surfaces in certain areas may be indicative of chute deposits which migrated across the surface of the bar after its formation (Fig. 6.9). If this were true, the scrolls which appear on the outer bend of the supposed chute deposit would actually be older than those on the inside. Alternatively, if considered reorientation surfaces, the outer scroll patterns would have been formed through onlapping tangentially into the reorientations and simply produced an obscure surface geometry not normally seen.

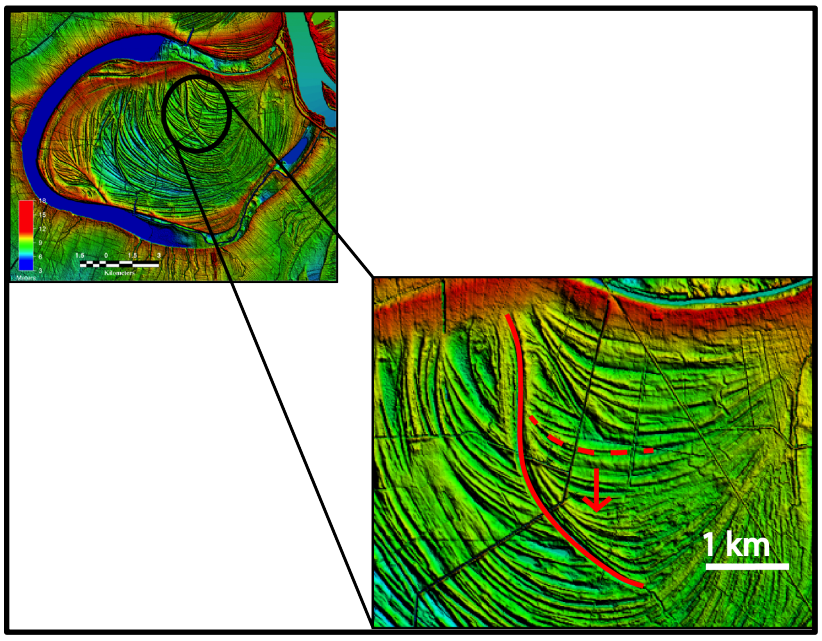

Figure 6.9. Close-up of area where abrupt onlapping is visible, indicating a possible migrating chute deposit with early deposition depicted by the dashed red line. The red arrow shows the direction of migration, and ends with the solid red line.

Unfortunately, although in some systems chute deposits are easily identifiable in the subsurface, chutes deposited with the same lateral migration direction as the scrolls are much more difficult to resolve when deciding between a laterally migrating chute and a reorientation surface. Ideally a chute deposit would exhibit a modest fining upwards trend caused by lateral accretion at a small scale, but this trend would likely be indistinguishable solely within a log from those deposits at the bar top because of the shallowness of the deposit (Fig. 6.10). In order to definitively prove a reorientation surface is actually a chute deposit, data from more closely spaced well pairs and/or seismic data would be needed in order to identify the smaller laterally accreting units within the chute deposit. Additionally, when focusing mainly on how sediment is distributed between large growth events, possible bar top reworking is less important compared to identifying reorientation surfaces that would bound accretionary sets. Because of this consideration, this study treats these surfaces as reorientations.

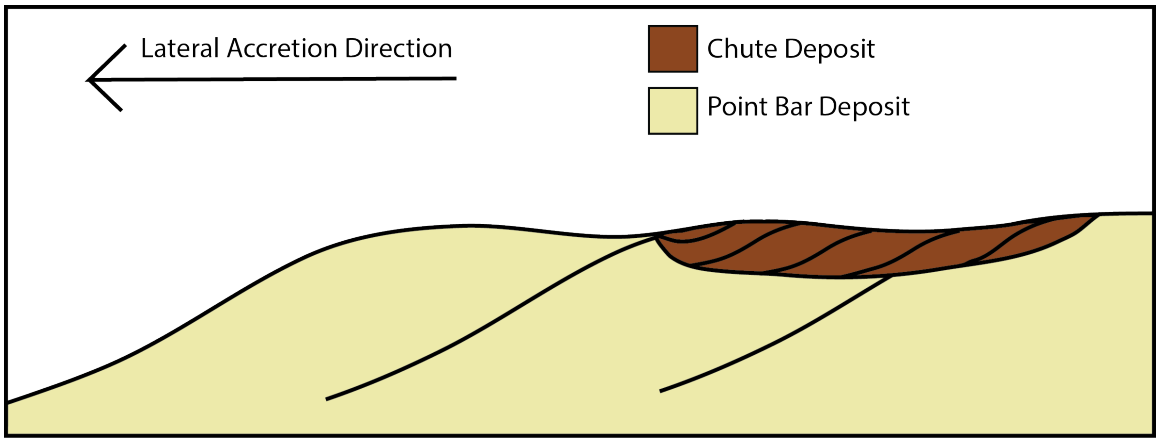

Figure 6.10. Example of a chute deposit migrating parallel to point bar growth within the upper units of the bar.

6.5 Hydraulic Conductivity (K)

Hydraulic conductivity (K) is a measurement of how easily a fluid is able to move through a pore space when influenced by a hydraulic gradient (McCall, 2011). The equation for hydraulic conductivity (6.1) can be derived from Darcy's law (6.2), where k is intrinsic

permeability, ρ is the fluid density, g is the gravitational force, μ is the viscosity of the fluid, A is the area of flow, L is the length over which the pressure drops, and (ρb-ρa) is the total pressure drop. Fluid density (ρ) is a product of the dissolved ion content within a fluid (Bennett, 1976; McCall, 2011). Because electrical conductivity is also affected by dissolved ions (which most effectively carry the flow an electric current), it reasons that when ρ changes, EC should also change. In contrast, viscosity (μ) is primarily a factor of temperature change, and in a system such as ours should remain relatively similar at equal depths in different locations.

$$K = k\frac{\rho g}{\mu} \tag{6.1}$$

$$Q = \frac{-KA(\rho b - \rho\, a)}{\mu L} \tag{6.2}$$

Based on this equation, if two facies packages are at equal depths with equal electrical conductivity values, any changes in the hydraulic conductivity would be directly correlated to the permeability (k) of the sediment, and more importantly grain size differences not related to differing facies values such as sand vs. clay, which would registered by the EC. This is important in areas where the EC and gamma alone would indicate a similar facies which in reality have different permeabilities and hydraulic conductivities, which is apparent in the False River point bar.

As the bar fines upwards and outwards and the coarseness of the sand decreases within the packages of the trough cross-bedded sand facies as a whole, it follows that if averaged by thickness for each studied part of the bar, hydraulic conductivity would be highest where the sand packages are thickest, such as in the Jumonville logs (Sites J1-J3), and lowest downstream (Sites W1-W4). However, when K is evaluated on the basis of individual sand packages within

the larger high net facies, quantitative differences are apparent within sands that otherwise would appear, and have been classified in past models, as being identical facies.

The best example of this trend is seen in the logs from Sites J3 and W1 (Fig. 6.11). If facies packages are evaluated solely on their values as measured by EC, equal EC values at the same depths at different locations would be characterized as the same facies, and should have equal hydraulic conductivities. Despite this, although sediments at Sites J3 and W1 both have approximately equal EC values (20 mS/m) at 65 ft (19.8 m) in depth, their hydraulic conductivity values differed. The sand section at Site J3 has a much higher K value of 50 ft/day, while the W1 package has a K of 37 ft/day. Based on the factors which affect K in equation 6.1, these differences in K are related to permeability differences, and thus grain size differences in the sand packages that are not registered by the EC.

This hydraulic conductivity difference is a good indicator that essentially, not all sands are created equal. As the river flows around the apex of the bar and further downstream there is a change in flow performance, which results in deposition of sands that are more finely grained and more poorly sorted than those deposited upstream. Previously, this flow difference was recognized by the increasing occurrence of IHS beds and the decreasing net to gross (less sand), but did not take into account the quantitative differences in seemingly identical lithologies deposited at different locations. Furthermore, this trend has likely been overlooked and/or missed in the past because the gamma and EC values are most significantly affected by the presence or absence of clay. This is problematic in sand-rich sections, because without core sections for comparison, the finer grained nature of packages may be overlooked if only gamma and electrical conductivity logs are available.

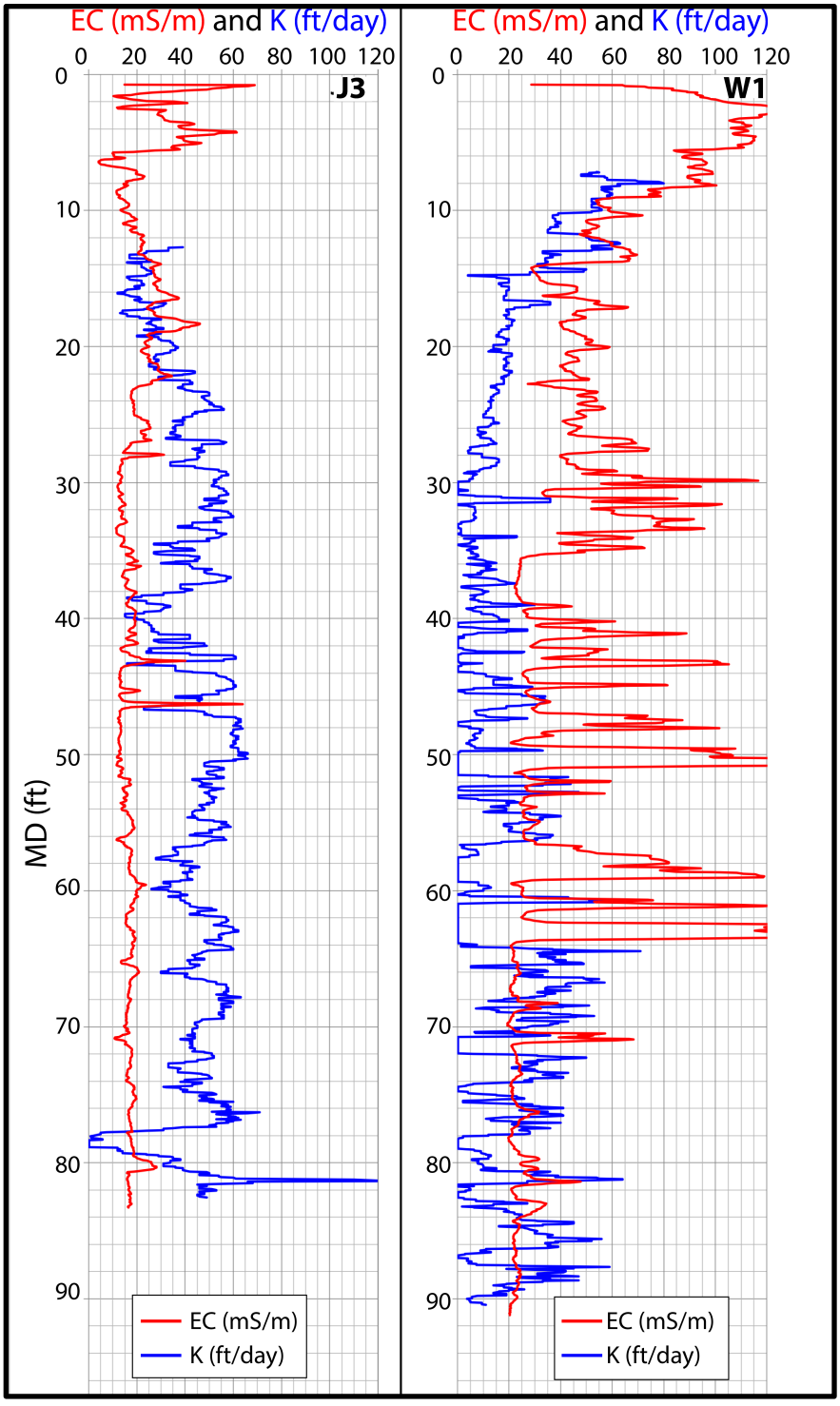

Figure 6.11. Stacked electrical conductivity (EC) and hydraulic conductivity (K) graphs from Sites J3 and W1.

7. SUMMARY, CONCLUSIONS, AND FUTURE RESEARCH RECOMMENDATIONS

7.1 Summary

The False River point bar is an ideal analogue for ancient, large scale meandering fluvial systems, and also builds on our understanding of how smaller scale fluvial systems function. Past research created a model of development, but lacked the complexity inherent in a high-order, compound system, especially in relation to heterogeneity at a fine scale. Developing a more detailed subsurface model was necessary in order to understand spatial heterogeneities throughout a large bar, as well as to answer questions regarding trends within stacking patterns.

Initially, a LIDAR DEM of the False River point bar was utilized in order to choose field locations in areas of interest throughout the bar which give the best over-all understanding of heterogeneities at different stages of formation. The DEM was also used to map supposed reorientation surfaces with the intention of later identifying them in the logs. However, due to a lack of both dip data and unique uncertain identifying features, it was not possible to recognize reorientation surfaces in the log. Initial core sampling in the field yielded poor sample recovery because the sampling techniques were not adequate for the material state. Later data acquisition of electrical conductivity, hydraulic profile tooling, and gamma logs was successful Interval coring was also possible using a different type of rig.

A 3D model of the point bar with smaller sector models of each borehole property were created by loading all of the data into Petrel software. Three general facies within the bar were identified within the logs, and allowed for a separation between the lower bar sand-rich units and the upper heterolithic units to be mapped, as well as the bar top

deposits. Nevertheless, despite good results, borehole spacing was too great to map continuity of individual strata. Although facies identification and the subsequent fining upwards and outward trend matched that predicated by small-scaled models, heterogeneities in certain logs proved that high order point bars, of the type I address here, are more complex and require a more detailed model, especially regarding processes such as cutoff.

7.2 Conclusions

7.2.1 Point Bar Architecture

1. Overall, the goal of defining the internal architecture of the point bar was met as applies to bulk facies patterns, constructional history, and spatial variability in key areas of the bar. At such a large scale the logging data cannot be interpolated throughout the entire point bar. However, the model created serves as a good framework for a general understanding of a large point bar
2. The facies identified matched those seen previously documented in the literature, and are found in both large and small-scale system. These are: bar top deposits, interbedded heterolithic strata, and the lower bar sand-rich facies. As expected, the ratio of sand to IHS decreases upwards and downstream, though this simplistic definition does not account for events capable of changing the energy and thus the depositional style of the point bar.
3. Variations in these typical stacking patterns are caused by abandonment and cut-off, as evidenced by the geophysical logs form the Bueche area. This is the result of high energy current activity during insipient or active abandonment, and leads to a change in the rate of lateral accretion versus vertical aggradation.

Subsequently, not only is the subsurface stratigraphy of the IHS and sand-rich facies different in these areas (at the apex of the bar), but large inner levees deposited by slow river channel abandonment begin to top the outer perimeter and apex areas of the bar.

4. Abandonment and cut-off from the main river channel were not immediate, but occurred at a slow rate. Though Fisk (1947) originally theorized this, the logs taken at Site B3 are further evidence for this event, as the fining upwards section throughout the log and an absence of sand-rich facies point to periodic flooding events after cut-off began.
5. The goal of better understanding how sediment is transported through large meandering systems was met and expanded upon. Simply put, sands are deposited mostly in the upstream part of the meander loops, and fine-grained sediments are deposited on top and mostly downstream as a result of recirculation after rounding the apex. Though seasonal discharge variability and the bank materials through which the river is cutting may cause a point bar to become asymmetrical and compound in nature, generalized facies trends and packages can be predicted in most areas before abandonment. Even after abandonment when the facies trends become unpredictable, understanding the method of this deposition is made possible based on how the energy of the river, and thus sediment transportation, would change.
6. New information regarding changes in sand quality from the head to the tail of the bar was identified. Sand packages are expected to become progressively less

permeable due to changes in flow performance. Though seemingly identical on the gamma and EC logs, these sands should differ in grain size and sorting.

7. Though the exact depth of reorientation surfaces were unidentifiable in the logs, the data provided from the boreholes in the downstream Woody area shows that basic stratigraphic trends and stacking patterns are maintained within accretionary sets bounded by these surfaces, though the continuity of individual strata across them cannot be known without first knowing the dip angle of the surfaces.

7.2.2 Use as a Modern Analogue to Ancient Systems-Stratigraphically and from an Industry Perspective

1. False River is a useful analog to ancient systems because it shows more accurately how sediment is distributed between large growth events in a compound system.
2. Stratigraphically, position within the bar is likely to be the most important factor regarding fine- scaled heterogeneity.
    a. Although the logs were too far from each other to map individual stratal continuity, this study is useful as a guide when choosing where within a point bar it might be possible to make correlations within the accretionary sets. This is important, because if predictions are to be made possible with respect to ancient systems, the ability to correlate at the bed scale is needed.
    b. Within the False River point bar and the Mississippi River, correlations between facies trends and formational history were possible because of the accuracy and spatial data provided by the DEM. In contrast, 3D seismic data is needed in order to know with accuracy the orientation of a single

well within an ancient system. Thus, the spatial data provided in this analog is greatly needed.

3. Characterizing unique events like those in the geophysical logs from Sites B1, B2 and B3 is critical in a model that is to be used as an analog, especially if the event was cutoff. This shows that in any system cut-off will have a very large impact on depositional style, and variations in sediment heterogeneity must be taken into account, especially when considering the large inner levee deposits caused by the event.
4. When applying this analog as an industry tool, the data from the Jumonville area proves that reservoir quality will be the best in the more headward areas of the bar as a result of the low occurrence of impermeable layers and the presence of characteristic boundaries at expected intervals. Areas at the final stage apex of the bar in the inner levee deposits are unpredictable when compared to those located more headward, and should be avoided as a potential hydrocarbon reservoir. Areas downstream of the apex, as applies to the Woody property, exhibited a large amount of fine-grained, interbedded strata. If quantified and understood these areas could be used for steam assisted gravity drainage (SAGD) operations, as understanding continuity is critical here when considering that fine grained facies at even the centimeter scale can hinder fluid flow.

7.3 Future Research Recommendations

1. Geophysical and geological infilling of data between current borehole locations is recommended as a necessary tool to:
    a. Determine the angle of accretion of the point bar.

b. Assess the continuity of the fine grained interbedded strata within the applicable distance as determined by the angle of accretion.

2. Seismic acquisition efforts by the geophysical team* must be continued as a means to:

    a. Determine the proper seismic acquisition techniques needed for good resolution in a point bar deposit.

    b. Determine the angles of reorientation and accretionary surfaces.

    c. Determine if strata are continuous both within and through reorientation sets.

3. Data from the Geotek MSCL Core Logger must be analyzed and depth aligned with the current log data in order to better classify individual facies.

4. All cores must be split, logged and correlated with the geophysical logs. Facies as determined by the cores must be matched to the Geotek MSCL Core Logger data and the geophysical log data as an additional method of facies interpretation. Ground trothing the geophysical logs is an essential step in deriving the most amount of information from this data source.

5. Samples taken from the cores must be age dated.

    a. The ages of initial bar formation and cut-off are estimated in the literature (Fisk, 1947; Saucier, 1969) and need to be defined more precisely in order to truly understand the time frame of large-scale point bar formation.

* This study is one-half of a joint project between myself (sedimentology) and a geophysical seismic team that is aiming to image the dipping surfaces within the point bar.

a. Age dating in an unamalgamated compound point bar has not been done in depth. Dating from all three borehole properties will aid in understanding why and how quickly compound bars form.

6. Laser particle size analysis (LPSA) needs to be conducted in order to verify inferences make about grain size based on hydraulic conductivity trends within this study.
7. Care must be taken when obtaining geophysical and geological data as pertains to the logging equipment in a point bar setting.
    a. Pressure differentials between the inside and outside of the sample rods may cause loss of recovery during coring. Because of the already saturated nature of the sediments (reflecting the high water table), further introduction of water by dual tube sampling systems should always be avoided, especially when paired with a Roto-Sonic drill rig, as the subsequent fluidization of the sediments results in sample loss when the inner tool string is pulled out.
    b. Though a 6610DT Direct Push machine is adequate for electrical conductivity and hydraulic profile tooling logging, a machine capable of exerting more force is needed if a greater borehole depth is to be reached, such as to the base of a point bar equal in depth and size to False River. However, the Geoprobe 6610DT Direct Push machine is an ideal tool in small-scale point bar systems or in large-scale systems where only the upper interbedded units need to be logged.

c. Gamma logging was a useful and cost effective tool. However, a slower logging speed should be used in future research to eliminate noise within the data

REFERENCES

Bennett, G. D., 1976. Introduction to ground-water hydraulics, a programed text for self instruction. U.S. Geological Survey techniques of water-resources investigations, book 3, ch. B2.

Bernard, H.A., Major, C.F., 1963. Recent meadner belt deposits of the Bazos River: An alluvial "sand" model. American Association of Petroleum Geologists Bulletin, v. 47 (2), p. 350 (abstract).

Brekke, H., and Evoy, R., 2004. Use of Dipmeter data in the definition of the internal architecture of point bar deposits in the Athatbasca oil sands: implications for the Middle McMurray Formation in the Hangingstone Area, Alberta (abst): American Association Petroleum Geologists Annual Meeting, Dallas, v. 13, p. 17.

Bridges, P.H. and Leeder, M.R., 1976. Sedimentary model for intertidal mudflat channels, with examples from the Solway Firth, Scotland. Sedimentology, v 23, p. 533-552.

Blum, M. D., Martin, J., Milliken, K. and Garvin, M., 2013. Paleovalley systems: Insights from Quaternary analogs and experiments. Earth Science Reviews, v. 116, p. 128-169, doi: 10.1016/j.earscirev.2012.09.003.

Blum, M. D., and Roberts, H. H., 2012. The Mississippi delta region: past, present, and future. The Annual Review of Earth and Planetary Sciences, v. 40, p. 655-683, doi: 10.1146/annurev-earth-042711-105248

Coleman, J.M., 1966. Ecological changes in a massive fresh-water clay sequence. Transactions, Gulf Coast Association of Geological Societies XVI, 159-174.

Connolly, W.M., Mazzullo, J., 1986. Morphology and sedimentology of a central Brazos River point bar, Boxley Bend, Brazos County, Texas. American Association of Petroleum Geology Bulletin, v. 70 (9).

Davies, D.K., 1966. Sedimentary Structures and Subfacies of a Mississippi River Point Bar. The Journal of Geology, v. 74 (2), p. 234-239.

Diaz- Molina, M., 1993. Geometry and lateral accretion patterns in meander loops: examples from the Upper Oligocene- Lower Miocene, Loranca Basin, Spain. Special Publications International Association of Sedimentologists, v. 17, p. 115-131.

Direct Image, 1994. A Percussion Probing Tool For the Direct Sensing of Soil Conductivity. Geoprobe® Technical Paper No. 94-100.

Ensmigner, P, A., 1998. Bathymetric survey and physical and chemical-related properties of False River, Louisiana, June and July 1998. U.S. Geological Survey, U.S. Department of the Interior, Water-Resources Investigations Report 99-4193.

Farrell, K.M., 1987. Sedimentology and facies architecture of overbank deposits of the Mississippi River, False River region, Louisiana. *In*: Etheridge, F.G., Flores, R.M., and Harvey, M.D. (eds): Recent development in fluvial sedimentology. Society of Economic Paleontologists and Mineralogists Special Publication 39, p. 111-120.

Fisk, H.N., 1944. Geological investigations of the alluvial valley of the Lower Mississippi River. U.S. Army Corps of Engineers, Mississippi River Commission, Vicksburg, MS, p. 1-69.

Fisk, H.N., 1947. Fine-grained alluvial deposits and their effect on Mississippi River Activity. U.S. Army Corps of Engineers, Mississippi River Commission, Waterways Experiment Station, Vicksburg, MS, v. 1, p. 1-82.

Friend, P.F., Slater, M.J., and Williams, R.C., 1979. Vertical and lateral building of river sandstone bodies, Ebro Basin, Spain. Journal of the Geological Society of London 136, p. 39–46.

Fustic, M., Hubbard, S.M., Spencer, R., Smith, D.G., Leckie, D.A., Bennett, B., and Larter, S., 2012. Recognition of down-valley translation in tidally influenced meandering fluvial deposits, Athabasca Oil Sands (Cretaceous), Alberta, Canada. Marine and Petroleum Geology, v. 29, p. 219-232.

Fustic, M., 2007. Stratigraphic dip analysis- a novel application for detailed geological modeling of point bars and predicting bitumen grade, McMurray Formation, Muskeg River Mine, Northeast Alberta. Natural Resources Research, v. 16, No. 1, March 2007.

Gibling, M. R., and B. R. Rust. 1993. "Alluvial ridge-and-swale topography; a case study from the Morien Group of Atlantic Canada." Special Publication of the International Association of Sedimentologists, v. 17, p. 133-150.

Gibling, M. R., 2006. Width and thickness of fluvial channel bodies and valley fills in the geological record: a literature compilation and classification. Society for Sedimentary Geology, v. 76 (5), p. 731-770, doi: 10.2110/jsr.2006.060.

Gesch, D., Oimoen, M., Greenlee, S., Nelson, C., Steuck, M., and Tyler, D., 2002. The National Elevation Dataset. Journal of the American Society for Photogrammetry and Remote Sensing, v. 68 (1).

Gouw, M.J.P., 2007. Alluvial architecture of fluvio-deltaic succession: a review with special reference to Holocene setting. Netherlands Journal of sciences, v. 86, p. 221-227.

Gouw, M.J.P., Autin, W.J., 2008. Alluvial architecture of the Holocene Lower Mississippi Valley (U.S.A.) and a comparison with the Rhine-Muse delta (Netherlands). Sedimentary Geology, v. 204, p. 106-121, doi: 10.1016/j.sedgeo.2008.01.003.

Howell, A.L., Bentley, S.J., Xu, K., Ferrell, R.E., Muhammad, Z., and Septama, E., 2014. Fine sediment mineralogy as a tracer of latest Quaternary sediment delivery to a dynamic continental margin: Pandora Trough, Gulf of Papua, Papua New Guinea. Marine Geology, v. 357, p. 108-122.

Hubbard, S.M., Smith, D.G., Nielsen, H., Leckie, D.A., Fustic, M., Spencer, R.J., Bloom, L., 2011. Seismic geomorphology and sedimentology of a tidally influenced river deposit, Lower Cretaceous Athabasca oil sands, Alberta, Canada. The American Association of Petroleum Geologists Bulletin, v. 95 (7), p. 1123-1145.

Jackson II, R.G. 1975. Velocity-bedform-texture patterns of meander bends in the lower Wabash River of Illinois and Indiana. Geological Society of America Bulletin, v. 86, p. 1511–1522.

Jackson II, R.G., 1981. Sedimentology of muddy fine-grained channel deposits in meandering streams of the American Middle West. Journal of Sedimentary Petrology, v. 51, p. 1169–1192.

Jordan, D.W., and Pryor, W.A., 1992. Hierarchical levels of heterogeneity in a Mississippi River meander belt and application to reservoir systems. American Association of Petroleum Geologists, Bulletin 76, p. 1601–1624.

Labrecque, P.A., Hubbard, S. M., Jensen, J.K., and Nielsen, H., 2011. Sedimentology and stratigraphic architecture of a point bar deposit, Lower Cretaceous McMurrary Formation, Alberta, Canada. Bulletin of Canadian Petroleum Geology, v. 59(2). p. 147-171, doi: 10.2113/gscpgbull.59.2.147.

Langbein, W.B., and Leopold, L.B., 1966. River meanders- theory of minimum variance. Physiographic and hydraulic studies of rivers, Geological Survey Professional Paper 422-H, United States Government Printing Office, Washington.

McCall, W., 1996. Electrical conductivity logging to determine control of hydrocarbon flow paths in alluvial sediments. Paper presented at: Outdoor Action Conference. NGA 1996: National Groundwater Association Annual Meeting; Las Vegas, NV. [accessed 2015 June 22]. http://geoprobe.com/literature/electrical-conductivity-paper-by-wes-mccall-ms.

McCall, W., 2011. Application of the Geoprobe® HPT logging system for geo-environmental investigations. Geoprobe® Technical Bulletin No. MK3184, p. 1-35.

Musial, R.G., Reynaud, J., Murray, G.K., Fenies, H., Labourdette, R., and Parize, O., 2012. Subsurface and outcrop characterization of large tidally influenced point bars of the Cretaceous McMurray Formation (Alberta, Canada). Sedimentary Geology, v. 279, p.156-172.

Nanson, G.C., 1980. Point bar and floodplain formation of the meandering Beatton River, Northeastern British Columbia, Canada. Sedimentology, v. 27(1), p. 3-29, doi: 10.1111/j.1365-3091.1980.tb01155.x.

Paola, C., Parker, G., Seal, R., Sinha, S.K., Southard, J.B., and Wilcock, P.R. 1992. Downstream fining by selective deposition in a laboratory flume.
Science, v. 258, p. 1757–1760.

Reading, (1986). Sedimentary environments and Facies. Blackwell Scientific Publications, Oxford, London, p. 20-54.

Renslow, M.S., 2012. Manual of airborne topographic LIDAR. Imaging and Geospatial Information Society, p. 246.

Revil, A., Glover, P.W.J., 1998. Nature of surface and electrical conductivity in natural sands, sandstones, and clays. Geophysical Research Letters, v. 25 (5), p 691-694.

Rittenour, T.M., Blum, M.D., Goble, R.J., 2007. Fluvial evolution of the lower Mississippi River valley during the last 100-kyr glacial cycle: response to glaciation and sea- level change. Geological Society of American Bulletin, v(119, p. 586-608.

Saucier, R. T., 1969. Geological investigation of the Mississippi River area, Artonish to Donaldsonville, LA. Technical Report S-69-4, U.S. Army Corps of Engineers, Waterways Experiment Station, Vicksburg, MS.

Saucier, R.T., 1974. Quaternary geology of the Lower Mississippi Valley. Arkansas Archeological Survey Research Series 6, p. 0-28.

Saucier, R.T., 1994. Geomorphology and Quaternary geologic history of the Lower Mississippi Valley. U.S. Army Corps of Engineers, Waterways Experiment Station, Vicksburg, MS, v. 1, p. 0-364.

Smith, D.G., Hubbard, S.M., Leckie, D.A., and Fustic, M., 2009. Counter point-bar deposits: Lithofacies and reservoir significance in the meandering modern Peace River and ancient McMurray Formation, Alberta, Canada. Sedimentology, V. 56, p. 1655-1669, doi: 10.1111/j.1365-3091.2009.01050.x.

Smith, D.G, Hubbard, S.M., Lavigne, J.R., Lecki, D.A., and Fustic, M., 2011. Stratigraphy of counter- point- bar and eddy- accretion deposits in low- energy meander belts of the Peace- Athabasca Delta, northeast Alberta, Canada. Society of Sedimentary Geology, Special Publication No. 97.

Strobl, R.S., Muwais, W.K., Wightman, D.M., Cotterill, D.K. and Yuan, L., 1997. Geological modeling of McMurray Formation reservoirs based on outcrop and subsurface analogues. In: Petroleum Geology of the Cretaceous Mannville Group, Western Canada. S.G.

Pemberton and D.P. James (eds.). Canadian Society of Petroleum Geologists, Memoir 18, p. 292–311.

Thomas, R.G., Smith, D.G., Wood, J.M., Visser, J., Calverley-Range, E.A. and Koster, E.H. 1987. Inclined heterolithic stratification-terminology, description, interpretation and significance. Sedimentary Geology, v. 53, p. 123–179.

Willis, B.J. 1989. Palaeochannel reconstructions from point bar deposits: a three-dimensional perspective. Sedimentology, v. 36, p. 757–766.

Willis, B.J., Tang, H, 2010. Three-dimensional connectivity of point-bar deposits. Journal of Sedimentary Research. v. 80, p. 440-454.

Zinger, J.A., Rhoads, B.L., and Best, J.L., 2011. Extreme sediment pulses generated by bend cutoffs along a large meandering river. Nature Geoscience, v. 4, p. 675-678, doi: 10.1038/NGEO1260.

APPENDIX A: PETREL 3D GRID INPUT AND SETTINGS

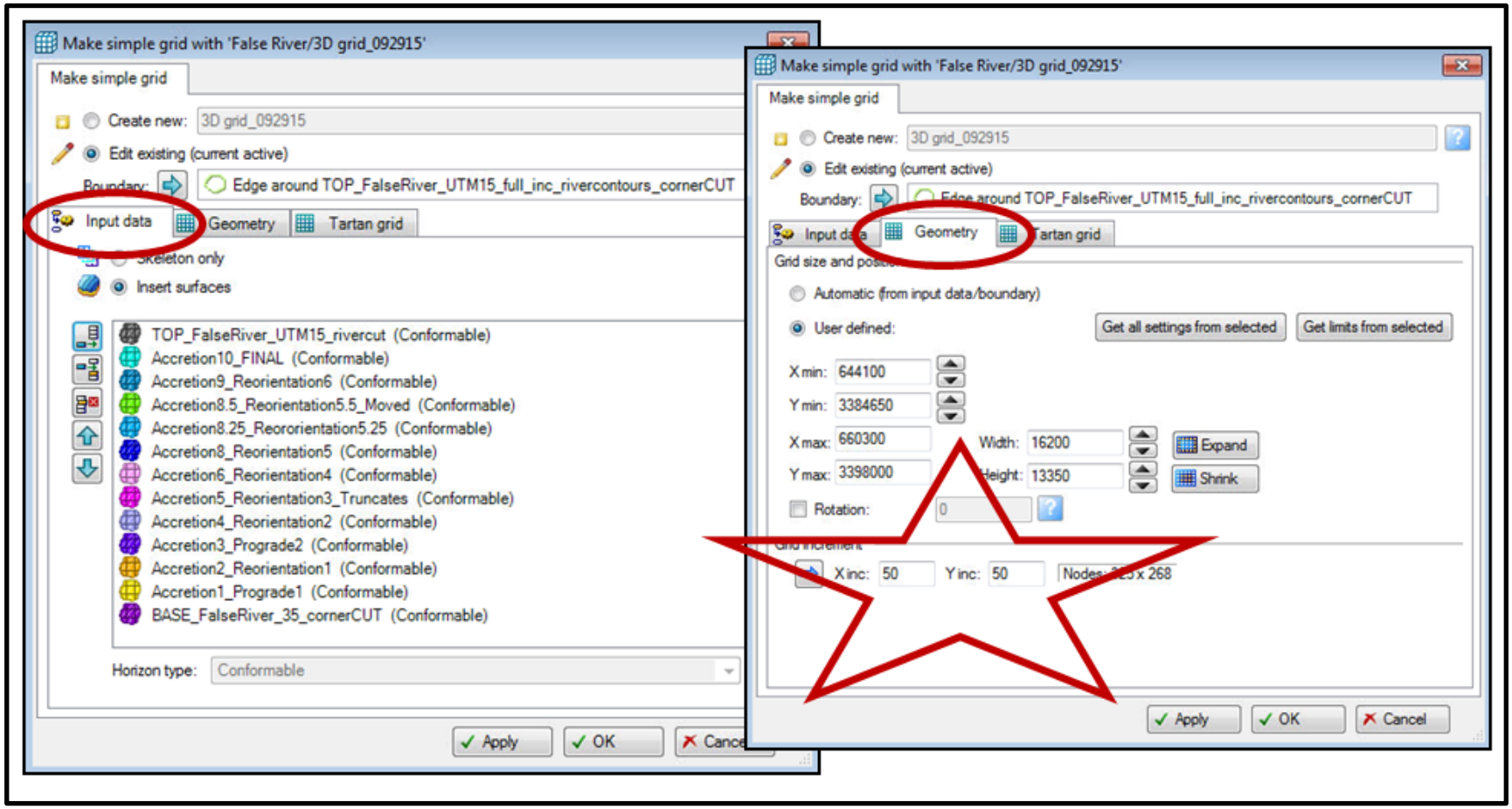

A.1. 3D grid input and geometry settings for the model of False River.

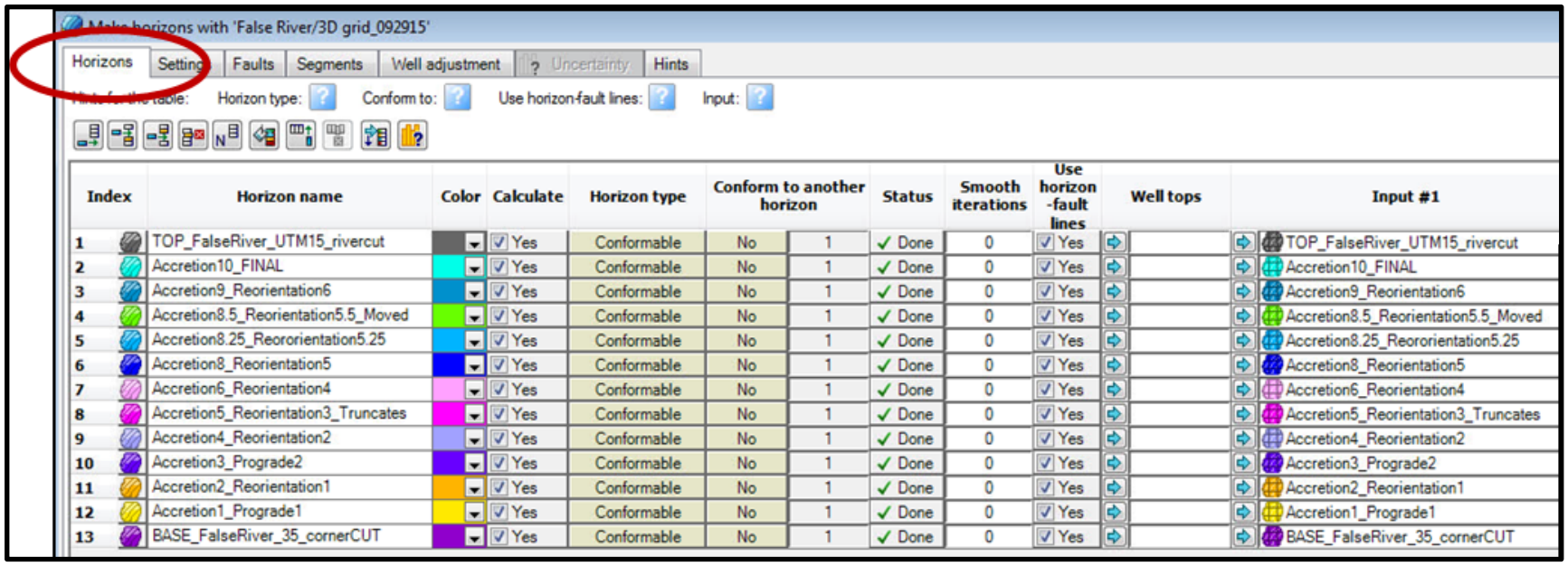

Index	Horizon name	Color	Calculate	Horizon type	Conform to another horizon		Status	Smooth iterations	Use horizon-fault lines	Well tops	Input #1
1	TOP_FalseRiver_UTM15_rivercut		Yes	Conformable	No	1	Done	0	Yes		TOP_FalseRiver_UTM15_rivercut
2	Accretion10_FINAL		Yes	Conformable	No	1	Done	0	Yes		Accretion10_FINAL
3	Accretion9_Reorientation6		Yes	Conformable	No	1	Done	0	Yes		Accretion9_Reorientation6
4	Accretion8.5_Reorientation5.5_Moved		Yes	Conformable	No	1	Done	0	Yes		Accretion8.5_Reorientation5.5_Moved
5	Accretion8.25_Reororientation5.25		Yes	Conformable	No	1	Done	0	Yes		Accretion8.25_Reororientation5.25
6	Accretion8_Reorientation5		Yes	Conformable	No	1	Done	0	Yes		Accretion8_Reorientation5
7	Accretion6_Reorientation4		Yes	Conformable	No	1	Done	0	Yes		Accretion6_Reorientation4
8	Accretion5_Reorientation3_Truncates		Yes	Conformable	No	1	Done	0	Yes		Accretion5_Reorientation3_Truncates
9	Accretion4_Reorientation2		Yes	Conformable	No	1	Done	0	Yes		Accretion4_Reorientation2
10	Accretion3_Prograde2		Yes	Conformable	No	1	Done	0	Yes		Accretion3_Prograde2
11	Accretion2_Reorientation1		Yes	Conformable	No	1	Done	0	Yes		Accretion2_Reorientation1
12	Accretion1_Prograde1		Yes	Conformable	No	1	Done	0	Yes		Accretion1_Prograde1
13	BASE_FalseRiver_35_cornerCUT		Yes	Conformable	No	1	Done	0	Yes		BASE_FalseRiver_35_cornerCUT

A.2. Horizons settings for the False River 3D grid model.

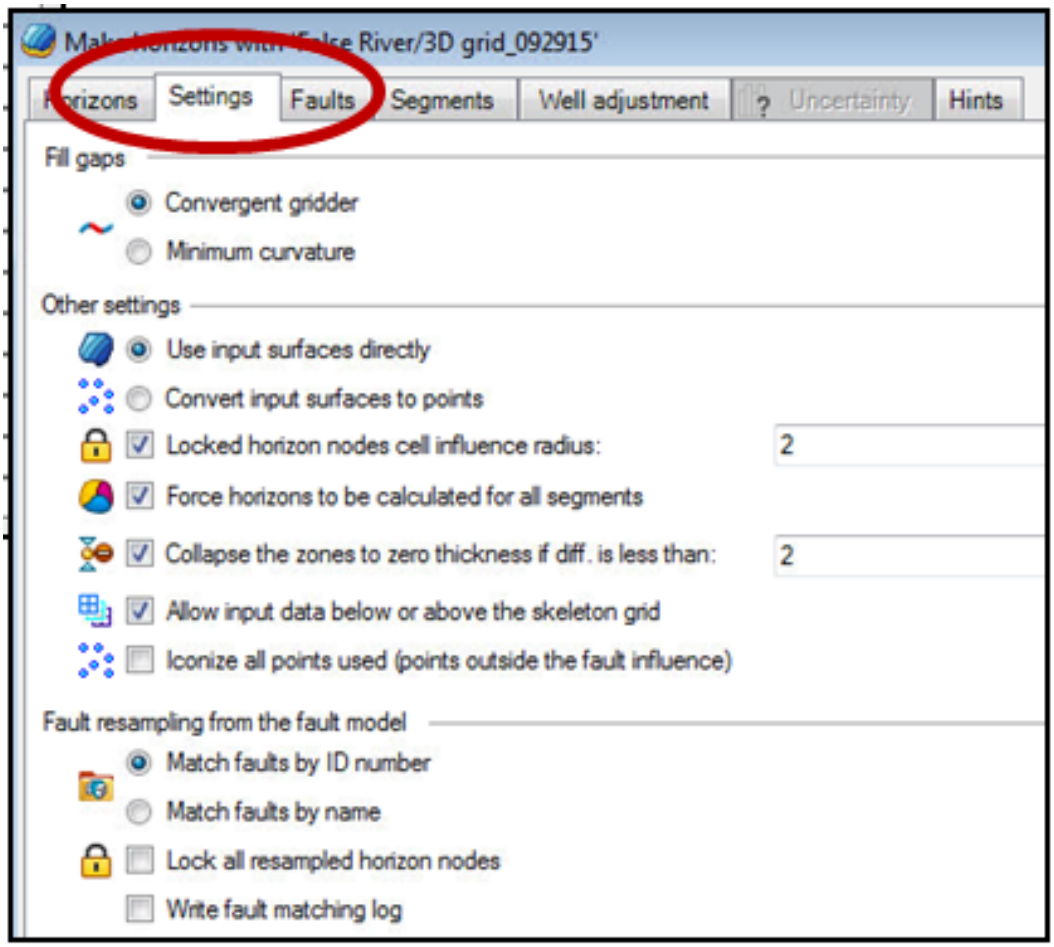

A.3. Horizons settings for the False River 3D model.

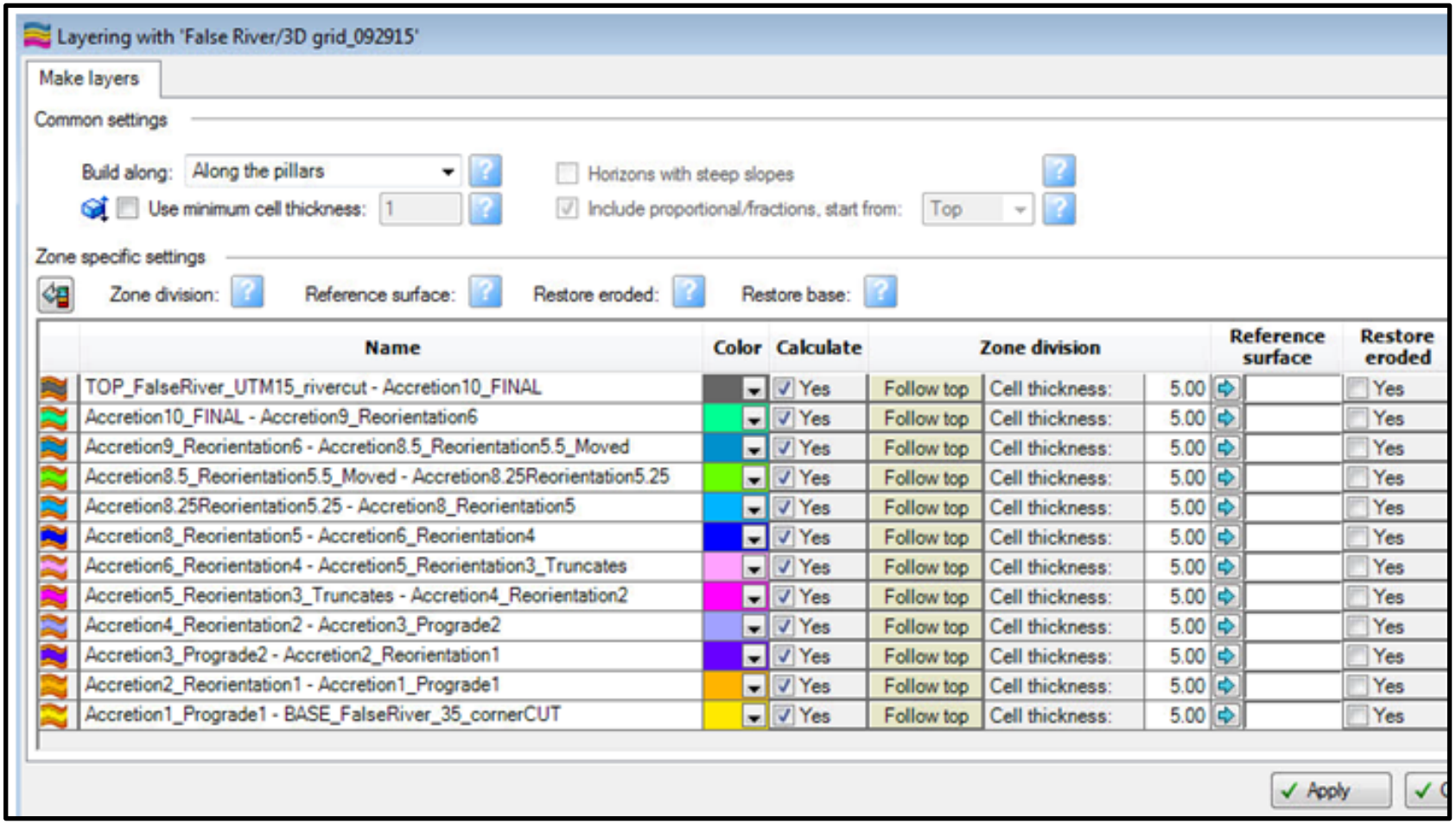

A.4. Layering settings for the False River 3D model.

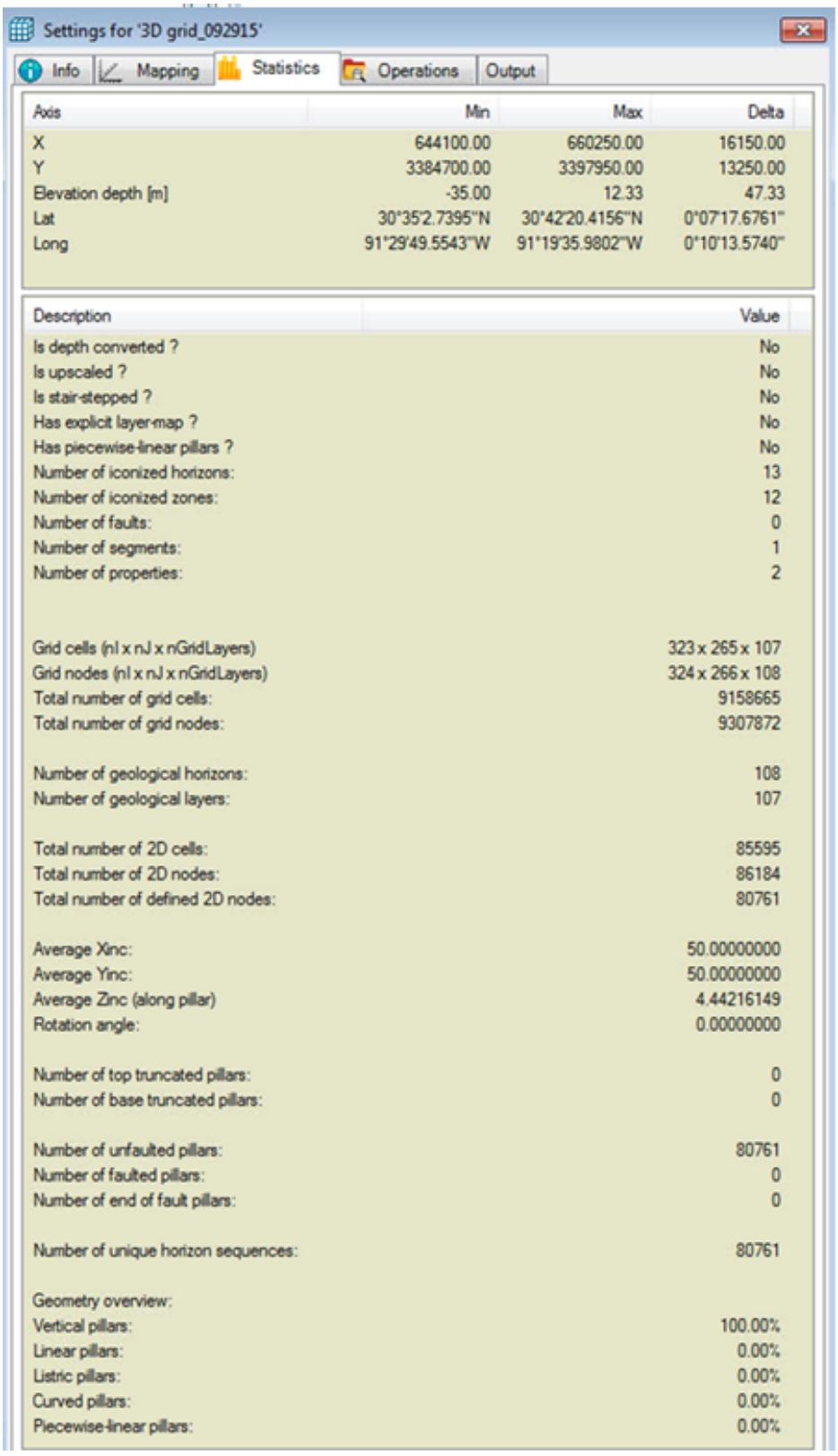

Axis	Min	Max	Delta
X	644100.00	660250.00	16150.00
Y	3384700.00	3397950.00	13250.00
Elevation depth [m]	-35.00	12.33	47.33
Lat	30°35'2.7395"N	30°42'20.4156"N	0°07'17.6761"
Long	91°29'49.5543"W	91°19'35.9802"W	0°10'13.5740"

Description	Value
Is depth converted ?	No
Is upscaled ?	No
Is stair-stepped ?	No
Has explicit layer-map ?	No
Has piecewise-linear pillars ?	No
Number of iconized horizons:	13
Number of iconized zones:	12
Number of faults:	0
Number of segments:	1
Number of properties:	2
Grid cells (nI x nJ x nGridLayers)	323 x 265 x 107
Grid nodes (nI x nJ x nGridLayers)	324 x 266 x 108
Total number of grid cells:	9158665
Total number of grid nodes:	9307872
Number of geological horizons:	108
Number of geological layers:	107
Total number of 2D cells:	85595
Total number of 2D nodes:	86184
Total number of defined 2D nodes:	80761
Average Xinc:	50.00000000
Average Yinc:	50.00000000
Average Zinc (along pillar)	4.44216149
Rotation angle:	0.00000000
Number of top truncated pillars:	0
Number of base truncated pillars:	0
Number of unfaulted pillars:	80761
Number of faulted pillars:	0
Number of end of fault pillars:	0
Number of unique horizon sequences:	80761
Geometry overview:	
Vertical pillars:	100.00%
Linear pillars:	0.00%
Listric pillars:	0.00%
Curved pillars:	0.00%
Piecewise-linear pillars:	0.00%

A.5. 3D grid model settings.

APPENDIX B: SECTOR MODEL PROPERTIES

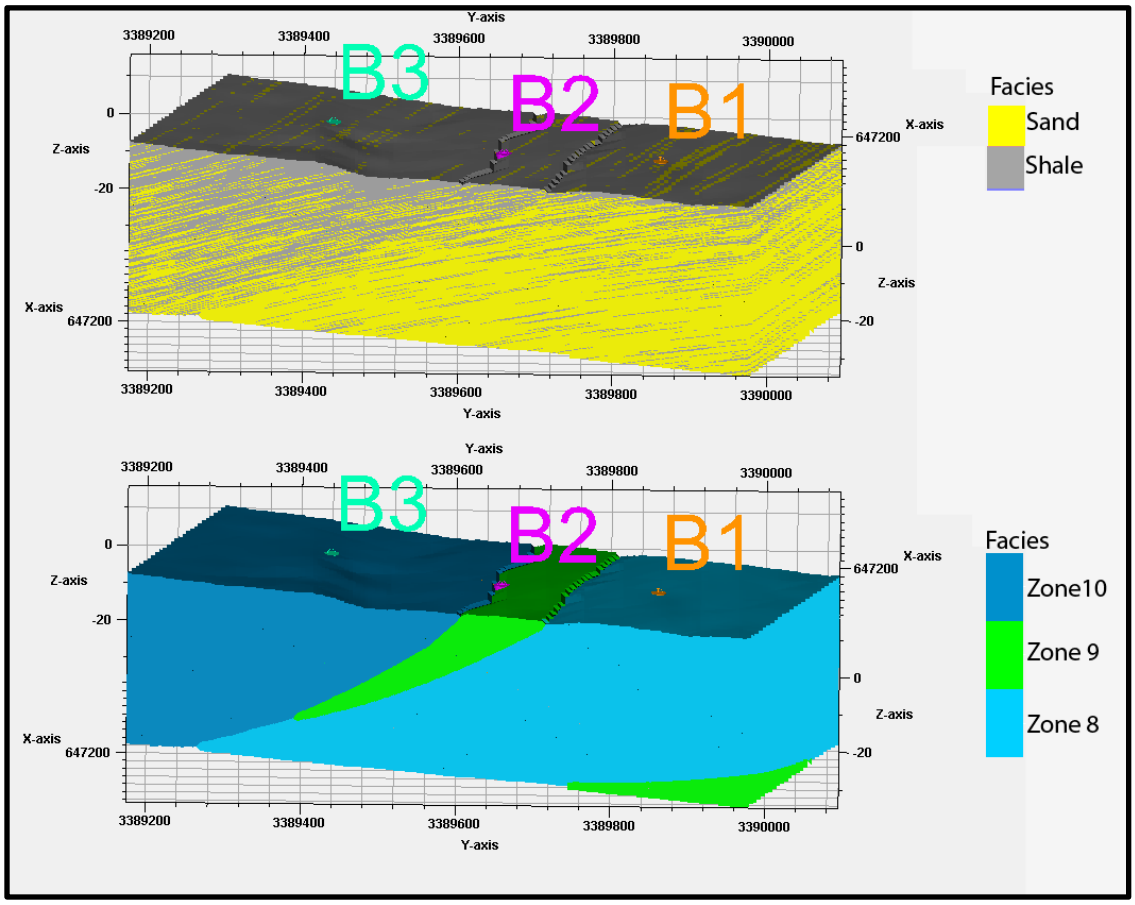

B.1. Sector model from Bueche property displaying the facies (top) and zones (bottom) properties. Vertical exaggeration is 5.

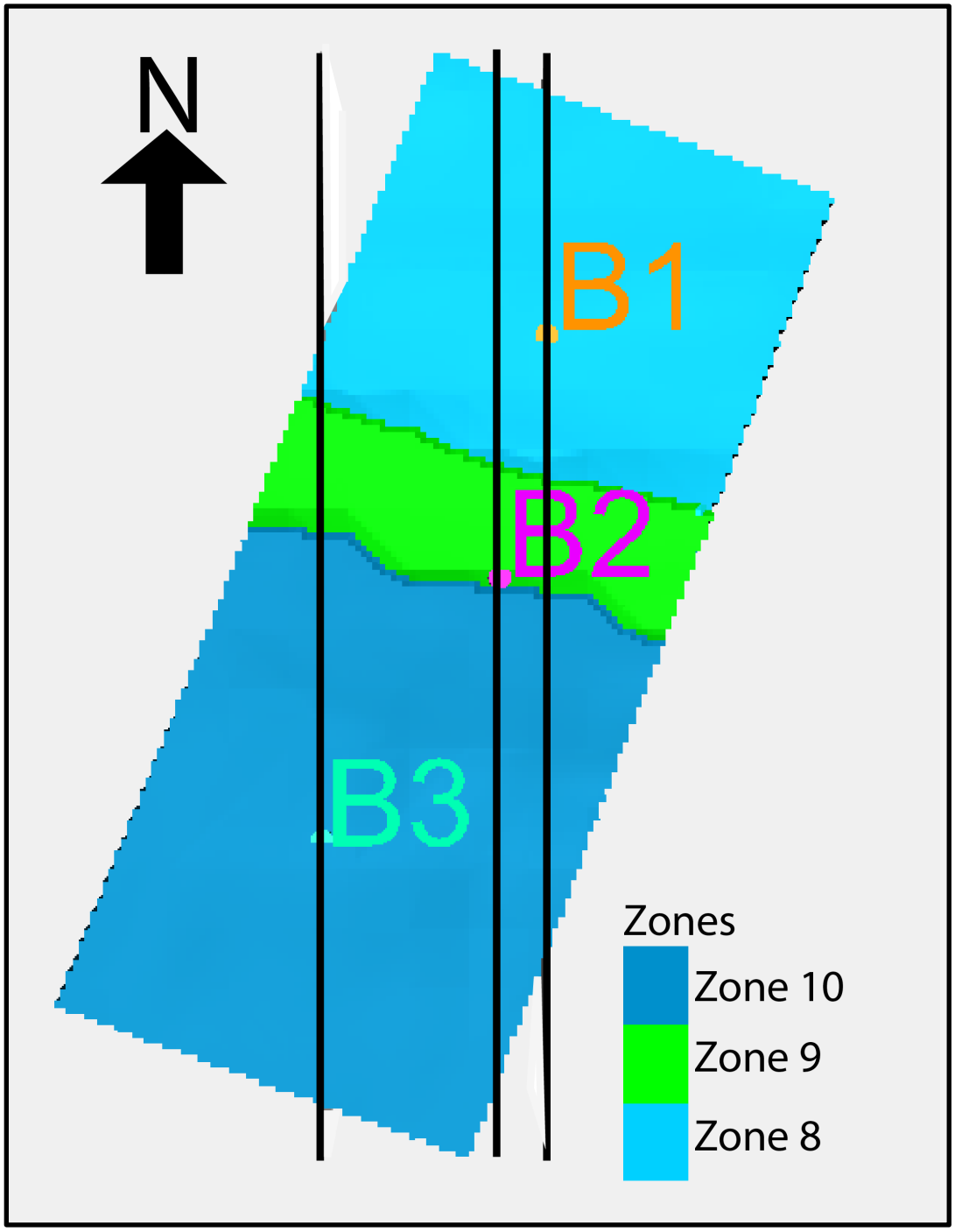

B.2. Cross section location through each of the Bueche borehole Sites within the Bueche sector model. Vertical exaggeration is 5.

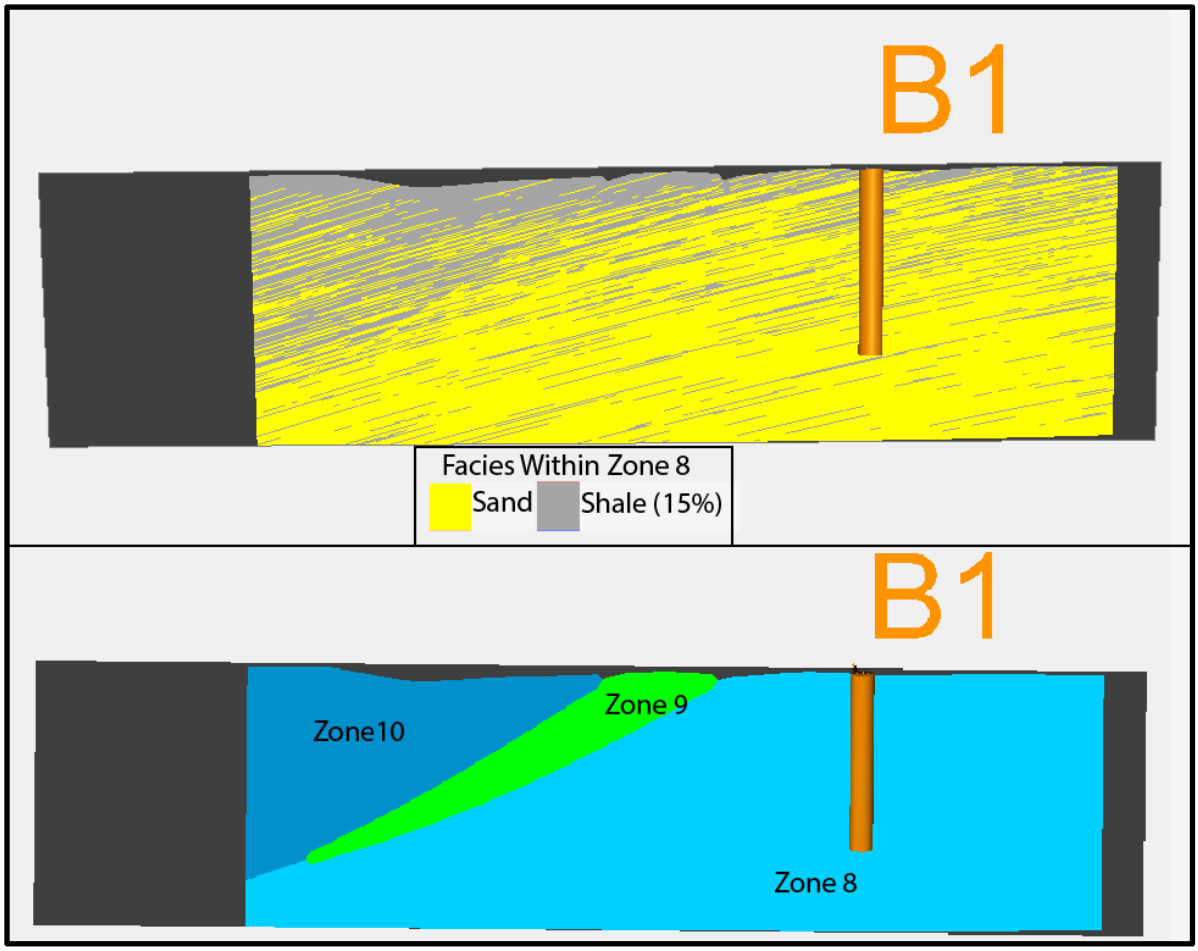

B.3. Cross section through B1 with the facies (top) and zones (bottom) displayed. The location of the cross section is displayed in Figure B.2 and runs from N to S. Vertical exaggeration is 5.

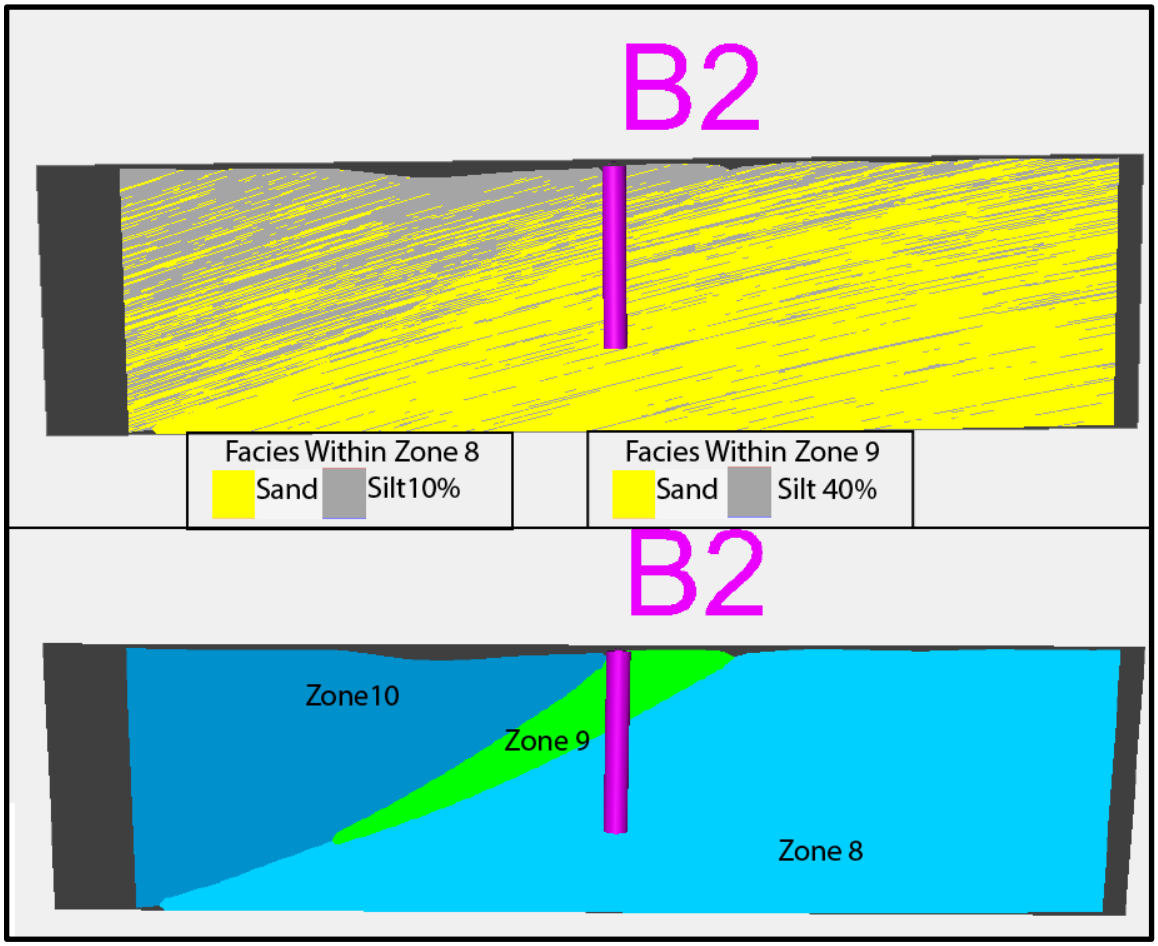

B.4. Cross section through B2 with the facies (top) and zones (bottom) displayed. The location of the cross section is displayed in Figure B.2 and runs from N to S. Vertical exaggeration is 5.

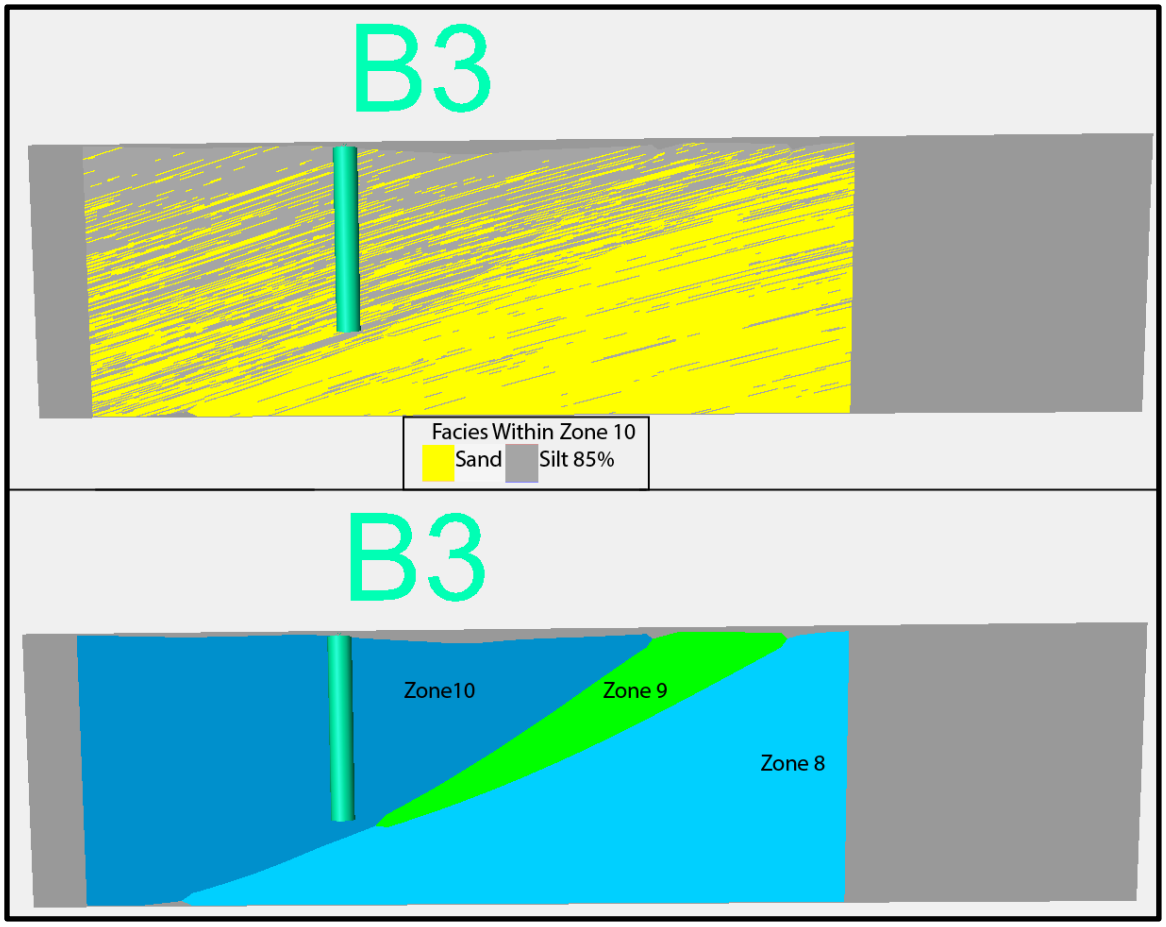

B.5. Cross section through B3 with the facies (top) and zones (bottom) displayed. The location of the cross section is displayed in Figure B.2 and runs from N to S. Vertical exaggeration is 5. The grey section on each side of the sector model is the remainder of the intersection window, and is not part of the silt facies.

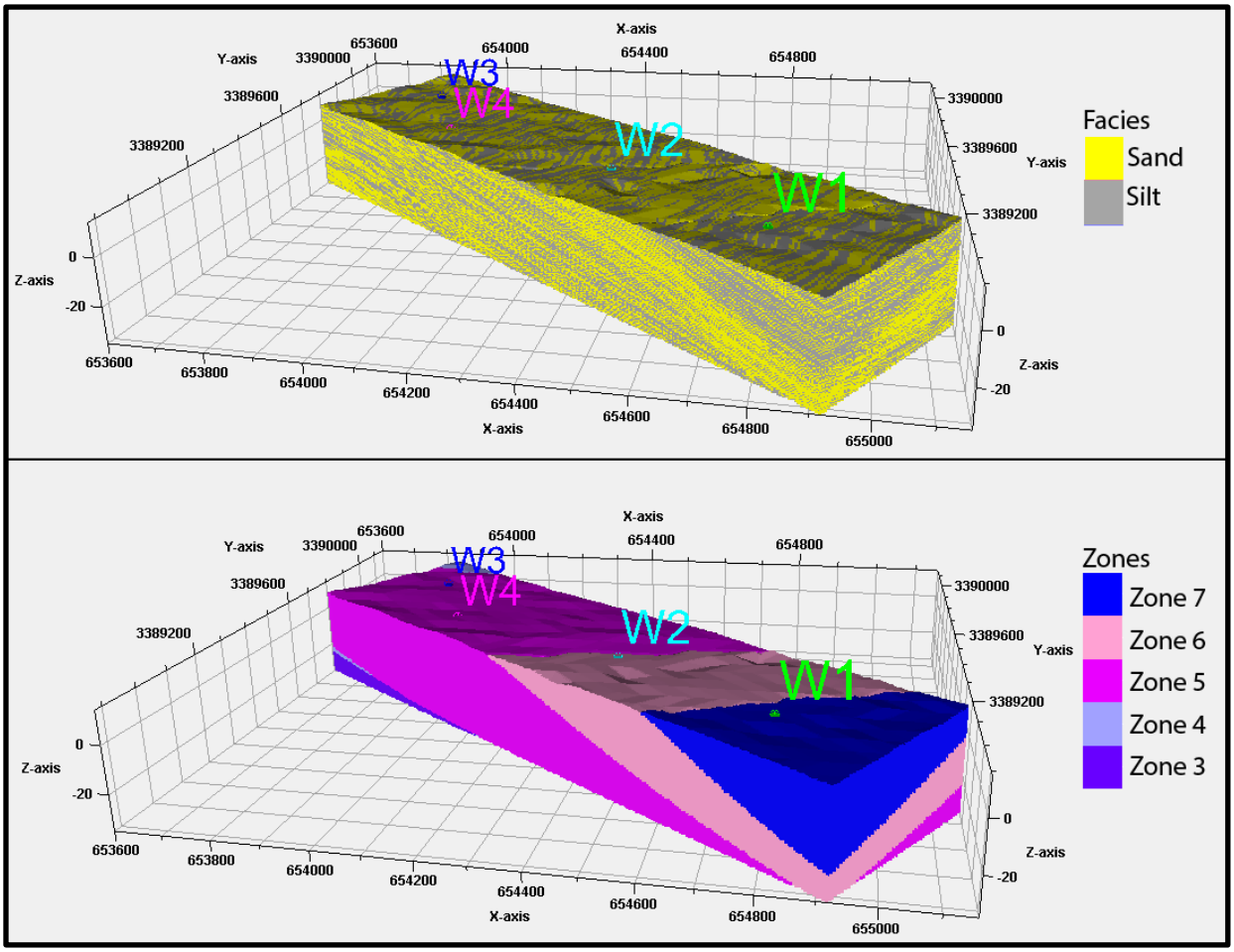

B.6. Sector model from the Woody property displaying the facies (top) and zones (bottom) properties. Vertical exaggeration is 5.

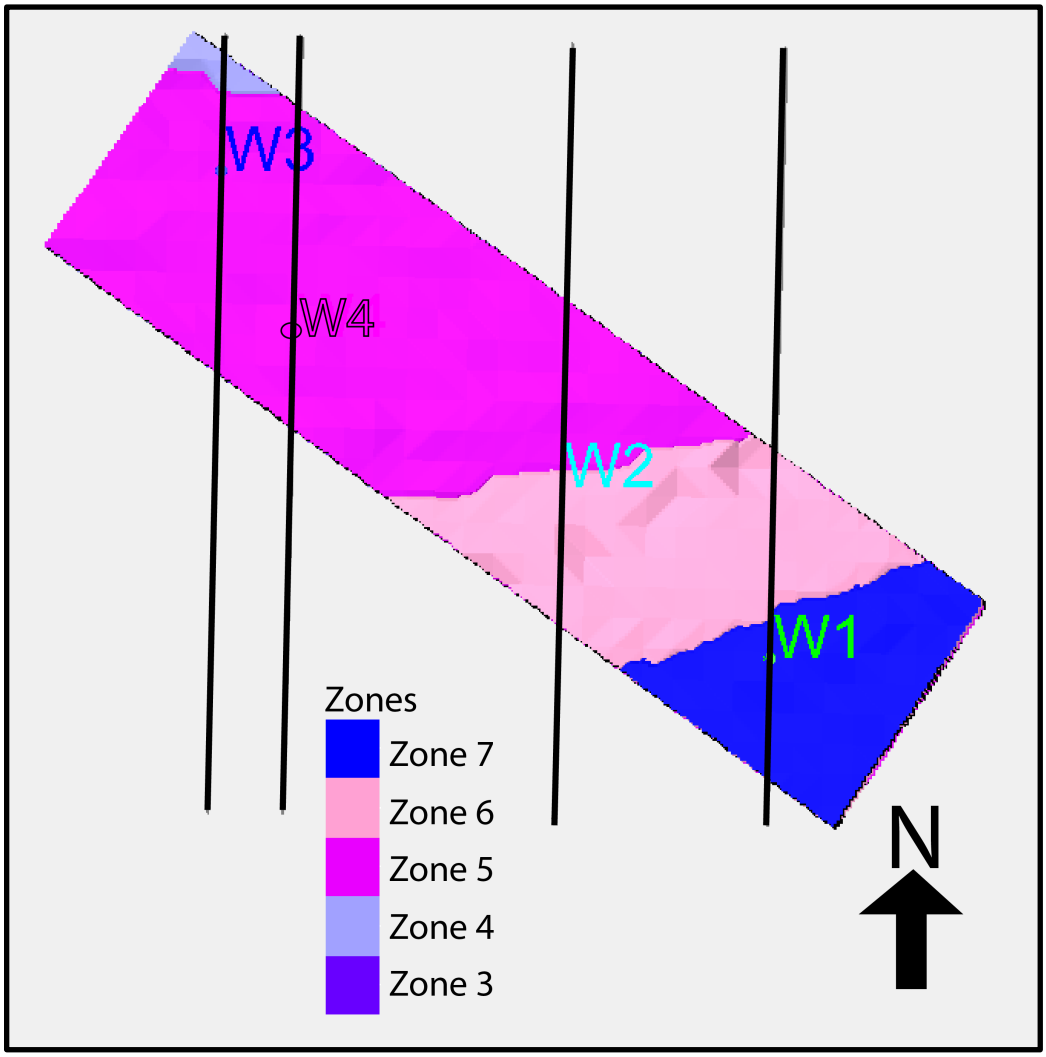

B.7. Cross section location through each of the Woody borehole Sites within the Woody sector model.

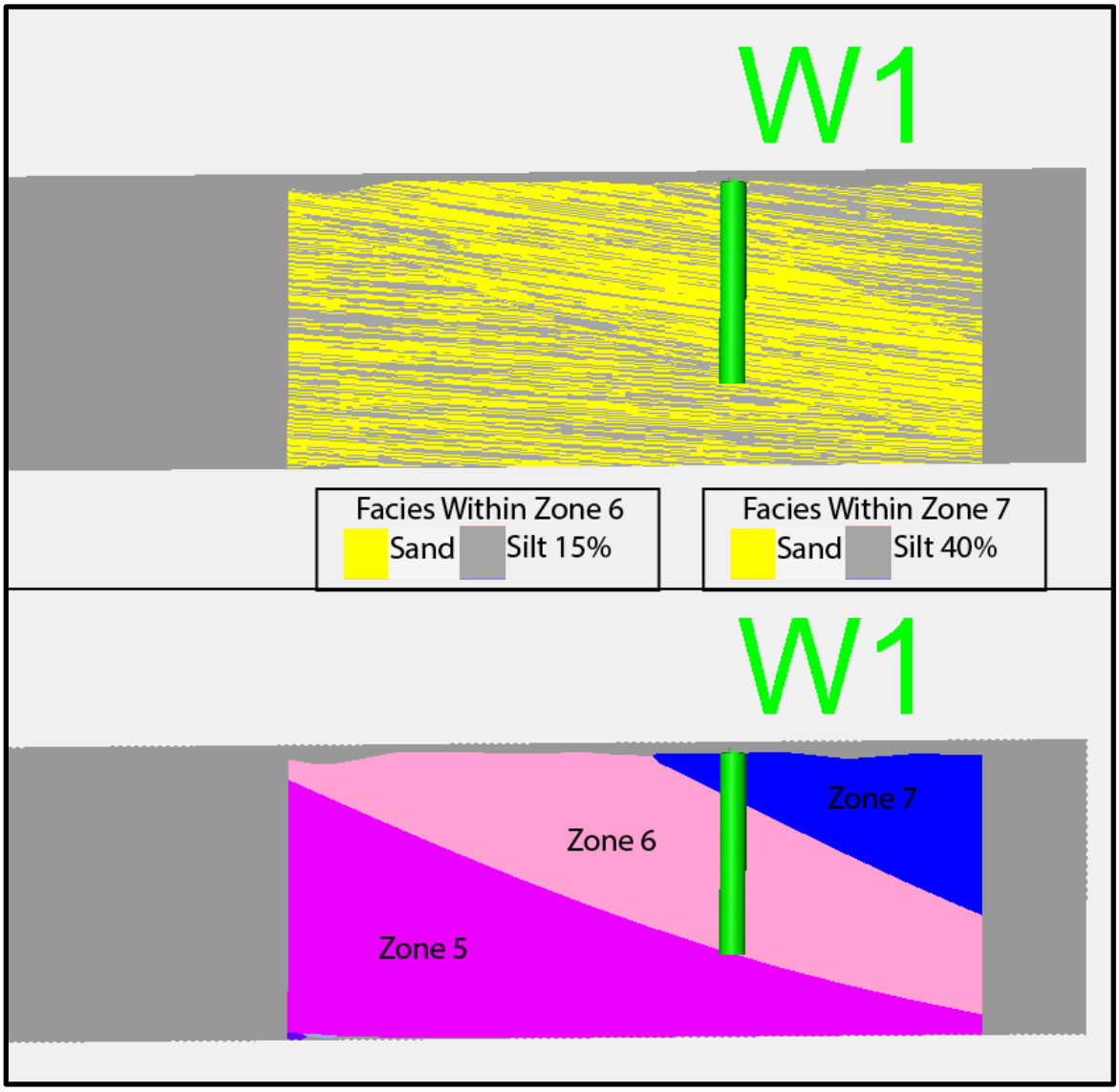

B.6. Cross section through W1 with the facies (top) and zones (bottom) displayed. The location of the cross section is displayed in Figure B.7 and is oriented SW to NE from left to right. Vertical exaggeration is 5. The grey section on each side of the sector model is the remainder of the intersection window, and is not part of the silt facies.

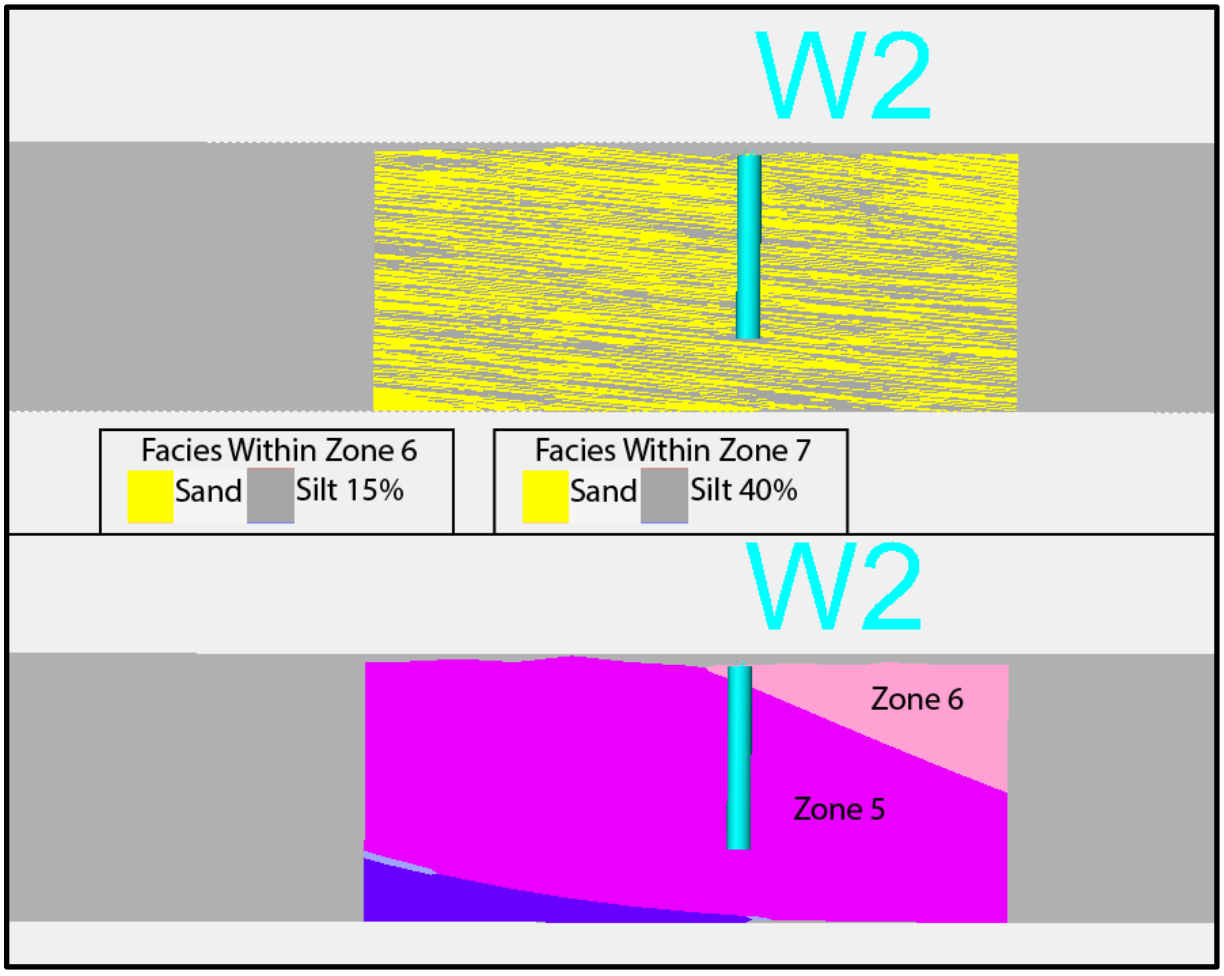

B.7. Cross section through W2 with the facies (top) and zones (bottom) displayed. The location of the cross section is displayed in Figure B.7 and is oriented SW to NE from left to right.. Vertical exaggeration is 5. The grey section on each side of the sector model is the remainder of the intersection window, and is not part of the silt facies.

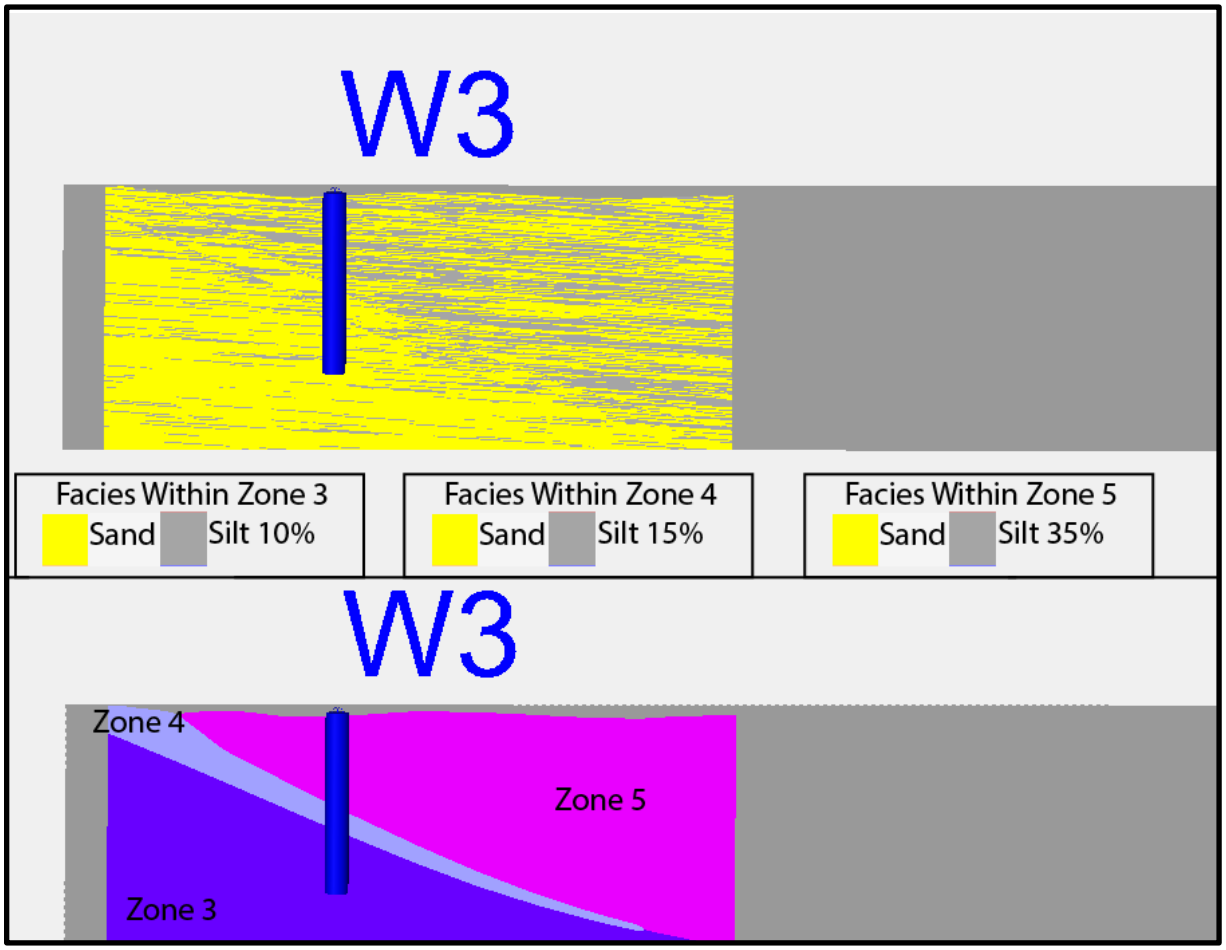

B.8. Cross section through W3 with the facies (top) and zones (bottom) displayed. The location of the cross section is displayed in Figure B.7 and is oriented SW to NE from left to right..Vertical exaggeration is 5. The grey section on each side of the sector model is the remainder of the intersection window, and is not part of the silt facies.

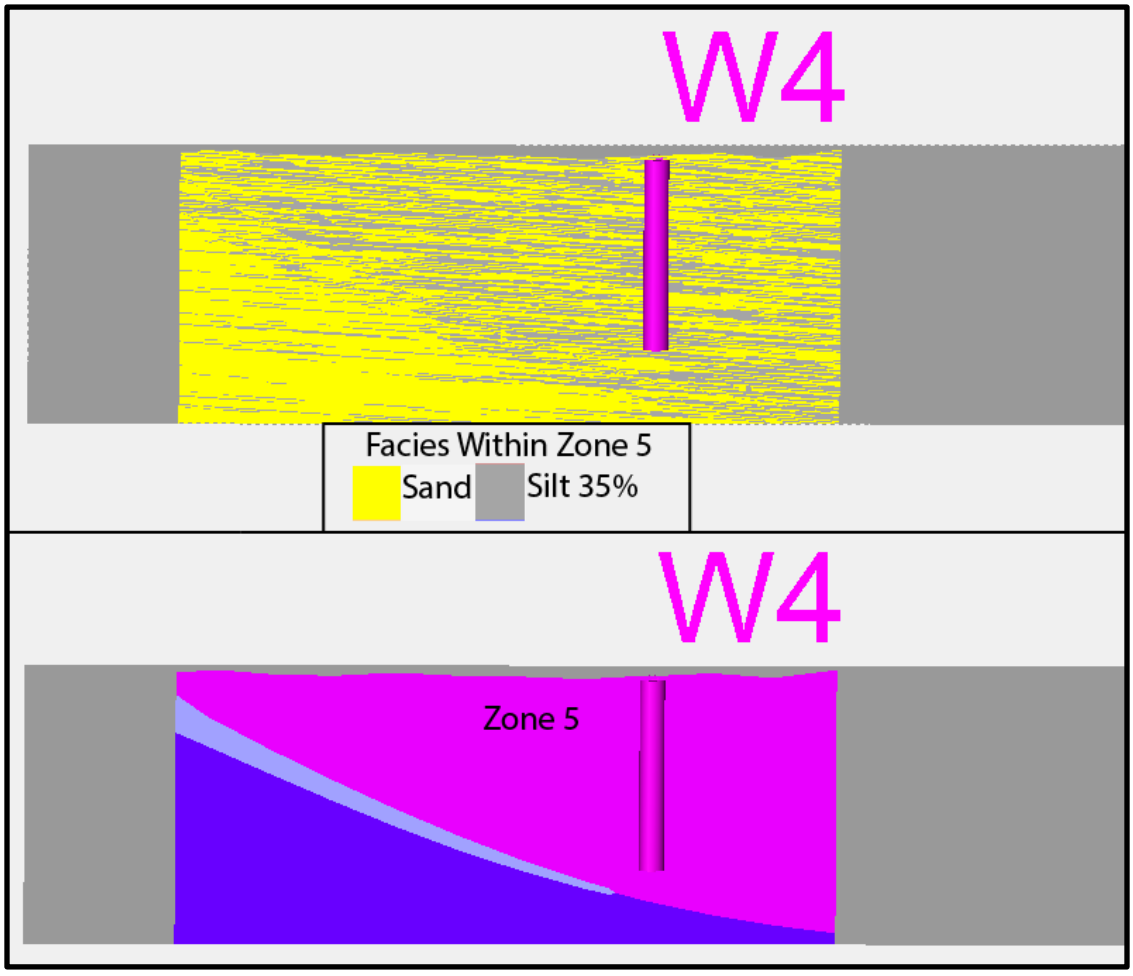

B.9. Cross section through W4 with the facies (top) and zones (bottom) displayed. The location of the cross section is displayed in Figure B.7 and is oriented SW to NE from left to right. Vertical exaggeration is 5. The grey section on each side of the sector model is the remainder of the intersection window, and is not part of the silt facies.

APPENDIX C: REMAINING EC AND K COMPARISON GRAPHS

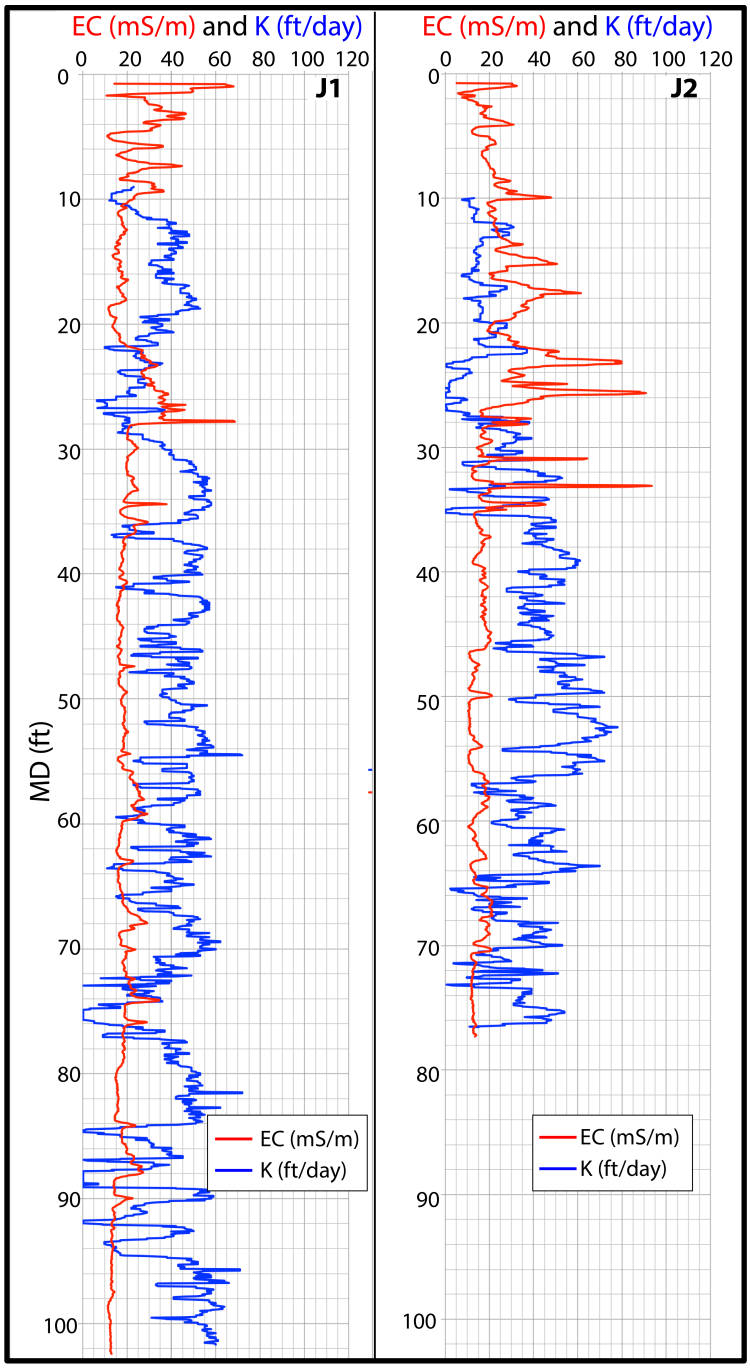

B.1. Stacked electrical conductivity (EC) and hydraulic conductivity (K) graphs from Sites J1 and J2.

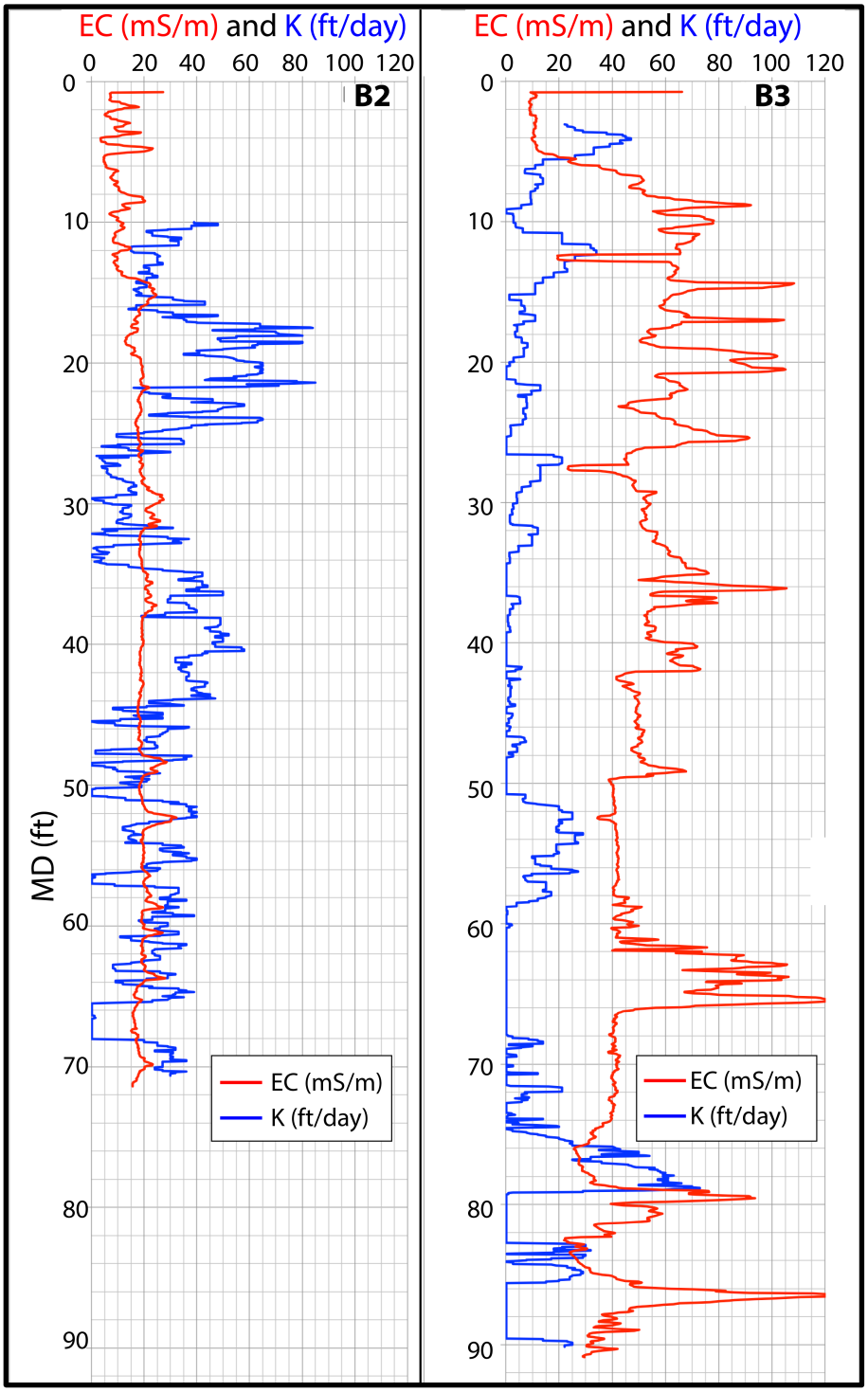

C.2. Stacked electrical conductivity (EC) and hydraulic conductivity (K) graphs from Sites B2 and B3.

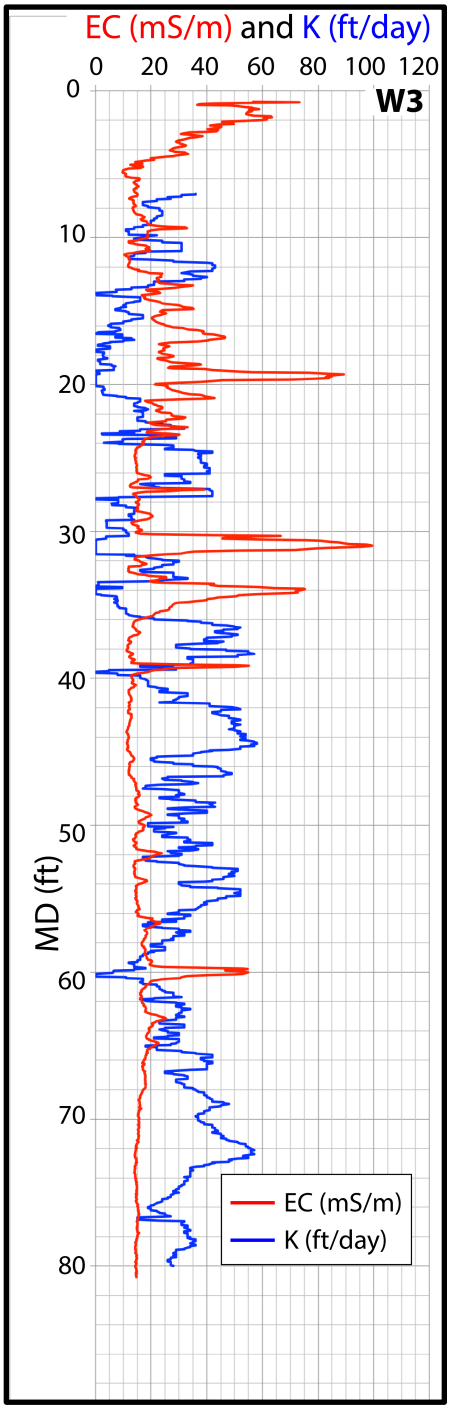

C.3. Stacked electrical conductivity (EC) and hydraulic conductivity (K) graphs from Site W3.

VITA

Alexandra Lechnowskyj was born and raised in San Diego, California. It was there that she began her studies to become a geologist, and graduated with an undergraduate degree in Engineering Geology from San Diego State University. She moved to Baton Rouge, LA, in Fall of 2013 to start her graduate degree at Louisiana State University in the Department of Geology and Geophysics.